Government of **Western Australia**
Department of **Mines, Industry Regulation and Safety**

RECORD 2018/7

3RD LITHOSPHERE WORKSHOP
5–6 NOVEMBER 2017
THE UNIVERSITY OF WESTERN AUSTRALIA

compiled by
W Gorczyk and K Gessner

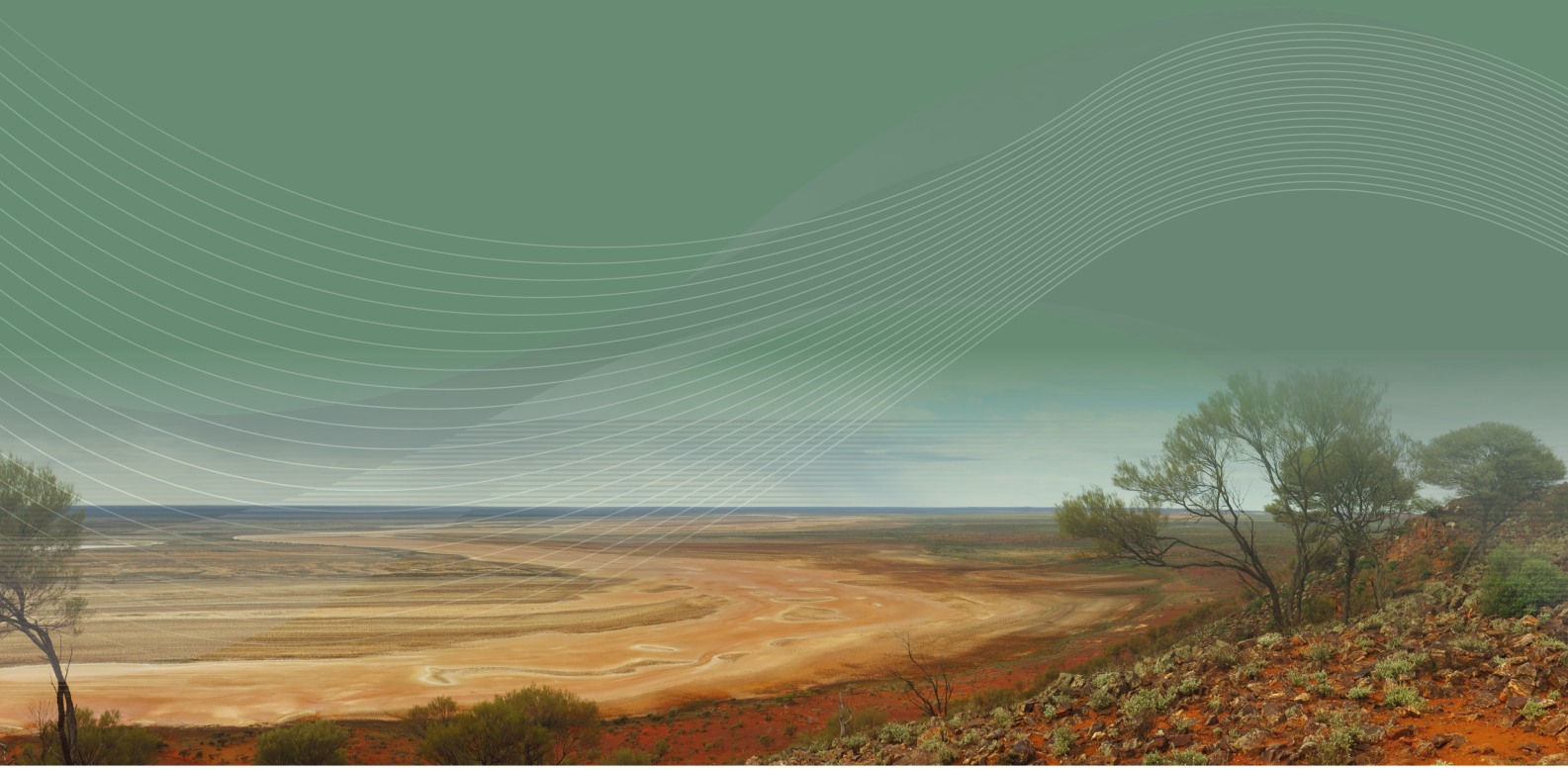

Geological Survey of Western Australia

Centre for EXPLORATION TARGETING

EXPLORATION INCENTIVE SCHEME

CCFS

Government of **Western Australia**
Department of **Mines, Industry Regulation and Safety**

RECORD 2018/7

3RD LITHOSPHERE WORKSHOP 5–6 NOVEMBER 2017 THE UNIVERSITY OF WESTERN AUSTRALIA

compiled by
W Gorczyk and K Gessner

PERTH 2018

Geological Survey of Western Australia

MINISTER FOR MINES AND PETROLEUM
Hon Bill Johnston MLA

DIRECTOR GENERAL, DEPARTMENT OF MINES, INDUSTRY REGULATION AND SAFETY
David Smith

EXECUTIVE DIRECTOR, GEOSCIENCE AND RESOURCE STRATEGY
Jeff Haworth

REFERENCE
The recommended reference for this publication is:
Gorczyk, W and Gessner, K (compilers) 2018, 3rd Lithosphere workshop, 5–6 November 2017, The University of Western Australia: Geological Survey of Western Australia, Record 2018/7, 63p.

ISBN 978-1-74168-812-2

About this publication
This Record presents the final abstracts for the 3rd Lithosphere workshop which was held 5–6 November 2018 at The University of Western Australia. The scientific content of the Record is the responsibility of the authors. No editing has been undertaken by GSWA.

Published 2018 by the Geological Survey of Western Australia
This Record is published in digital format (PDF) and is available online at <www.dmp.wa.gov.au/GSWApublications>.

Further details of geological products and maps produced by the Geological Survey of Western Australia are available from:
Information Centre
Department of Mines, Industry Regulation and Safety
100 Plain Street
EAST PERTH WESTERN AUSTRALIA 6004
Telephone: +61 8 9222 3459 Facsimile: +61 8 9222 3444
www.dmp.wa.gov.au/GSWApublications

Cover image: Elongate salt lake on the Yilgarn Craton — part of the Moore–Monger paleovalley — here viewed from the top of Wownaminya Hill, 20 km southeast of Yalgoo, Murchison Goldfields. Photograph by I Zibra, Department of Mines, Industry Regulation and Safety

Contents

Speaker abstracts

Poster abstracts

PROGRAM: 3rd Lithosphere workshop, 5–6 November 2017, UWA, Perth

Day 1: Core to crust – advances in modelling and not only

8.15 – 8.30	**Annette George**	Welcome
8.30 – 9.30	**Hrvoje Tkalčić**	From the Crust to the Core Using Recent Advances in Global Seismology, Global Interferometry and Mathematical Geophysics
9.30 – 10.30	**Dietmar Muller**	Stability of LLSVP's through deep geological time: Fact of fiction?
10.30 – 11.00	Morning tea	
11.00 – 12.00	**Louis Moresi**	Subduction Dynamics, Continental Collision and Some Thoughts on the Early Earth
12.00 – 12.45	Lunch	
12.45 – 13.45	**Craig O'Neill**	Deep mantle processes: rheology, mixing, and how it's changed.
13.45 – 14.45	**Tim Stern**	Migrating uplift-subsidence in continental interiors due to convective delamination of mantle lithosphere
14.45 – 15.00	Afternoon tea	
15.00 – 16.00	**Zhonghai Li**	Subduction-induced mantle hydration and overriding craton destruction: numerical modeling
16.00 – 17.00	2 min poster presentations	
17.00 – on	Posters and sundowner	

Day 2: Construction and destruction of cratons

8.30 – 9.30	**Keith Priestley**	Structure and evolution of the continents
9.30 – 10.00	**Klaus Gessner**	Mapping the Yilgarn Craton's deep crustal structure by integrating time constrained geochemical data with geophysics
10.00 – 10.30	**Yongjun Lu**	From Archean craton to Tibet: application of isotopic mapping, whole-rock fertility indicator and zircon compositions to understanding lithospheric evolution and mineral systems
10.30 – 11.00	Morning tea	
11.00 – 12.00	**Ling Chen**	Mid-lithospheric discontinuity and its roles in the evolution of cratons
12.00 – 13.00	Lunch	
13.00 – 14.00	**Chris Kirkland**	Charting crust generation via the supercontinent cycle through deep time
14.00 – 15.00	**Fawna Korhonen**	Cratonization revisited: insights from a long-lived intraplate orogen
15.00 – 15.30	Afternoon tea	
15.30 – 16.30	**Tom Raimondo**	Fluid- and melt-rock interaction enable intraplate orogeny
16.30 – 17.00	**Marco Fiorentini**	Closing remarks and best student poster prize

Speaker abstracts

Mid-lithospheric discontinuity and its roles in the evolution of cratons

by

L Chen[1,2]

Detailed knowledge of the structure and properties of lithosphere is essential for understanding the origin and evolution of continents. Recent seismic studies reveal a sharp discontinuity with a velocity decrease at ~60–160 km depth, with majority clustering at ~70–100 km depth beneath continents (Fig. 1; Chen, 2017 and references therein). In young tectonic regions where the lithosphere is generally thin (~100 km), this discontinuity is considered to be the lithosphere-asthenosphere boundary (LAB). However, beneath stable cratons where the lithosphere usually extends to >200 km depth, the discontinuity is interpreted as a mid-lithosphere discontinuity (MLD). The MLD marks the top boundary of a relatively low-velocity layer within the cold, high velocity cratonic mantle keel. Its common appearance is therefore a manifestation of vertical structural variation or layering within the subcontinental lithospheric mantle (SCLM) of cratons. The nature and origin of the MLD and the formation of such SCLM layering are closely associated with the process of generating a thick, buoyant and strong cratonic root in the Archean time, and with the long-term evolution of the SCLM.

The MLD and the underlying (relatively) low velocity layer may indicate a mechanically weak layer within the overall strong cratonic SCLM. How such a weak layer in the SCLM could have affected the ensuing evolution of cratons may provide valuable clues for elucidating the ways of destroying presumably stable cratons. The weak layer may act as the focus of ductile deformation at mantle depths, playing a similar role as the pre-existing laterally weak belts that are expected to be areas of intense heating and strain concentration in the continental lithosphere during tectono-thermal events. Ductile deformation at the MLD depths within the SCLM does have been invoked to explain the nucleation of some mantle earthquakes beneath continents (Prieto et al., 2017), and proven to be capable of leading to delamination of the lower lithospheric mantle under compression regime (Gorczyk et al., 2012). On the other hand, geodynamic modelling indicates that the weak layer does not play a dominant role in craton destruction during lithospheric extension processes (Liao et al., 2013).

The common presence of the MLD beneath stable cratons also suggests that it might not have significantly affected on the long-term stability of cratons. However, the role of the weaker layer could be considerably amplified under the strong influence of oceanic plate subduction, especially with the injection of water-rich fluids, disturbance by subduction-induced unsteady mantle circulations and large-scale extension of the lithosphere associated with slab rollback, as happened beneath the eastern North China Craton during the Early Crateceous. In this case, the presence of such a weak layer within the SCLM may have facilitated simultaneous modifications at the base and in the middle of the lithosphere, eventually leading to the severe lithospheric thinning and destruction recorded in this part of the craton (Chen et al., 2014). Indeed, the eastern North China Craton has been regarded as the best example of craton destruction among others that were affected by oceanic plate subduction (e.g. Carlson et al., 2005; Zhu et al., 2011). A better understanding of this issue and potential roles of the MLD and vertical lithospheric layering in continental evolution demands further detailed investigations of the structure and behaviors of the mantle weak layer in various real tectonic settings (e.g. subduction, collision, mantle plume etc.) and in areas with or without a weak lower crust.

1 State Key Laboratory of Lithospheric Evolution, Institute of Geology and Geophysics, Chinese Academy of Sciences, Beijing, China

2 CAS Center for Excellence in Tibetan Plateau Earth Sciences, Beijing, China

References

Carlson, RW, Pearson, DG and James, DE 2005, Physical, chemical, and chronological characteristics of continental mantle: Review of Geophysics, 43, RG1001, doi: 10.1029/2004RG000156.

Chen, L 2017, Layering of subcontinental lithospheric mantle: Science Bulletin, 62, 1030-1034.

Chen, L, Jiang, MM, Yang, JH, Wei, ZG, Liu, CZ and Ling, Y 2014, Presence of an intralithospheric discontinuity in the central and western North China Craton: Implications for destruction of the craton: Geology, v. 42(3),p. 223–226.

Gorczyk, W, Hobbs, B, Gerya, T, 2012, Initiation of Rayleigh-Taylor instabilities in intra-cratonic settings: Tectonophysics, 514–517, p. 146–155.

Liao, J, Gerya, T and Wang, Q 2013, Layered structure of the lithospheric mantle changes dynamics of craton extension: Geophysical Research Letter, v. 40, p. 5861–5866.

Prieto, GA, Froment, B and Yu, CQ 2017, Earthquake rupture below the brittle-ductile transition in continental lithospheric mantle: Science Advance, 3, e1602642.

Zhu, RX, Chen, L, Wu, FY and Liu, JL 2011, Timing, scale and mechanism of the destruction of the North China Craton: Science China Earth Science, v. 54, p. 789–797.

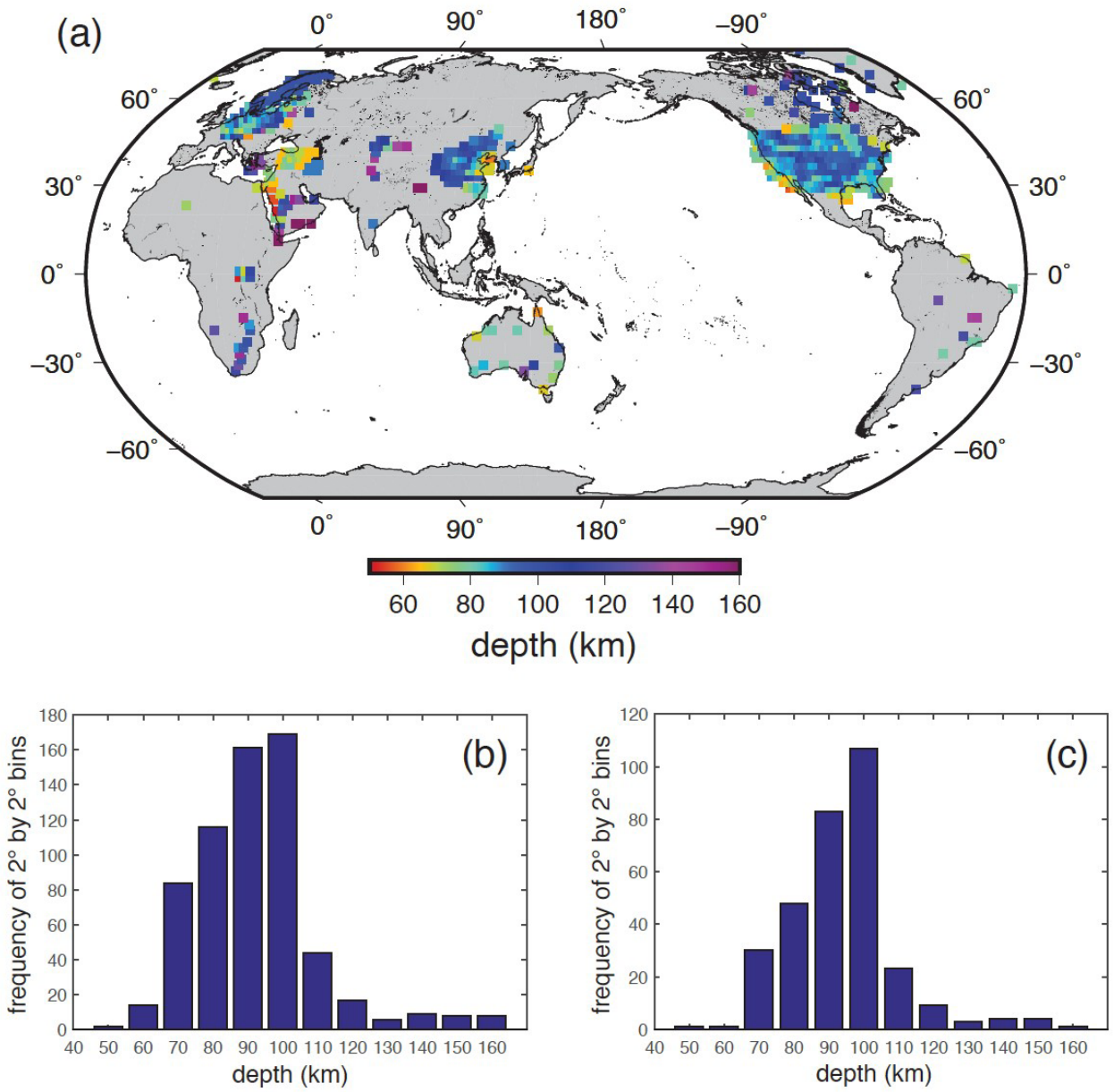

Figure 1. **Depths to the discontinuity with a downward velocity decrease in the shallow upper mantle (≤160 km) beneath continents (from Chen, 2017): (a) geographic distribution of discontinuity depths. Data are averaged into 2° by 2° bins to avoid geographic sampling biases. Color indicates depth; (b) spatial frequency of observed depths shown in (a). Histogram bins are 10 km; (c) same as (b) but only for depths of the mid-lithosphere discontinuity (MLD) beneath cratons.**

Mapping the Yilgarn Craton's deep crustal structure by integrating time constrained geochemical data with geophysics

by

K Gessner[1], RH Smithies[1], Y-J Lu[1], CL Kirkland[2], and H Yuan[1,3,4]

Major progress in the availability of high-quality and spatially extensive time constrained, geochemical and isotopic data and their integration with deep geophysical information allows unprecedented insights into the Yilgarn Craton, one of Earth's best studied segments of ancient continental crust. New and expanded geochemical datasets reveal breaks and gradients in Nd isotope compositions and in trace element ratios that differ significantly from established interpretations of upper crustal structure from surface geological mapping and shallow level geophysical imaging.

The combination of isotopic ($^{143}Nd/^{144}Nd$ and $^{176}Hf/^{177}Hf$) and trace element ratios that reflect the degree of mantle contribution and the depth of melting in magmatic rocks (e.g. Eu/Eu*, La/Yb and Sr/Y ratios), respectively, reveal information on the earliest deep structure of the craton. Specifically, these results suggest that the prominent north-northwesterly to northwesterly trending shear zones overprint an older, east-northeasterly trending fabric that predates the segmentation of the Yilgarn Craton into tectonic domains, specifically the formation of the Ida Fault. This large-scale east-northeasterly trending fabric is also visible in long wavelength geophysical datasets, and is subparallel to the Yilgarn Craton's northern and southern Proterozoic margins. We speculate that this east-northeasterly trending fabric represents the oldest known structural grain of the Yilgarn Craton and reflects early earth geodynamic processes during craton formation. This early fabric may also play a role in the localization of previously reported structural elements, such as early faults with strong north–south movement components, east-trending basin transfers and local Au-mineralization trends.

The application of our combined imaging approach has the potential to re-evaluate other Archean cratons and the processes that shaped them.

1 Geological Survey of Western Australia, East Perth WA 6004

2 Centre for Exploration Targeting – Curtin Node, John de Laeter Centre, Institute of Geoscience Research (TIGeR); Curtin University, Bentley WA 6045

3 ARC Centre of Excellence for Core to Crust Fluid Systems, Department of Earth and Planetary Sciences, Macquarie University, Sydney NSW 2109

4 Centre for Exploration Targeting, The University of Western Australia, Crawley WA 6009

Subduction-induced mantle hydration and overriding craton destruction: numerical modelling

by

Z-H Li*

The continental craton is generally stable due to its buoyancy and rigidity; however, it may also be significantly thinned or even destructed during the long-term evolution, e.g. the North China craton. The mechanism of craton destruction is widely debated, which may include: 1) extension induced thinning (e.g. Liao et al., 2014), 2) compression induced delamination (e.g. Li et al., 2016), 3) plume erosion (e.g. Gorczyk et al., 2017), 4) thermal convection induced erosion in the big mantle wedge (e.g. He, 2014), 5) hydrous mantle transition zone upwelling and erosion (e.g. Wang et al., 2016), and 6) flat subduction and (de)hydration erosion.

The first three models are generally related to the simple mechanisms, i.e. extension, compression, or mantle plume, which are however more difficult to achieve. For example, a stable continental craton requires too large stress, no matter extensional or compressional, to be destructed, which thus limit their applications. The other three models are generally related to the subduction-induced mantle flow, especially the accompanied (de)hydration and melting processes (Fig. 1). In one set of model (Fig. 1a), the subducting slab flatly lies in the mantle transition zone, which triggers the small scale convection in the big mantle wedge. The mantle flow with fluid and melt activity erodes the bottom of the craton and thus leads to the thinning of the lithosphere. In a similar set of model (Fig. 1b), the hydrous mantle transition zone is highlighted, which migrates upward during subduction and then erodes the overriding craton. These two models could be defined as a regime 'from the bottom up'. In contrast, the final model (Figure 1c) highlights the dehydration of flatly subducting slab as well as the hydration and erosion of the overriding craton, which may be followed by the transition to steep subduction. Thus, this regime can be regarded as 'from the top down'.

In order to study the deep mantle hydration and its effects on the craton destruction, we conducted systematic numerical models which combined thermo-mechanical method and thermodynamic data. Firstly, we apply the 'Perplex' (Connolly, 2005) to calculate the phase diagram of water content up to 30 GPa (i.e. the lower mantle depth) for both the mafic and ultramafic rocks. These thermodynamic databases are further integrated to the thermo-mechanical code 'I2VIS' (Gerya and Yuen, 2007) for the subduction modelling.

The numerical models demonstrate that the water contained in the oceanic crust are rather difficult, or even impossible, to be transferred into the mantle transition zone. However, the hydrated and/or serpentinized mantle can do that in the models with cold subducting slab and relatively fast convergence. Due to the uncertainties for the water content and solubility in the mantle transition zone, it is rather difficult to establish a very reliable model for the big mantle wedge hydration, i.e. 'from the bottom up'. Conversely, the flat subduction model (from the top down) is more solid, with much more reasonable datasets. The effects on the overriding craton are also notable in the later case, which may thus provide as a good candidate for the craton destruction.

References

Connolly, JAD 2005, Computation of phase equilibria by linear programming: A tool for geodynamic modelling and an application to subduction zone decarbonation, Earth and Planetary Science Letters, v. 236, p. 524–541

Gerya, TV and Yuen, DA 2007, Robust characteristics method for modelling multiphase visco-elasto-plastic thermo-mechanical problems, Physics of Earth Planetary Interiors, v. 163, p. 83–105.

Gorczyk, W, Mole, DR and Barnes, SJ 2017, Plume-lithosphere interaction at craton margins throughout Earth history, Tectonophysics, doi.org/10.1016/j.tecto.2017.04.002.

He, L 2014, Numerical modelling of convective erosion and peridotite-melt interaction in big mantle wedge: Implications for the destruction of the North China Craton, Journal of Geophysical Research: Solid Earth, v. 119, p. 3662–3677.

Li, ZH, Liu, M and Gerya, T 2016, Lithosphere delamination in continental collisional orogens: A systematic numerical study: Journal of Geophysical Research: Solid Earth, 121, 5186–5211.

Liao, J and Gerya, T 2014, Influence of lithospheric mantle stratification on craton extension: Insight from two-dimensional thermo-mechanical modelling, Tectonophysics, v. 631, p. 50–64.

Wang, Z, Kusky, TM and Capitanio, FA 2016, Lithosphere thinning induced by slab penetration into a hydrous mantle transition zone, Geophysical Research Letters, v. 43(22).

* University of Chinese Academy of Sciences, Beijing, China

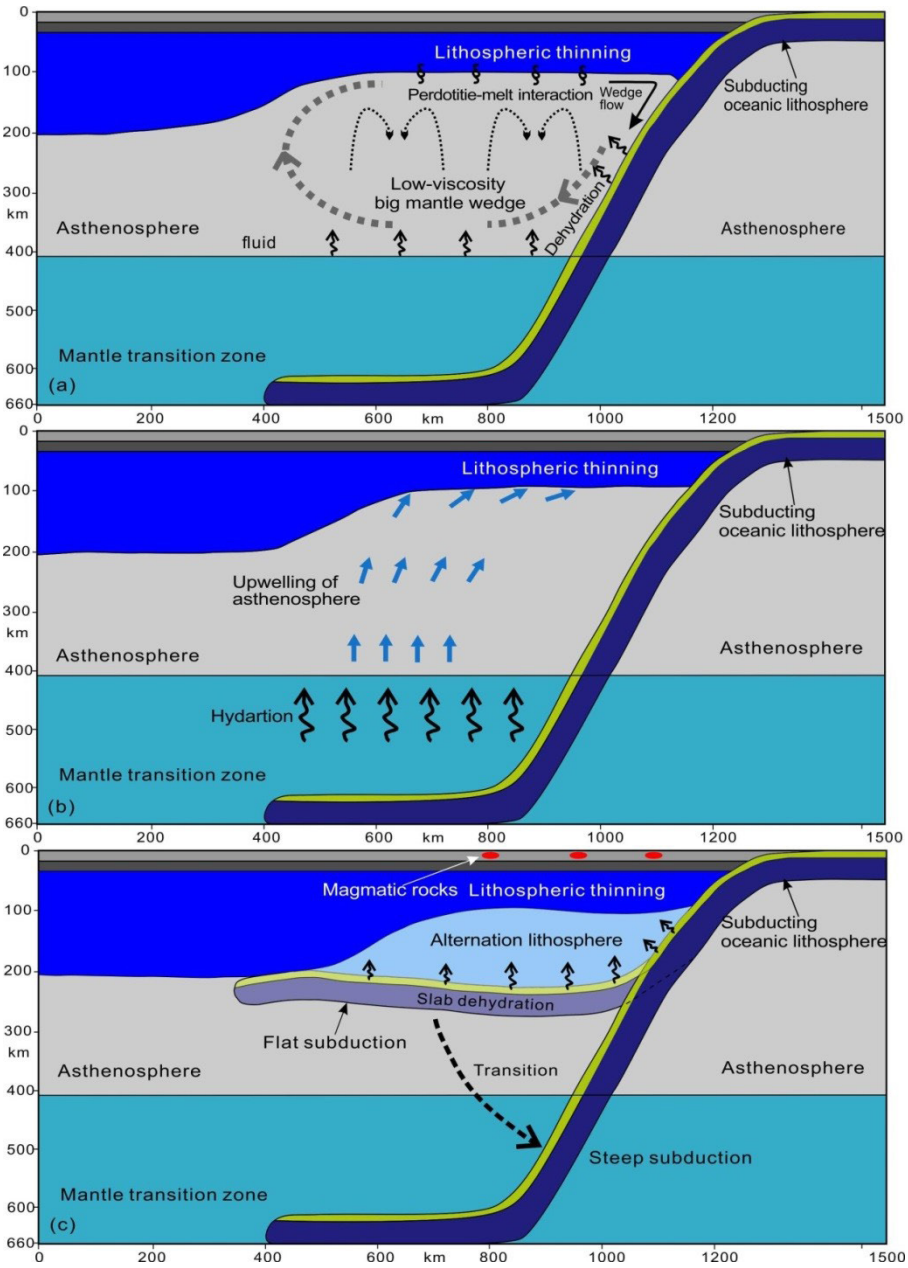

Figure 1. Three candidate models for the subduction-induced mantle hydration and overriding craton destruction: (a) thermal convection induced erosion in the big mantle wedge; (b) hydrous mantle transition zone upwelling and erosion; (c) flat subduction and (de)hydration erosion

Charting crust generation via the supercontinent cycle through deep time

by

CL Kirkland, NJ Gardiner and MIH Hartnady

Crustal growth and the supercontinent cycle

In the modern paradigm, heat energy from our planet's interior escapes through the operation of plate tectonics, driving the generation of primary crust which spreads apart, moves horizontally, stacks up and recycles back into the mantle via subduction zones. The rate of these processes, which is responsible for the generation of Earth's continental crust, is an enduring controversy fostered in part by the progressively more incomplete geological record back into deep time. There have been many models proposed for the rate and timing of crust formation, although two main end members are evident. One end member suggests that most crust formed early in Earth history and has been recycled ever since through uniformitarian plate tectonics (Armstrong, 1991; Scholl and von Heune, 2007). The alternative model suggests that crust grew at a relatively constant rate since the early Archean (c. 4.2 Ga), or perhaps the end of the Archean (2.5 Ga: Taylor and McLellan, 1985; Kramers, 2002; Valley et al., 2005; Belousova et al., 2010). Equally contentious is whether crustal growth was linked to the periodic organization of the supercontinent cycle (e.g. Condie, 1998; Pearson et al., 2007; Condie and Aster, 2010; Hawkesworth et al., 2010). Many recent papers have sought to address the rates and timing question through the use of geochemical evolution datasets, where a geochemical proxy for Earth processes is linked to a precise age (e.g. oxygen U/Pb; Lu/Hf–U/Pb). For such evolution datasets a critical question is to what extent is the preserved record biased and to what extent it captures geological information (Hawkesworth et al., 2009, 2010; Bradley, 2011; Gardiner et al., 2016).

The supercontinent cycle

The supercontinent cycle describes the episodic assembly of most or all of the continental masses which occurs on a quasi-regular timescale of 200–500 Myr (Condie, 1998). The supercontinent cycle is a primary expression of the escape of thermal energy from the lower levels of the planet and fundamentally drives the prevailing global tectonic style and potentially ultimately controls the rate of crust production (Condie et al., 2011). The progression of a single cycle is recorded through the episodic dominance of subduction and supercontinent assembly leading to amalgamation versus rifting and supercontinent dispersal leading to subduction and assembly of the next supercontinent. Recently debate has been centred on the extent to which plate tectonics and supercontinent cycles have shaped and/or biased the isotopic record as preserved in rocks and their eroded remains, and how this is reflected in both the U–Pb and Lu–Hf isotopic datasets (see Hawkesworth et al., 2009 and contrast with Gardiner et al., 2016).

In this contribution we present time-constrained isotope analyses that act as proxies of crust generation (Fig. 1). We show how the data confirm the operation of Earth's supercontinent cycle through to at least 3000 Ma. Furthermore, the importance of the supercontinent cycle to continental growth is demonstrated by a link between periods of enhanced crustal recycling and elevated geochemical proxies of subduction flux (Van Kranendonk and Kirkland, 2016).

The Hf record

Newly generated crust extracted from the mantle can be considered to have an initial $^{176}Hf/^{177}Hf$ ratio equivalent to that of a depleted mantle model. A juvenile zircon Hf signal will be measured in magmas derived from material recently extracted from depleted mantle with minimal to no older crustal contamination. Hf analyses recording a lower initial $^{176}Hf/^{177}Hf$ than a depleted mantle model may reflect a source of reworked existing older crust with no significant new mantle, or alternatively a mix between juvenile and evolved sources. Hence, the zircon Hf isotopic system can be used as a tool to monitor the degree to which a melt source reflects juvenile mantle addition versus reworking of pre-existing crust.

In this work we consider the Hf compilation of Roberts and Spencer (2014) that represents a near-continuous record of magmatism sampled from a variety of tectonic settings and localities and encompasses the assembly of at least four major supercontinents: Pangaea, Gondwana, Rodinia and Columbia (Nuna), although much the same trends are evident in other compilations (Belousova et al., 2010). We calculate a de-trended evolution line for the juvenile 95% signal which is most sensitive to collision and breakup processes, a feature which has been interpreted as a consequence of it being least affected by mixtures with crustal components (Gardiner et al., 2016). De-trending of this isotopic signal fits a linear regression to the dataset as a means to evaluate significant changes around the broad evolutionary trend (Van Kranendonk and Kirkland, 2016).

Periodicities within the global zircon Hf signal, treated in this way, correlate with high statistical confidence to the supercontinent cycle as determined through independent geological evidence (Gardiner et al., 2016).

The total amplitude of the juvenile Hf signal during supercontinent cycles varies with time, reaching a maximum intensity immediately prior to the final assembly of Pangaea and markedly diminishing thereafter, which may reflect a secular change in subduction style leading to enhanced subduction erosion during Gondwana assembly. Alternatively this pattern of decreasing signal strength may reflect the loss of information through one supercontinent cycle into the next.

Biased by selective preservation — not in the way most think?

Some have proposed that the population peaks evident in the U–Pb zircon record are an artefact of preservation rather than supercontinent assembly processes (Hawkseworth et al., 2009). Such an interpretation is founded on a model where the preservation potential for early subduction-related (early assembly) and later extensional-related (breakup) magmatism is less than for collision-related magmatism. Roberts and Spencer (2014) considered a similar phenomenon to affect the Hf isotope record. We suggest that the global Hf record is less sensitive to selective preservation, as the Hf record is less influenced by the frequency of observations and more by the relative compositional value. Although selective preservation may erode the signal by reducing the number of analyses at a given age the pattern of low preservation potential affects those parts of a supercontinent cycle with a dominance of juvenile material. Hence, during these intervals, selective removal of some of the juvenile analyses through erosion may move the average of that group towards more evolved values. However due to the distribution of data, this process is unlikely to move the average to the type of values seen in those parts of the cycle with a dominance of evolved material which are also likely to have the greatest preservation potential (Fig. 2). Furthermore, Gardiner et al., (2016) found no correlation between the number of analyses and the deviation from a juvenile reference signal, consistent with a lack of significant preservation bias in the global Hf signal.

Although tectonic process are encoded into isotopic evolution signals, the extent to which other processes — such as preservation artefacts — modify this primary signal is not well constrained but potentially accessible through comparison of disparate datasets which will respond differently to earth surface processes. Importantly, we observed systematic differences between signals in whole rock and grain-based isotopic systems. By comparing these two sample mediums we suggest it is possible to assess the affect that zircon preservation biases have on isotopic evolution patterns.

It has been shown that preservation biases in the Hf isotope record are not to the extent that they obscure the supercontinent signal (Gardiner et al., 2016). Nonetheless, biases may be imposed by the amount of the isotopic signal held within sedimentary basins which may not be recycled on the same timescale as other crustal components. These differences in isotopic signal from different mediums allow us to determine how much signal, and by extension, juvenile crust is carried through one supercontinent cycle into the next and provide a means to understand how much geological information in the isotopic record may be lost transitioning between supercontinents. Considering these preservation factors in decoding isotopic signals reveals a profound increase in mineral grain-based isotopic systems over whole-rock isotope evolution signals at the start of the Phanerozoic. This change is consistent with the volume of sedimentary rock mass at the Earth's surface dramatically increasing at this time. We ascribe the difference in grain and whole-rock signals as the consequence of grain based systems capturing information from the previous supercontinent cycle, whereas whole-rock systems, based on magmatic rocks, losing this information through subduction. Importantly, the difference in signal strength can be used to approximate the volume of material that gets carried through one supercontinent cycle into the next via sedimentary basins.

Conclusions

The temporal fluxes in crustal recycling rate match periods of supercontinent assembly and dispersal, as well as variations in the volume of mantle-derived magmas, demonstrating the profound linkage between deep, shallow and surface Earth system processes arising from the aggregation and dispersal of supercontinents. Broad-scale secular excursions in Hf isotopes towards more juvenile or evolved signals can be used to infer globally prevailing tectonic style. Although grain-based evolution signals carry with them a strong signal from the supercontinent cycle that is not extensively influenced by selective preservation, a higher order signal component documents the increase in global sedimentary mass at the start of the Phanerozoic. The discrepancy between whole-rock igneous and grain-based detrital signals charts the volume of material preserved through one supercontinent cycle into the next.

References

Armstrong, RL 1991, The persistent myth of crustal growth. Australian Journal of Earth Sciences, v. 38, p. 613–630.

Belousova, EA, Kostitsyn, YA, Griffin, WL, Begg, GC, O'Reilly, SY and Pearson, NJ 2010, The growth of the continental crust: Constraints from zircon Hf-isotope data. Lithos, v. 119, p. 457–466.

Bradley, DC 2011, Secular trends in the geologic record and the supercontinent cycle. Earth-Science Reviews, v. 108(1), p. 16–33.

Condie, KC, Bickford, M, Aster, RC, Belousova, E and Scholl, DW 2011, Episodic zircon ages, Hf isotopic composition, and the preservation rate of continental crust. Geological Society of America Bulletin, v. 123(5–6), p. 951–957.

Condie, KC 1998, Episodic continental growth and supercontinents: a mantle avalanche connection? Earth and Planetary Science Letters, v. 163(1), p. 97–108.

Condie, KC and Aster, RA 2010. Episodic zircon age spectra of orogenic granitoids: The supercontinent connection and continental growth. Precambrain Research, v. 180, p. 227–236.

Gardiner, NJ, Kirkland, CL and Van Kranendonk, MJ 2016, The Juvenile Hafnium Isotope Signal as a Record of Supercontinent Cycles. Scientific Reports, 6, doi:10.1038/srep38503.

Cratonization revisited: insights from a long-lived intraplate orogen

by

FJ Korhonen and SP Johnson

The stabilization of continental crust to form cratons plays a fundamental role in the evolution of our planet. These coherent domains of crust are the end product of intense magmatic, tectonic, and metamorphic episodes that progressively organize the crust and underlying lithosphere into a stable compositional and thermal profile. However, few terranes preserve a detailed record of the processes leading to cratonization. In this contribution we synthesize the results of detailed studies in the Capricorn Orogen, Western Australia, to document the cumulative events that lead to stabilization of the crust. Our understanding of these events provides new insights into the processes related to protracted cratonization.

The Proterozoic Capricorn Orogen is a complex region that records the punctuated assembly of the Archean Pilbara and Yilgarn Cratons with the Glenburgh Terrane to form the West Australian Craton (Cawood and Tyler, 2004). Following the final assembly of the West Australian Craton, the orogen was structurally and thermally reworked during at least five intraplate orogenic events (Fig. 1), with metamorphism and deformation partitioned into discrete tectonic corridors (Sheppard et al., 2010) that progressively narrow with time. Many of the events, particularly the older ones, were accompanied by the intrusion of voluminous felsic magmatic rocks. The overall crustal evolution has been well characterized using Sm–Nd whole-rock data, and Lu–Hf and $\delta^{18}O$ isotopic data from magmatic and inherited zircon from the four main magmatic suites (Johnson et al., 2017). These data reveal a near-complete record of crustal differentiation, with a significant period of crustal growth along a subduction margin just prior to continental collision (Cycle 2; Fig. 1). Subsequent magmatic cycles become increasingly dominated by reworking of older crustal sources, with the final magmatic cycle (Cycle 4) formed exclusively by crustal reworking.

Following Cycle 4 magmatism, the orogenic crust displays a broad secular change to more rigid behavior (Fig. 1), allowing the emplacement of abundant mafic dykes and sills into the shallow crust and the formation of thick intracontinental sedimentary basins. However, the granitic rocks generated during the reworking events show an increasing enrichment in heat-producing elements (HPE; Korhonen and Johnson, 2015), demonstrating that differentiation of the orogenic crust culminated in an enriched, radiogenic upper crust. The present-day heat production values exceed values for typical granitic rocks and those for the bounding Pilbara and Yilgarn Cratons. A radiogenic mid to upper crust will elevate the thermal gradient, potentially making the crust more susceptible to deformation and reworking (McLaren et al., 2005), despite the overall refractory nature of the crustal profile. Following Cycle 4 magmatism and the deposition of up to 10 km of siliciclastic sedimentary rocks into the Edmund Basin (Cutten et al., 2016), those areas dominated by a highly radiogenic batholith emplaced during Cycle 4 were reworked during the Mesoproterozoic Mutherbukin Tectonic Event (Fig. 1). Numerical models show that slight thickening of this HPE-rich crust during transpressional deformation formed a thermal lid, which elevated the regional thermal gradient and sustained metamorphism over prolonged timescales (>110 Ma; Korhonen and Johnson, 2015; Korhonen et al., 2017). The timing of this event was coincident with numerous mid-Mesoproterozoic events around the West Australian Craton, suggesting that thick cratonic roots may play a significant role in propagating stresses generated at distant plate boundaries.

In contrast to the reworking events that are partitioned into progressively narrower corridors, orogen-scale reactivation of faults and shear zones occurred immediately after the final reworking event (Fig. 1; Piechocka et al., in press). Field observations are consistent with lateral extrusion of the crust during north–south compression between the bounding Pilbara and Yilgarn Cratons. The reactivation of these structures at this time is interpreted as the transition from reworking to cratonized behavior (Piechocka et al., in press; Holdsworth et al., 2001).

References

Cawood, PA and Tyler, IM 2004, Assembling and reactivating the Proterozoic Capricorn Orogen: lithotectonic elements, orogenies, and significance: Precambrian Research, v. 128, p. 201–218.

Cutten, HN, Johnson, SP, Thorne, AM, Wingate, MTD, Kirkland, CL, Belousova, EA, Blay, OA and Zwingmann, H 2016, Deposition, provenance, inversion history and mineralization of the Proterozoic Edmund and Collier Basins, Capricorn Orogen: Geological Survey of Western Australia, Report 127, 80p.

Holdsworth, RE, Hand, M, Miller, JA and Buick, IS 2001, Continental reactivation and reworking, *in* Continental reactivation and reworking *edited by* JA Miller, RE Holdsworth, IS Buick and M Hand: Geological Society, London, Special Publications: v. 184, p. 1–12.

Johnson, SP, Korhonen, FJ, Kirkland, CL, Cliff, JB, Belousova, EA and Sheppard, S 2017, An isotopic perspective on growth and differentiation of Proterozoic orogenic crust: From subduction magmatism to cratonization: Lithos, v. 268–271, p. 76–86.

Korhonen, FJ and Johnson SP 2015, The role of radiogenic heat in prolonged intraplate reworking: The Capricorn Orogen explained?: Earth and Planetary Science Letters, v. 428, p. 22–32.

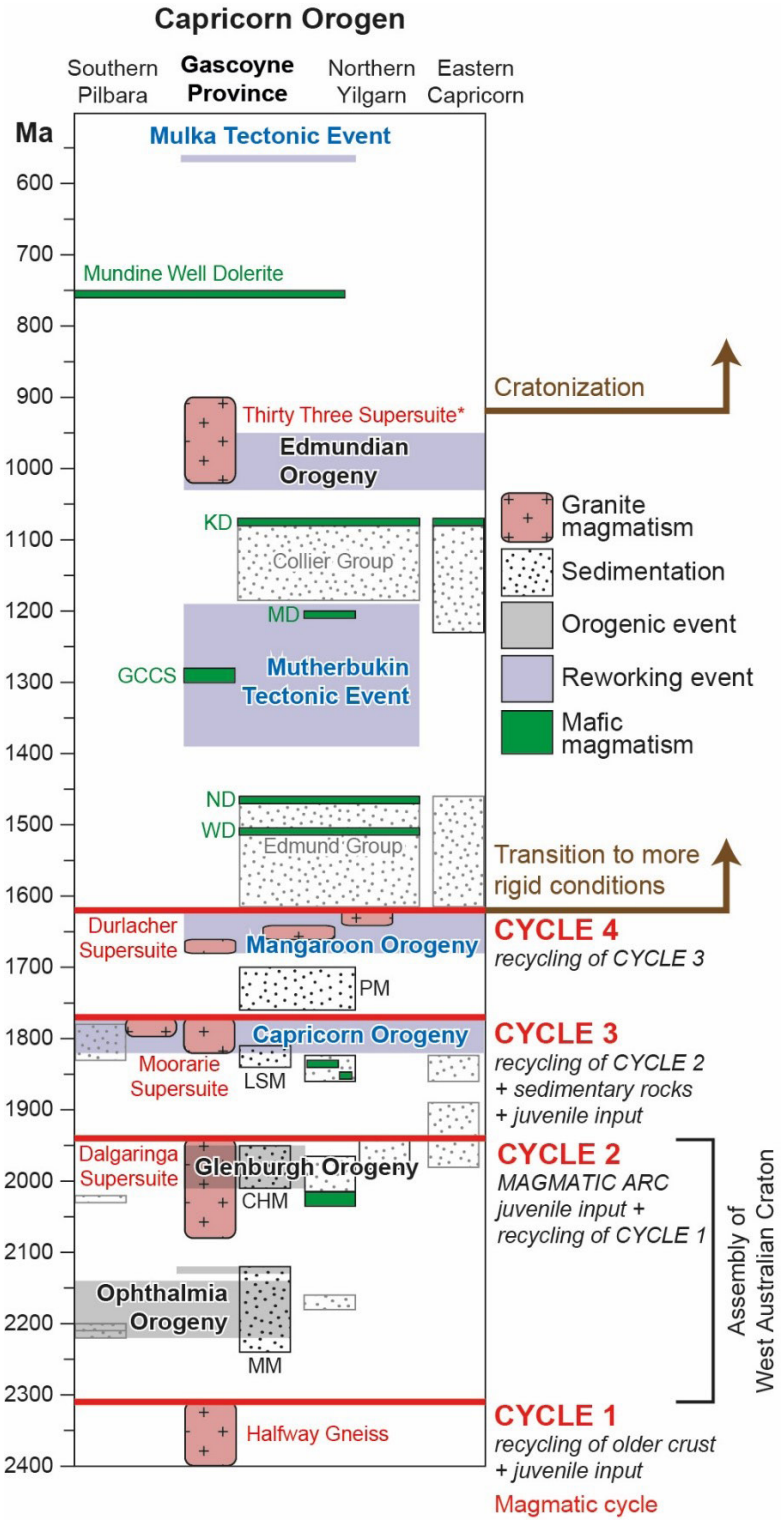

Figure 1. Time–space event summary of the Capricorn Orogen (after Korhonen and Johnson, 2015). Magmatic cycles shown in red; * denotes minor, localized intrusions. Abbreviations: CHM, Camel Hills Metamorphics; GCCS, Gifford Creek Carbonatite Suite; KD, Kulkatharra Dolerite; LSM, Leake Spring Metamorphics; MD, Muggamurra Dolerite; MM, Moogie Metamorphics; ND, Narimbunna Dolerite; PM, Pooranoo Metamorphics; WD, Waldburg Dolerite

Korhonen, FJ, Johnson, SP, Wingate, MTD, Kirkland, CL, Fletcher, IR, Dunkley, D, Roberts, MP, Sheppard, S, Muhling, JR and Rasmussen, B 2017, Radiogenic heating and craton-margin plate stresses as drivers for intraplate orogeny: Journal of Metamorphic Geology, v. 35, p. 631–661.

McLaren, S, Sandiford, M and Powell, R 2005, Contrasting styles of Proterozoic crustal evolution: a hot-plate tectonic model for Australian terranes: Geology, v. 33, p. 673–676.

Piechocka, AM, Sheppard, S, Johnson, SP, Rasmussen, B and Jourdan, F in press, Death of an orogen, birth of a craton: Geology.

Sheppard, S, Bodorkos, S, Johnson, SP, Wingate, MTD and Kirkland, CL 2010, The Paleoproterozoic Capricorn Orogeny: intracontinental reworking not continent-continent collision: Geological Survey of Western Australia, Report 108, 33p.

From Archean craton to Tibet: application of isotopic mapping, whole-rock fertility indicator and zircon compositions to understanding lithospheric evolution and mineral systems

by

Y-J Lu[1,2]

Isotopic mapping

Whole-rock Sm–Nd and zircon Lu–Hf isotopic mapping are powerful in imaging lithospheric architecture and crustal evolution through time in Archean cratons and Cenozoic orogens (Champion and Cassidy, 2007; Champion, 2013; Champion and Huston, 2016; Mole et al., 2014; Hou et al., 2015; Wang et al., 2016; Gardiner et al., 2017). I present here the most updated whole-rock Sm-Nd isotopic maps of the Archean Pilbara and Yilgarn Cratons in Western Australia and the zircon Lu–Hf isotopic maps in the Tibetan Plateau (Figs 1–3).

The T_{DM}^2 map of the Pilbara Craton shows that the east Pilbara is dominated by Eoarchean–Paleoarchean basement whereas the west Pilbara is dominated by Mesoarchean–Neoarchean basement (Fig. 1a,b). After 3.2 Ga, the felsic magmatism in the east Pilbara is derived mainly by reworking of existing crust, whereas the west Pilbara has juvenile crustal addition, suggesting two distinct geodynamic evolutions after 3.2 Ga (Fig. 1d).

The Nd isotopic map of the Yilgarn Craton subdivides the craton into an older Yilgarn proto-craton to the west (Narryer, South West and Youanmi Terranes) and the younger, more juvenile Eastern Goldfields Superterrane to the east (Kalgoorlie, Kurnalpi, Burtville and Yamarna Terranes; Fig. 2). The juvenile Kalgoorlie and Kurnalpi Terranes are interpreted to be rift produced by the c. 2.7 Ga mantle plume event, which produced thick sequences of komatiitic volcanic rocks and basalts of 2710–2690 Ma in the Kalgoorlie Terrane (Witt et al., in prep.).

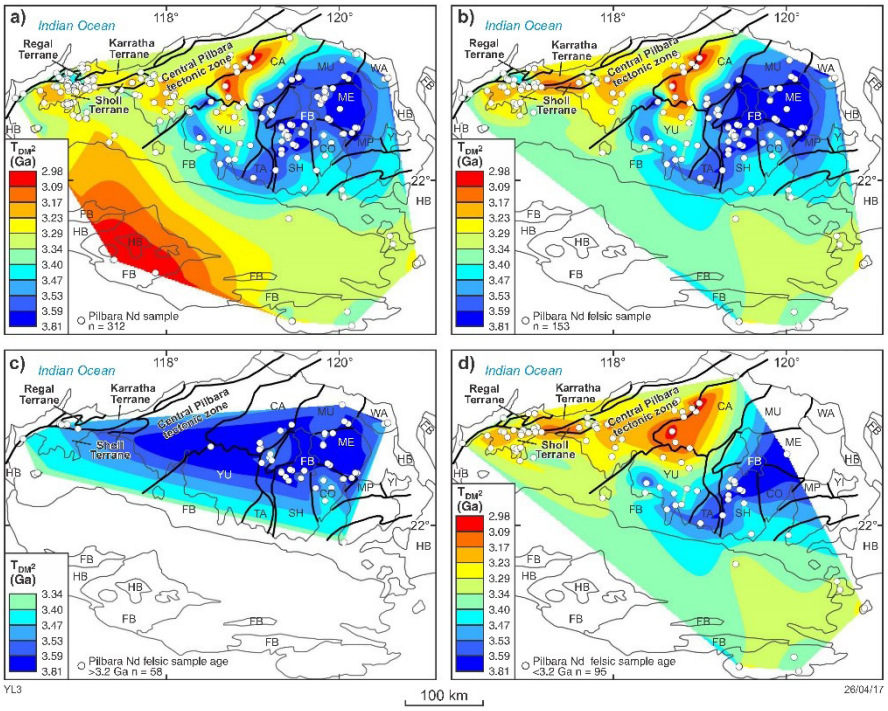

Figure 1. Whole-rock Sm–Nd model age (T_{DM}^2) maps of the Pilbara Craton

1 Geological Survey of Western Australia, 100 Plain Street, East Perth WA 6004

2 Centre for Exploration Targeting and Australian Research Council Centre of Excellence for Core to Crust Fluid Systems (CCFS), School of Earth Sciences, The University of Western Australia, Crawley WA 6009

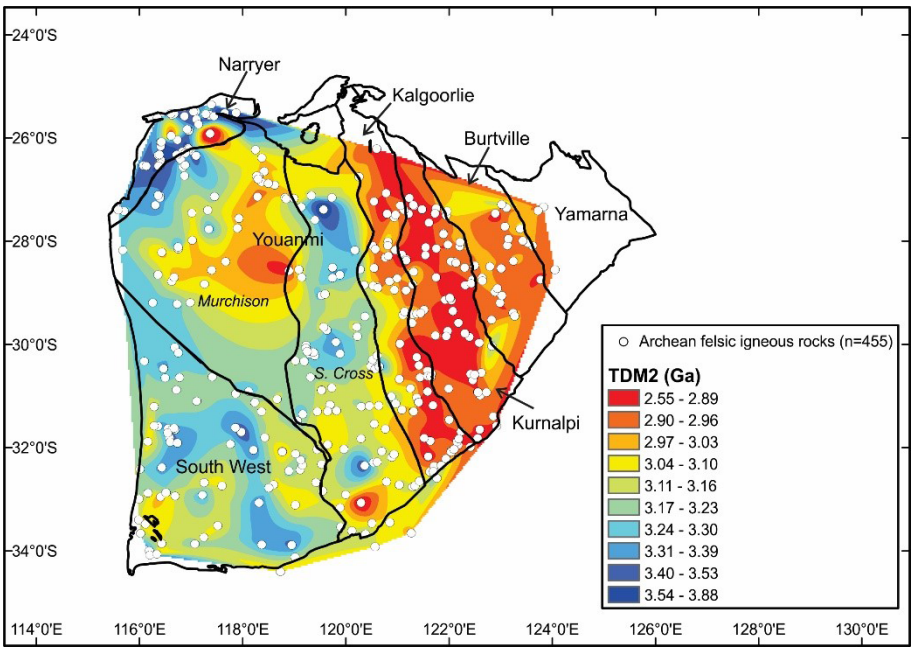

Figure 2. Whole-rock Sm–Nd model age (TDM2) map of the Yilgarn Craton

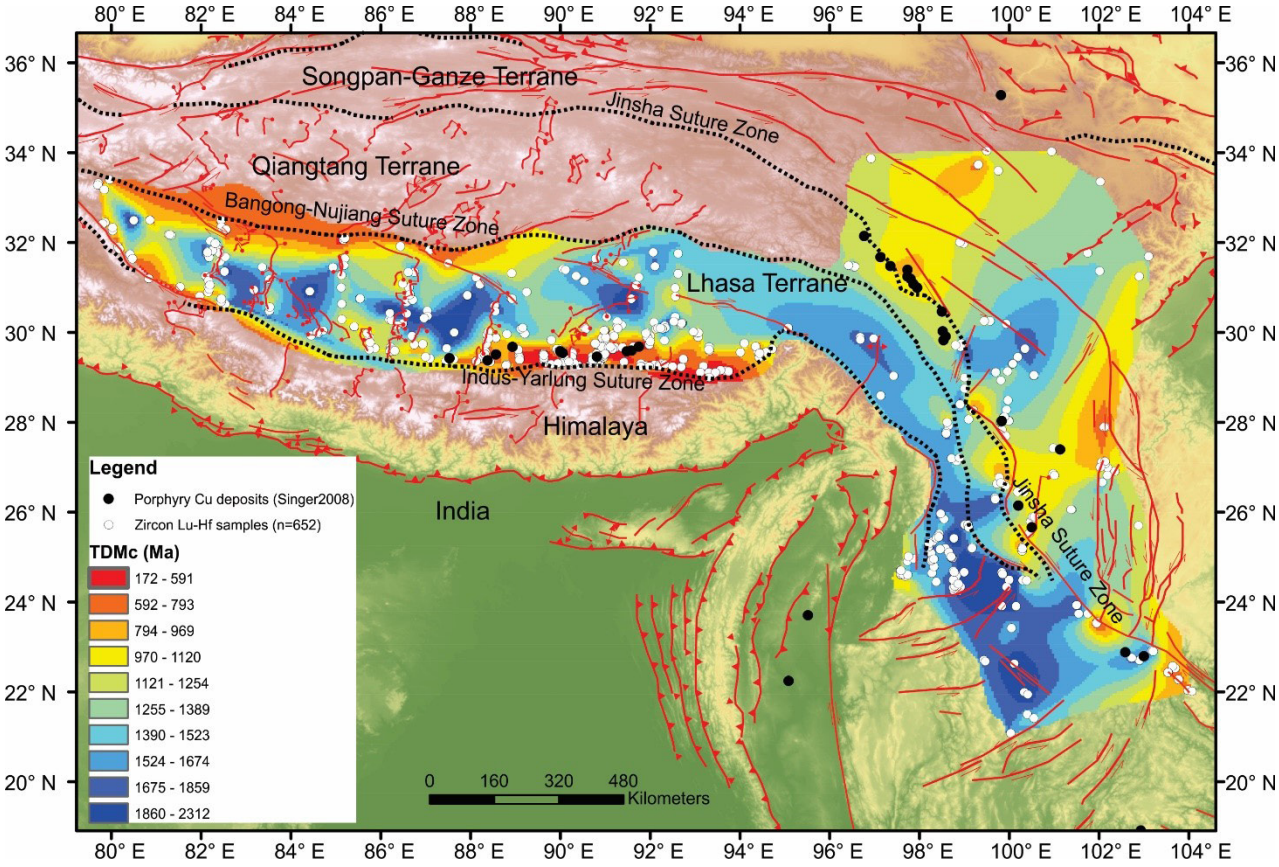

Figure 3. Contour map of zircon two-stage depleted mantle model ages (TDMc) for granitoid and felsic volcanic rocks in the Tibetan Plateau. Zircon data sources: Hou et al. (2015); Wang et al. (2016). Suture zones and faults of the Tibetan Plateau are from the HimaTibet Map (Styron et al., 2010). Locations of porphyry copper deposits are from Singer et al. (2008)

The zircon Hf isotopic map in the Tibetan Plateau constructed by using 652 zircon samples demonstrates that the majority of porphyry Cu deposits are associated with isotopically juvenile domains along two major suture zones of the Indus-Yarlung and Jinsha suture zones (Fig. 3). Such isotopic mapping can thus help narrow down search space from over 2500 km scale to about 500 km scale.

Whole-rock fertility indicator

Whole-rock geochemical mapping using about 1200 samples across the Lhasa Terrane is shown in Figure 4. All porphyry Cu deposits are located within high 10000*(Eu/Eu*)/Y (>800) domains. Other whole-rock fertility indicators such as V/Sc, Eu/Eu*, Sr/Y ratios (Loucks, 2014) are less effective in discriminating Cu-porphyries from barren ultrapotassic rocks on contour maps. Thus, the (Eu/Eu*)/Y ratio is the best whole-rock fertility indicator, and is interpreted to indicate extremely high magmatic water content which induces early and prolific hornblende fractionation and suppresses early plagioclase crystallization. Geochemical mapping using this ratio can significantly reduce exploration space.

Zircon trace element fertility indicator

Zircon U–Pb and trace element data were obtained from 66 igneous samples of Jurassic to Miocene (181–11 Ma) age in the eastern Gangdese belt (Fig. 5). Both xenocrystic and magmatic zircons show systematic temporal compositional evolution from Jurassic to Miocene. From c. 200 Ma to c. 55 Ma, zircon Eu/Eu* (0.1 – 0.4), 10000*(Eu/Eu*)/Y (0.1–10), and (Ce/Nd)/Y (0.001 – 0.05) ratios remain broadly similar (Lu et al., 2016). However, these zircon trace element ratios increase rapidly after c. 55 Ma and culminate at c. 13 Ma with Eu/Eu*, 10000*(Eu/Eu*)/Y, and (Ce/Nd)/Y ratios up to 1, 70, and 2, respectively (Fig. 5). This zircon compositional trend is interpreted to indicate increasing maturation of the collision-related magmas due to increased compression related to subduction of buoyant Indian continental lithosphere.

Zircon composition can distinguish fertile from infertile Phanerozoic magmatic suites with respect to porphyry Cu mineralization, and reflect processes previously determined through whole-rock fertility indicators (Lu et al., 2016). To investigate the fertility of Archean granites, the zircon compositions were determined for various Archean granites in the Yilgarn Craton (Fig. 6). Based on whole-rock compositions, the population of granite samples can be broadly divided into three groups. This includes sodic low Sr/Y granites, potassic low Sr/Y granites and TTGs. Each group shows broadly different zircon trace element compositions, all of which are transitional between Phanerozoic infertile (dry and reduced) and fertile (hydrous and oxidized) suites (Fig. 6). The Archean Yilgarn granites generally have lower zircon Ce/Ce* and Ce/sqrt(U*Ti) ratios than the Phanerozoic Cu-ore-forming fertile suites, suggesting the former are less hydrous and more reduced and are thus not favourable for Cu mineralization.

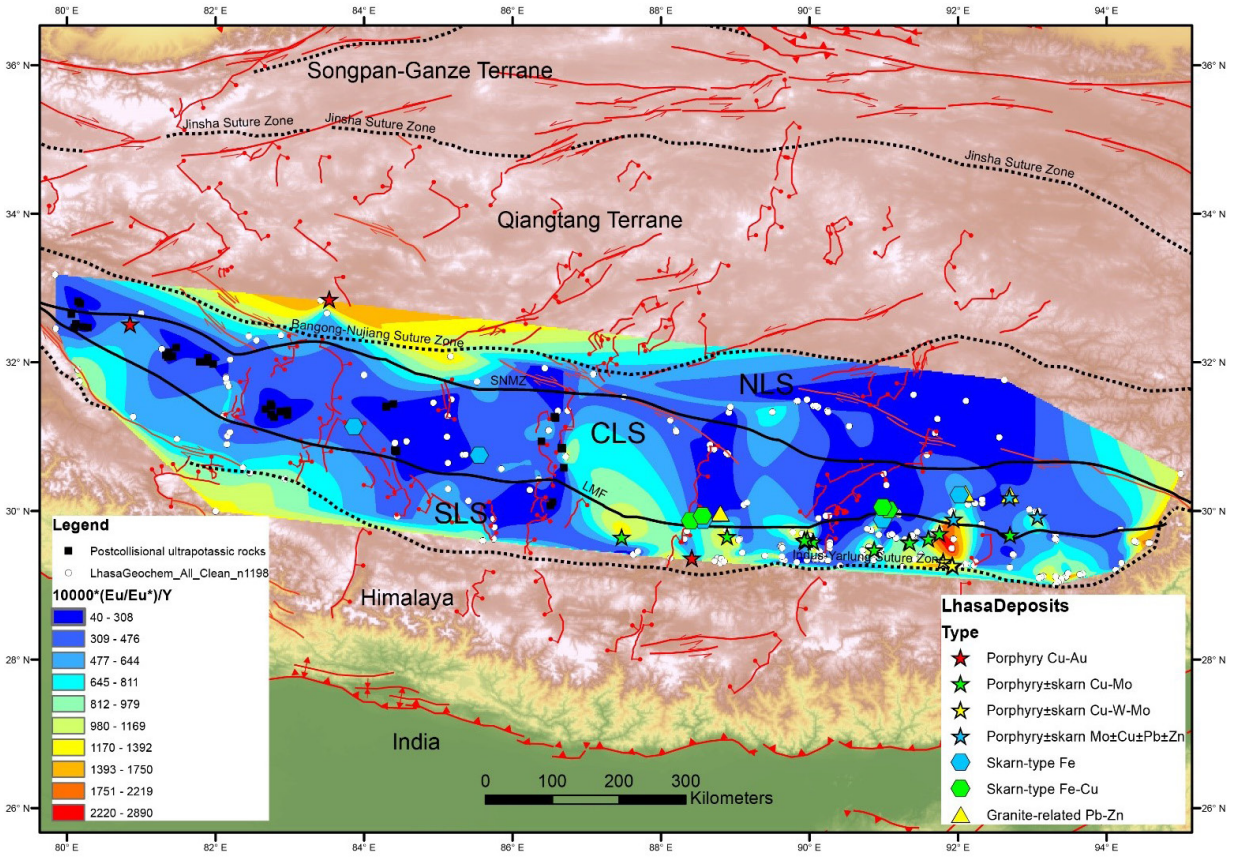

Figure 4. Contour map of whole-rock geochemical ratio of 10000*(Eu/Eu*)/Y for mafic to felsic intrusive and volcanic rocks in the Lhasa Terrane, southern Tibet. Also shown are major mineral deposits in the Lhasa Terrane (Hou et al., 2015; Yang et al., 2016). Whole-rock geochemistry of igneous rocks in the Lhasa Terrane were compiled from Hou et al. (2015), Yang et al. (2016) and Lu et al. (unpublished). Abbreviations: NLS, Northern Lhasa Subterrane; CLS, Central Lhasa Subterrane; SLS, Southern Lhasa Subterrane

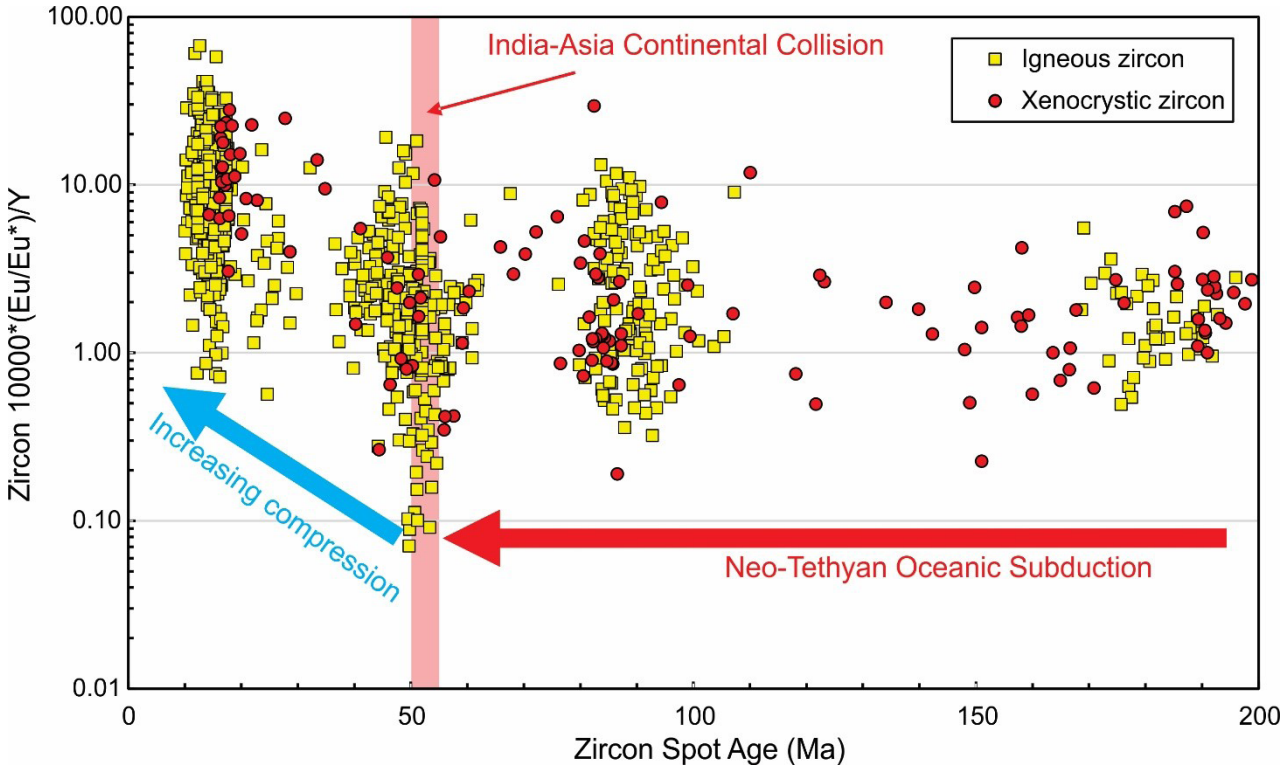

Figure 5. Zircon 10 000* (Eu/Eu*)/Yratio vs Age (Ma) for 66 magmatic rocks in the eastern Gangdese belt, Lhasa Terrane, southern Tibet. Data Source: Lu et al. (unpublished)

Conclusion

Whole-rock Sm-Nd isotopic mapping of the Archean Pilbara and Yilgarn Cratons demonstrate it is powerful in imaging lithospheric architecture and crustal evolution through time. Zircon Lu–Hf isotopic mapping of the Tibetan Plateau reveals that juvenile crust domains are preferable for porphyry Cu formation. Porphyry Cu deposits in the Lhasa Terrane have distinctly high whole-rock 10 000*(Eu/Eu*)/Y ratios (>800), which is the best fertility indicator. The combined isotopic mapping and whole-rock 10 000*(Eu/Eu*)/Y ratio mapping has great potential to help focus exploration on prospective areas. Zircon trace elements of Archean granites in the Yilgarn Craton suggest these granites are less hydrous and more reduced than Phanerozoic Cu-ore-forming granites, which can explain the scarcity of porphyry mineralization in the Archean.

References

Champion, DC 2013, Neodymium depleted mantle model age map of Australia: explanatory notes and user guide. Record 2013/44. Geoscience Australia: Canberra.

Champion, DC and Cassidy, KF 2007, An overview of the Yilgarn Craton and its crustal evolution. In: Berlin, F.P., Knox-Robinson, C.M. (Eds.), Proceedings of Geoconferences (WA) Inc. Kalgoorlie 07 Conference. Geoscience Australia Record 14, p. 8–13.

Champion, DC and Huston, DL 2016, Radiogenic isotopes, ore deposits and metallogenic terranes: novel approaches based on regional isotopic maps and the mineral systems concept. Ore Geology Reviews, v. 76, p. 229–256.

Gardiner, NJ, Hickman, AH, Kirkland, CL, Lu, YJ, Johnson, T and Zhao, JX 2017, Processes of crust formation in the early Earth imaged through Hf isotopes from the East Pilbara Terrane, Precambrian Research, v. 297, p. 56-76.

Hou, ZQ, Duan, LF, Lu, YJ, Zheng, YC, Zhu, DC, Yang, ZM, Yang, ZS, Wang, BD, Pei, YR, Zhao, ZD and McCuaig, TC 2015, Lithospheric architecture of the Lhasa Terrane and its control on ore deposits in the Himalayan-Tibetan orogeny: Economic Geology, v. 110, p. 1541–1575.

Loucks, RR 2014, Distinctive composition of copper-ore-forming arc magmas. Australian Journal of Earth Sciences, v. 61, p. 5–16.

Lu, YJ, Loucks, RR, Fiorentini, ML, McCuaig, TC, Evans, NJ, Yang, ZM, Hou, ZQ, Kirkland, CL, Parra-Avila, LA and Kobussen, A 2016, Zircon compositions as a pathfinder for porphyry Cu ± Mo ± Au deposits, Society of Economic Geologists Special Publication No. 19, p. 329–347.

Mole, DR, Fiorentini, ML, Thebaud, N, Cassidy, KF, McCuaig, TC, Kirkland, CL, Romano, N, Belousova, EA, Barnes, SJ and Mill, J 2014, Archean komatiite volcanism controlled by the evolution of early continents: PNAS 111, p. 10083–10088.

Singer, DA, Berger, VI and Moring, BC 2008, Porphyry copper deposits of the world: database and grade and tonnage models: U.S. Geological Survey Open-File Report 2008-1155, 45p., http://pubs.usgs.gov/of/2008/1155/.

Styron, R, Taylor, M and Okoronkwo, K 2010, HimaTibetMap-1.0: new 'web-2.0' online database of active structures from the Indo-Asian collision, Eos, v.91, no. 20.

Wang, CM, Bagas, L, Lu, YJ, Santosh, M, Du, B and McCuaig, TC 2016. Terrane boundary and spatio-temporal distribution of ore deposits in the Sanjiang Tethyan Orogen: Insights from zircon Hf-isotopic mapping. Earth-Science Reviews, v. 156, p. 39–65.

Witt, WK, Cassidy, K, Lu, YJ and Hagemann, S, The tectonic setting and evolution of the 2.7 Ga Kalgoorlie - Kurnalpi Rift, a world-class Archean gold province. Mineralium Deposita (under review).

Yang, ZM, Goldfarb, R and Chang, ZS 2016, Generation of Postcollisional Porphyry Copper Deposits in Southern Tibet Triggered by Subduction of the Indian Continental Plate, Society of Economic Geologists Special Publication No. 19, p. 279–300.

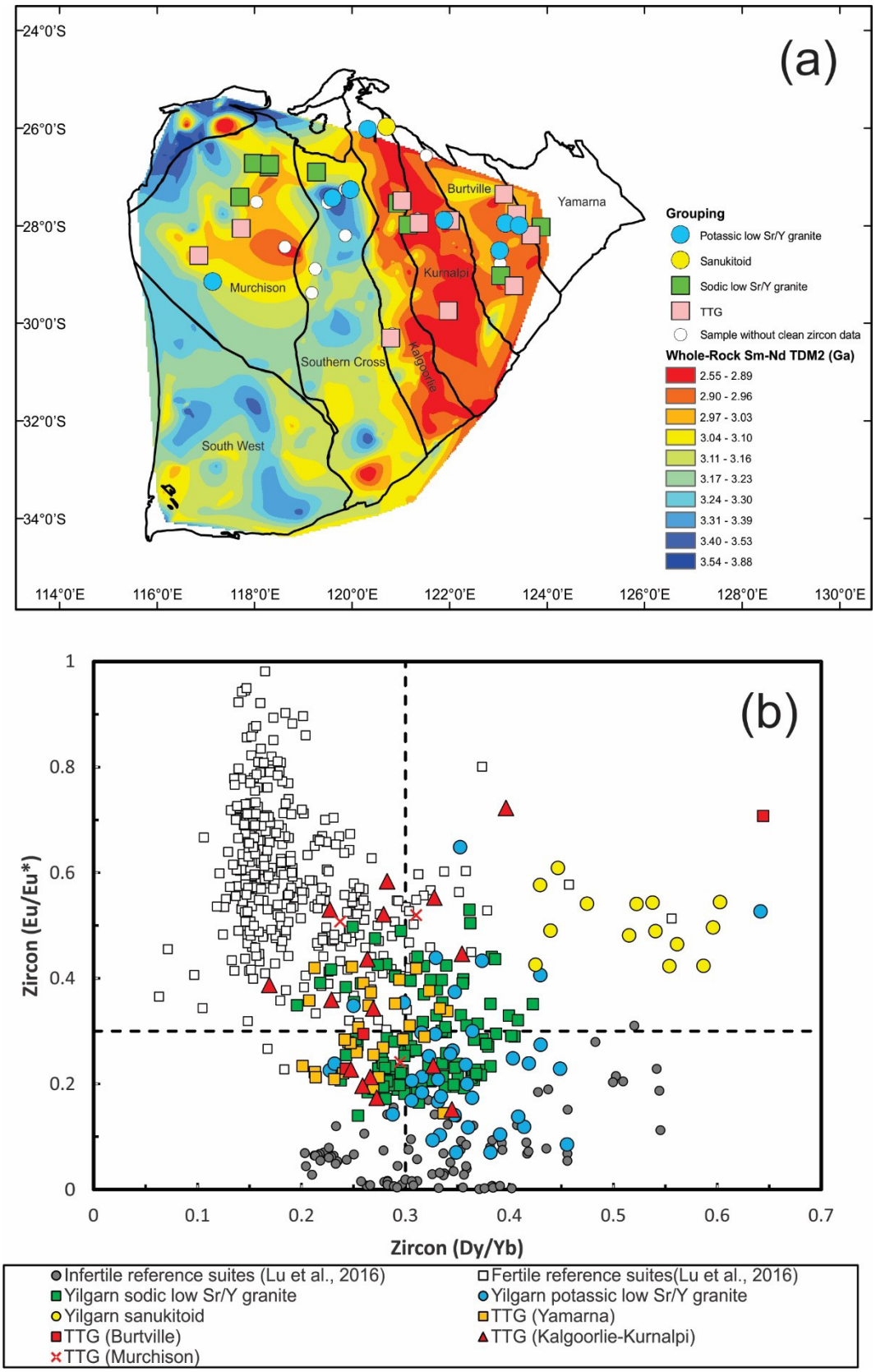

Figure 6. **Zircon compositions of Archean granites in the Yilgarn Craton: (a) zircon sample localities on top of the whole-rock Sm–Nd T_{DM}^2 contour map; (b) zircon Eu/Eu* vs Dy/Yb ratios for Archean granites compared with Phanerozoic infertile and fertile reference suites of Lu et al. (2016)**

Subduction dynamics, continental collision and some thoughts on the early Earth

by

L Moresi[1], A Beall[2], P Betts[3], K Cooper[4], and MS Miller[5]

In the modern Earth, processes such as accretion and continental collision are driven by the combined buoyancy forces of an entire length of subduction zone acting to overcome the resistance in the congested section (Moresi et al, 2014; Betts et al, 2015). This is a mechanism to amplify the typical stresses one might normally consider would be available to drive accretion and orogeny and this can be helpful in understanding the dynamics interaction of plate tectonics, mantle flow and continental deformation. See Figure 1 for an illustration.

It is interesting to consider how effective this mechanism would have been in the early Earth and consider if it would be a way to supply sufficient stress to construct a long-lived craton. Tectonic origins for the cratonic lithosphere have been favoured in recent discussions (e.g. Lee et al., 2011; McKenzie and Priestley, 2016) but there are reasons to suspect accretion and crustal thickening would have been more difficult under Archean conditions. We typically expect convective stresses to be lower for the early Earth when internal temperatures were higher and viscosities lower. Furthermore, the actual viability of subduction in the Archean Earth is still a subject of debate due to the need for thinner cold-boundary layers to 'outweigh' a thicker oceanic crust formed at high temperatures. Numerical models suggest subduction would have been thermally and mechanically viable in the Archean but slabs would have been weaker and more prone to breakoff (van Hunen and Moyen, 2012).

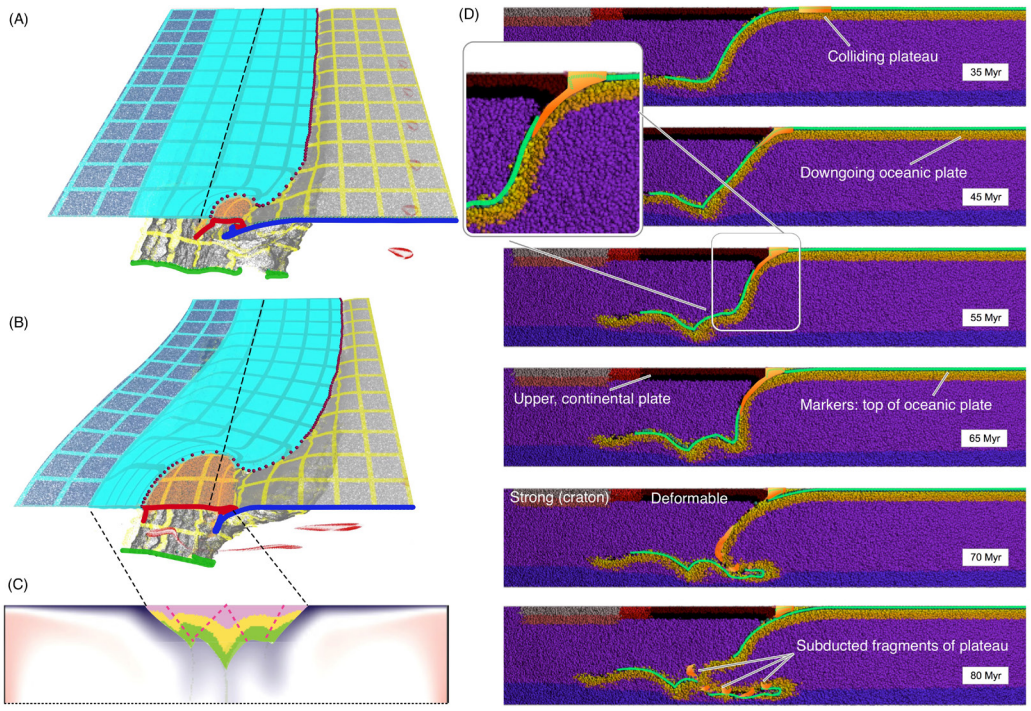

Figure 1. Simulations showing the collision of a continental fragment with an ocean-continent subduction zone. The buoyancy available to drive convergence and thickening of the overriding plate comes not only from the congested region of the plate boundary but from continued subduction in the unaffected. Even after slab breakoff, this mechanism can produce continued and significant convergence. Figure from Cooper et al. (2016)

1 School of Earth Sciences, University of Melbourne, Australia
2 School of Earth and Ocean Sciences, Cardiff University, UK
3 School of Earth Atmosphere and Environment, Monash University, Australia
4 School of the Environment, Washington State University, USA
5 Research School of Earth Sciences, Australian National University, Australia

How do we assemble cratonic lithosphere in the low-stress environment of the young Earth that is strong and resistant to tectonic recycling in the older Earth where higher stresses are available?

Recent work suggests that, very early in Earth's evolution, a heat-pipe mode of convection would have been favoured — this is a form of stagnant lid convection in which the internal heat is lost by magmatic pipes bypassing the upper boundary layer and depositing magma at or near the surface. A stagnant lid with the right combination of intrusive and extrusive heat-pipe magmatism, is potentially capable of satisfying the thermal and petrological constraints for the early Archean Earth. (e.g. Moore and Webb, 2013; Rozel et al., 2017). These models naturally become unstable with respect to mobile-lid convection models as the level of internal heat production decreases.

A possible resolution of this puzzle is to understand whether the transition phase between stagnant lid and a mobile lid or plate-tectonic style of convection is capable of building or assembling the cratonic lithosphere and not just destroying the stagnant lithosphere. The stresses during the collapse of the thick, stagnant lid can be significantly higher than the convective stresses in either the steady, stagnant lid or the mobile-lid convective regimes (Fig. 2B).

We discuss these models and compare the deep lithospheric structure with that which occurs when growth is driven by lateral accretion. This builds upon previous studies by Cooper and Miller (2013), Cooper et al (2016) and Beall (2017).

References

Beall, APJ 2017, Gravitational Instabilities Beneath Continents, PhD, University of Melbourne.

Betts, PG, Moresi, LN, Miller, MS and Willis, D 2015, Geodynamics of oceanic plateau and plume head accretion and their role in Phanerozoic orogenic systems of China, Geoscience Frontiers, 6(1), p. 49–59, doi:10.1016/j.gsf.2014.07.002.

Cooper, CM and Miller, MS 2014, Craton formation: Internal structure inherited from closing of the early oceans. Lithosphere 6**,** p. 35–42.

Cooper, C. M., M. S. Miller, and L. Moresi (2016), The structural evolution of the deep continental lithosphere, Tectonophysics, 695, p. 1–89, doi:10.1016/j.tecto.2016.12.004.

van Hunen, J and Moyen, JF 2012, Archean Subduction: Fact or Fiction? Annu. Rev. Earth Planet. Sci., 40(1), p. 195–219, doi:10.1146/annurev-earth-042711-105255.

Lee, CT, Luffi, P and Chin, EJ 2011, Building and destroying continental mantle, Annual Review of Earth and Planetary Sciences, doi:10.1146/annurev-earth-040610-133505.

McKenzie, D and Priestley, K 2016, Speculations on the formation of cratons and cratonic basins, Earth and Planetary Science Letters, 435(C), p. 94–104, doi:10.1016/j.epsl.2015.12.010.

Moore, WB, Moore, WB and Webb, AAG 2013, Heat-pipe Earth, Nature, 501(7468), p. 501–505, doi:10.1038/nature12473.

Moresi, L, Betts, PG, Miller, MS and Cayley, RA 2014, Dynamics of continental accretion, Nature, 508(7495), p. 245–248, doi:10.1038/nature13033.

Rozel, AB, Golabek, GJ, Jain, C, Tackley, PJ and Gerya, TV 2017, Continental crust formation on early Earth controlled by intrusive magmatism, Nature, p. 1–12, doi:10.1038/nature22042.

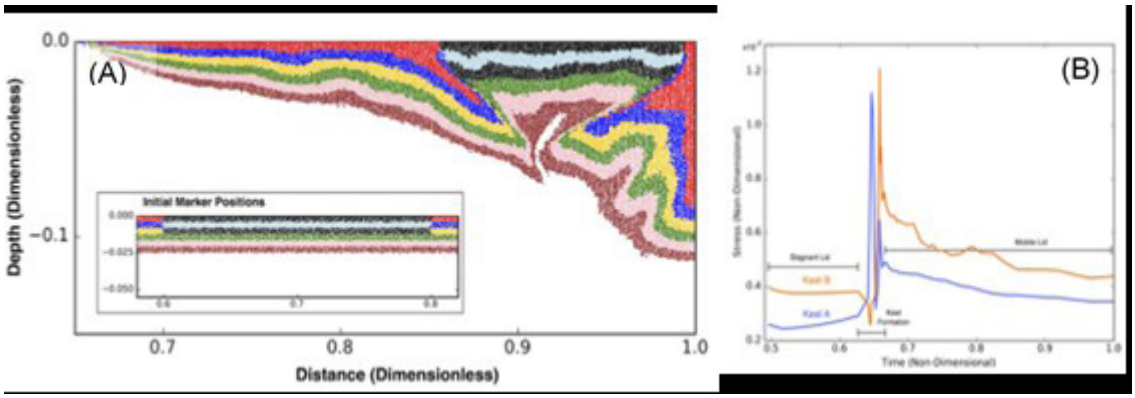

Figure 2. A collapsing stagnant lid produces an over-thickened, folded structure from an initially thin layer within the upper part of the stagnant lid that is strong enough to resist subsequent convective stresses. An anomalously strong region arbitrarily embedded within the stagnant lid can survive the lid collapse with very little deformation at the surface but with underthrusting and stacking of the lower crust and the mantle lithosphere

Stability of LLSVPs through deep geological time: fact or fiction?

by

RD Müller

Introduction

Coupled plate tectonic–geodynamic models for post-Pangea times have been developed for about two decades, and are relatively mature. They have led to a good and generally agreed-upon understanding that the large-scale mantle structure observed today, using seismic tomography, is the consequence of the post-Pangea subduction history, leading to a degree-2 mantle structure of two large upwellings, associated with large low shear velocity provinces (LLSVPs) in areas away from subduction in the last 250–200 Ma (Bower et al., 2015; Bunge et al., 1997; Zhong and Rudolph, 2015). This result implies that the current location and shape of LLSVPs, driving large-scale thermal upwellings, is a consequence of the post-Pangea subduction history (Flament et al., 2017). However, long-term stability of LLSVPs throughout most of the Phanerozoic has been proposed by reconstructing large igneous provinces and kimberlites relative to LLSVP edges, assumed to be the so-called plume generation zones, where deep mantle plumes originate (Torsvik et al., 2010). This inferred association has been used to then orient the longitudinal positions of plates through time (which are ill-constrained by paleomagnetic data) such that they comply with the assumption of lining up large igneous provinces (LIP) and kimberlites with plume generation zones assumed to be stable through time (Torsvik et al., 2014). However, there is a circularity in this line of arguments. One recent proposal for the origin of LLSVPs is that they represent chemically distinct regions that reflect mineralogically-distinct domains; such LLSVPs may have remained stable for most of the Earth's evolution (Ballmer et al., 2017). However, limitations of this recent 2D numerical model are that the proposed locations of these primordial LLSVP domains are arbitrary relative to the Earth's spin axis and the core-mantle boundary, and it is an open question to what extent 2D box models are useful to evaluate the complex thermal and chemical evolution of the mantle and its boundary layers.

Rules governing absolute plate motions

Reconstruction absolute plate motions is at the centre of the LLSVP stability discussion, as it has been suggested that following the assumption of an alignment of LIP and kimberlites is the only way to constrain the longitudinal position of plates through time (Torsvik et al., 2008), which is otherwise ill-constrained. If the assumed long-term stability of LLSVPs is used to orient the positions of plates through time, as has been done in some published plate models, independently testing the idea of LLSVP stability via geodynamic modelling with imposed plate motions is impossible, and fully dynamic models to answer these questions are still under development. There are alternative ways to orient the plates longitudinally through time, by utilising limits of net rotation of all plates and the migration speed of subduction zones through time. Recently developed tectonic models with continuously evolving plate boundaries (Müller et al., 2016) now provide us with an opportunity to analyse, and optimise, absolute plate motions such that they comply with 'rules of geodynamics' — this advance has been made possible by functionality available in the GPlates2.0 software, and associated development of optimization algorithms (Tetley et al., 2015). Plate reconstructions with continuously closing boundaries have been used to show that absolute continental plate speeds are largely limited to less than 10 cm/yr, with rare exceptions, and it has been shown that both the percentage of Proterozoic regions as well as cratonic area as part of any continent impedes plate motions, i.e. large, old continents with substantial lithospheric keels do not move very fast (Zahirovic et al., 2015). Global average continental RMS speeds, as a proxy for net plate rotation, in these models are below 5 cm/yr in the last 200 Ma, with a mean around 3 cm/yr (Zahirovic et al., 2015). Such rules can be used to optimise plate models (Merdith et al., 2017b), which in turn can be used to test LLSVP stability.

Another useful criterion is the migration speed of subduction zones. Subduction zone migration is known to be characterized in recent geological time by slow retreat between 0 and 3 cm/yr, ranging from relatively fast trench retreat of 5 cm/yr to rare, slow trench advance of up to 2 cm/yr (Williams et al., 2015). Subduction zone migration in published plate reconstructions with evolving plate boundary topologies back into the Paleozoic to 410 Ma (Domeier and Torsvik, 2014; Matthews et al., 2016) complies with a relatively constant mean rate of subduction zone migration, albeit with a increased standard deviation for pre-Pangea times. For times before the assembly of Pangea, many subduction zones cross over the present-day location of LLSVPs. The same holds for a recently published reconstruction back to 1 billion years (Merdith et al., 2017a). This opens the question whether these reconstructions are fundamentally wrong, or whether the assumption of LLSVP stability is fundamentally flawed, as it is unlikely that LLSVPs retained their current shape while the geometry of the global network of subduction zones was profoundly different from their post-Pangea arrangement.

Geodynamic modelling

We have used geodynamic models with imposed plate motions and subduction histories to model the evolution of LLSVPs for the last 230 million years, testing different plate reconstructions and mantle initial conditions. We use thermochemical models of the Earth's mantle under the extended-Boussinesq approximation (Christensen and Yuen, 1985) in a spherical shell. The equations for the conservation of mass, momentum, and energy are cast as a finite element problem and solved using CitcomS (Zhong and Rudolph, 2015), which has been modified to allow for progressive assimilation of surface plate motion and inferred slab material based on global plate reconstructions (Bower et al., 2015). The full spherical shell is composed of 12 parts, each subdivided into 128 3 128 3 64 elements, amounting to a total of 12.6 million elements. The mesh is refined radially to provide a vertical resolution of 15 and 27 km near the top and bottom boundary layers, respectively. The minimum radial resolution in the midmantle is 109 km. The lateral resolution is 50 km and 28 km at the surface and the core-mantle boundary (CMB), respectively. The petrological estimates of plume excess temperature (difference in temperature between plumes and ambient mantle) range between 200 and 300 K. At the CMB, we apply an isothermal and free-slip boundary condition, while at the surface we impose an isothermal and kinematic boundary condition, and use piecewise Arrhenius laws to describe the variation of viscosity with temperature, depth, and composition in the upper and lower mantle (Hassan et al., 2015). In these models, descending slab material generates large-scale upwellings and plume generation zones, which are well-matched to locations and geometries of tomographically mapped LLSVPs. These models confirm that LLSVP edges act as plume generation zones and nucleate deep mantle plumes, in those broad regions where they are observed today. Time-dependent subduction causes instabilities in the mantle basal flow regime, and thus generates plumes (Fig. 1), but also forces LLSVP boundaries to migrate if there is sufficient volume and proximity to this subducted material (Fig. 2).

As a consequence, LLSVP boundaries in the proximity of migrating subduction zones are more prone to deformation than those distal to subduction zones. We find that median rates of LLSVP boundary migration are between 8.8 and 11 km/my for the African LLSVP and between 10.5 and 17.1 km/my for the Pacific LLSVP. We have previously related the time-dependent migration of the Pacific LLSVP (fast before 50 Ma and slowing down afterwards) to the bend in the Hawaii-Emperor chain (Hassan et al., 2016), keeping in mind that a portion of this bend also reflects a global plate motion event. Our estimated LLSVP migration rates raise doubts as to the fixity of LLSVPs and plume generation zones over long geological time periods. However, it is noteworthy that in our models the western wall of the African LLSVP has remained relatively stable over time, within 1500 km of the location at 180 Ma up until the present day. The southern African LLSVP wall is equivalently stable. This result is significant in that the majority of the observations (LIP/kimberlites) pointing to African LLSVP stability are associated with the western and southern African LLSVP edges (Torsvik et al., 2010). It is thus possible that notions of LLSVP edge stability versus instability since the breakup of Pangea are dependent on which region is being investigated, that 'not all LLSVP edges are equal' and that some portions of LLSVPs are much more stable than others.

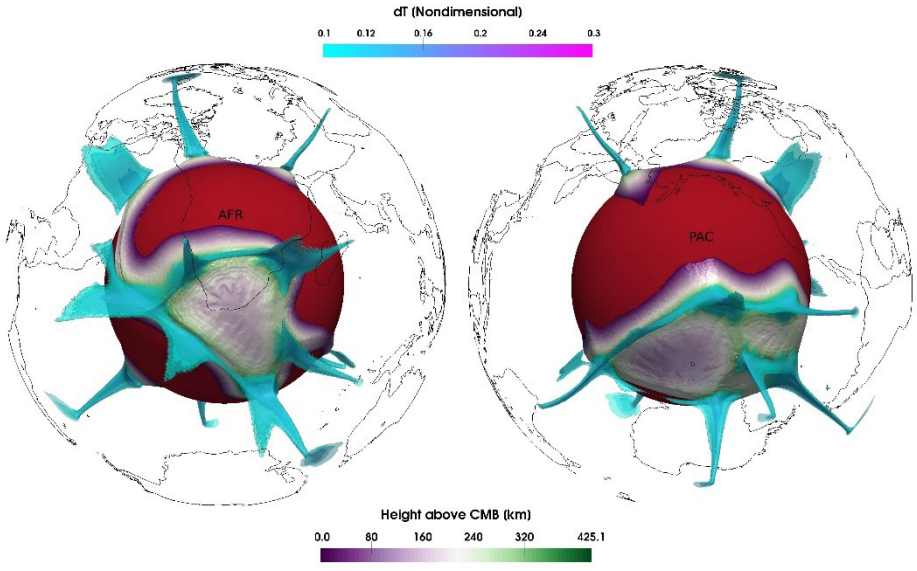

Figure 1. **3D view of a geodynamic model output centred on the African LLSVP (left) and the Pacific LLSVP (right). Plumes are generated fully dynamically in these models and generally form in regions where plumes are observed (see Hassan et al. (2016) for a detailed statistical analysis). The temperature field above mantle layer averages, dT, is plotted as isosurfaces in the range 0.1 – 0.3, delineating LLSVPs, plume generation zones along their edges and plume conduits at present-day for model M5 (Hassan et al., 2016). Topography of the 75% chemical concentration isosurface, above the core-mantle boundary, is also shown for the same model at present day. Coastlines are shown for geographical reference**

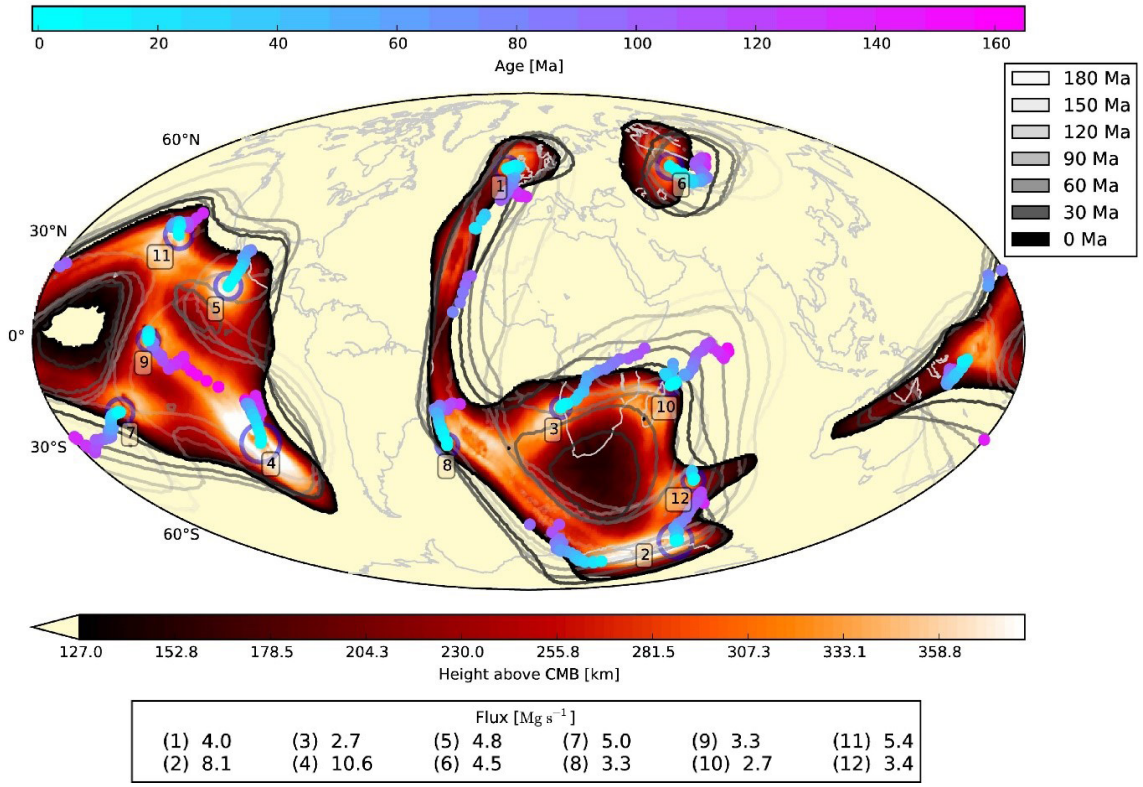

Figure 2. Topography of the 75% chemical concentration isosurface, above the CMB at present day for model M5 (Hassan et al., 2016). Contour lines show the evolution of the areal extent of the 75% chemical concentration isosurface since 180 Ma to present day. Age-coded model plume paths at a depth of 350 km are shown in the foreground and plumes at present-day are numbered. Radii of blue circles encircling present-day plumes are representative of their respective buoyancy fluxes, which are listed in the frame to the right. Note overall substantial migration of LLSVP boundaries through time, as well as the lack of significant migration along the western and southern boundaries of the African LLSVP. These boundaries are quite distal from subduction zones, while the northeastern boundary of the African LLSVP is proximal to Tehyan subduction slabs and predicted to be 'pushed' to the southwest by the significant Tehtyan slab volumes descending in the deep mantle in this region, spreading above the core-mantle boundary and pushing the African LLSVP edge towards the southwest

References

Ballmer, MD, Houser, C, Hernlund, JW, Wentzcovitch, RM and Hirose, K 2017, Persistence of strong silica-enriched domains in the Earth's lower mantle: Nature Geoscience 10, p. 236–240.

Bower, DJ, Gurnis, M and Flament, N 2015, Assimilating lithosphere and slab history in 4-D Earth models: Phys. Earth Planet. Inter. 238, p. 8–22.

Bunge, H-P, Richards, MA, Lithgow-Bertelloni, C, Baumgardner, JR, Grand, SP and Romanowicz, BA 1997, Geodynamic Earth models: Plate motion constraints, relevant timescales, and comparison with seismic tomography, submitted.

Christensen, UR and Yuen, DA 1985, Layered convection induced by phase transitions. Journal of Geophysical Research: Solid Earth 90, p. 10291–10300.

Domeier, M and Torsvik, TH 2014, Plate tectonics in the late Paleozoic: Geosci. Front. 5, p. 303–350.

Flament, N, Williams, S, Müller, R, Gurnis, M and Bower, DJ 2017, Origin and evolution of the deep thermochemical structure beneath Eurasia. Nature communications 8, 14164.

Hassan, R, Flament, N, Gurnis, M, Bower, DJ and Müller, D 2015, Provenance of plumes in global convection models. Geochem., Geophys., Geosyst. 16, p. 1465–1489.

Hassan, R, Müller, RD, Gurnis, M, Williams, SE and Flament, N 2016, A rapid burst in hotspot motion through the interaction of tectonics and deep mantle flow. Nature 533, p. 239–242.

Matthews, KJ, Maloney, KT, Zahirovic, S, Williams, SE, Seton, M and Müller, RD 2016, Global plate boundary evolution and kinematics since the late Paleozoic: Global and Planetary Change 146, p. 226–250.

Merdith, AS, Collins, AS, Williams, SE, Pisarevsky, S, Foden, JF, Archibald, D, Blades, ML, Alessio, BL, Armistead, S and Plavsa, D 2017a, A full-plate global reconstruction of the Neoproterozoic. Gondwana Research.

Merdith, AS, Williams, SE, Müller, RD and Collins, AS 2017b, Kinematic constraints on the Rodinia-Gondwana transition: Precambrian Research.

Müller, RD, Seton, M, Zahirovic, S, Williams, SE, Matthews, KJ, Wright, NM, Shephard, GE, Maloney, K, Barnett-Moore, N, Hosseinpour, M, Bower, DJ and Cannon, J 2016, Ocean Basin Evolution and Global-Scale Plate Reorganization Events Since Pangea Breakup. Annu. Rev. Earth Planet. Sci. 44.

Tetley, M, Williams, S, Hardy, S and Müller, D 2015, The Application of Optimisation Methods to Constrain Absolute Plate Motions, AGU Fall Meeting Abstracts.

Torsvik, TH, Burke, K, Steinberger, B, Webb, SJ and Ashwal, LD 2010, Diamonds sampled by plumes from the core-mantle boundary: Nature 466, p. 352–355.

Torsvik, TH, Steinberger, B, Cocks, LRM and Burke, K 2008, Longitude: linking Earth's ancient surface to its deep interior: Earth and Planetary Science Letters 276, p. 273–282.

Torsvik, TH, van der Voo, R, Doubrovine, PV, Burke, K, Steinberger, B, Ashwal, LD, Trønnes, RG, Webb, SJ and Bull, AL 2014, Deep mantle structure as a reference frame for movements in and on the Earth: Proc. Natl. Acad. Sci. U.S.A. 111, p. 8735–8740.

Williams, S, Flament, N, Müller, RD and Butterworth, N 2015, Absolute plate motions since 130 Ma constrained by subduction zone kinematics: Earth and Planetary Science Letters 418, p. 66–77.

Zahirovic, S, Müller, RD, Seton, M and Flament, N 2015, Tectonic speed limits from plate kinematic reconstructions. Earth and Planetary Science Letters 418, p. 40–52.

Zhong, S and Rudolph, ML 2015, On the temporal evolution of long-wavelength mantle structure of the Earth since the early Paleozoic: Geochem., Geophys., Geosyst. 16, p. 1599–1615.

Deep mantle processes: rheology, mixing, and how it's changed

by

C O'Neill*

Introduction

The mantle is a mixture of different mineral components, which may have very different rheological properties, which can influence interior dynamics. For instance, lower mantle domains enriched in bridgmanite, compared to ferripericlase, have been suggested to have significantly higher viscosity (up to ~1000 times), and may represent ancient unmixed mantle domains. Such mineralogical differences are reflected in bulk compositional measures such as Mg/Si ratios, which are highly variable in the meteorite population today. Furthermore, the mineralogical makeup is related to oxygen fugacity, which has been shown to affect mantle rheology, both at lithospheric levels, and in the deeper mantle. In this presentation I discuss the implications of these observations to mantle convection models of an evolving Earth. In particular, I explore how mixing in the mantle may have varied from the Hadean to the present, and how variable mantle mineral makeup, and fO_2, complicate the story.

Results

The model shown in Figure 1 was performed using the community code Aspect (aspect.dealii.org) with a distinct passive compositional field, which was modelled with both compositional field and particles. The model has diffusion creep in the lower mantle, and diffusion, dislocation, Peierls and yielding in the upper mantle/lithosphere. The model also includes evolving heat sources, and an evolving core-boundary condition.

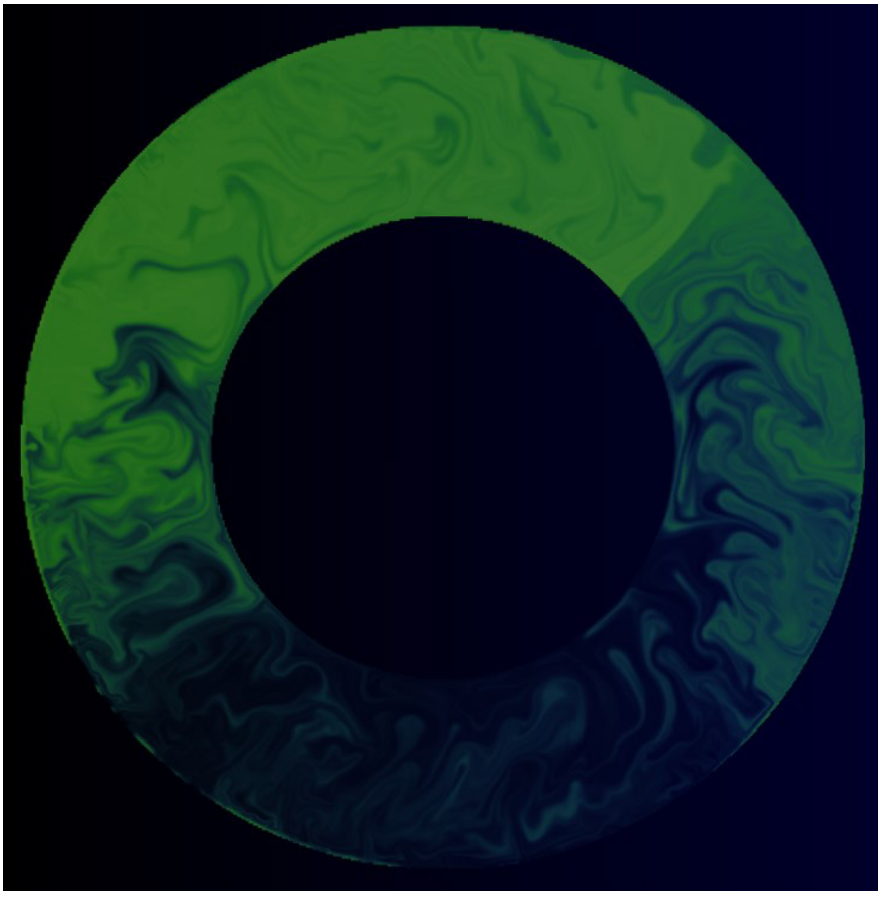

Figure 1. **Snapshot of an aspect convection model in a stagnant lid regime after 800 Myr of evolution. An initially offset compositional field still has not fully mixed laterally after this time**

* CCFS and Macquarie Planetary Research Centre, Macquarie University, NSW 2109

Structure and evolution of the continents

by

K Priestley*, D McKenzie* and T Ho*

Determining upper-mantle thermal variations

Tomographic images that are derived from the inversion of more than seven million, multi-mode surface waveforms provide high resolution images of the Earth's upper -mantle shear-wave (Vs) velocity structure to transition zone depths. Upper-mantle Vs is principally controlled by temperature and unknown grain size. Because of the grain size dependence, it is not straightforward to convert the shear-wave velocity to temperature using parameters determined from laboratory experiments. However, geophysical estimates of temperature within the oceanic lithosphere and petrological estimates from garnet peridotite nodules provide sufficient constraints to determine a Vs(P,T) relationship which is based on geophysical and petrological observations alone. This empirically-derived Vs(P,T) relationship is then used to estimate the unrelaxed shear modulus and its derivatives with respect to pressure and temperature, which agree reasonably with values from laboratory experiments. Relaxation occurs at high temperatures, causing the shear-wave velocity to depend on frequency. This behaviour is parametrised using a viscosity to obtain a Maxwell relaxation time. The relaxation behaviour is described using a dimensionless frequency, which depends on an activation energy E and volume Va . The values of E and Va obtained from the geophysical models agree well with those from laboratory experiments on high temperature creep (Priestley and McKenzie, 2006, 2013). We use the Vs(P,T) relationship to map the seismic velocity of the upper mantle as a function of depth into temperature as a function of depth. The resulting lateral variation in upper-mantle temperature agrees well with independent temperature estimates from the composition of intraplate basalts.

Lateral variation in lithospheric thickness

We use the lateral changes in temperature gradient (from advecting to conducting) to determine lateral variations in the depth of the base of the lithosphere (Fig. 1).

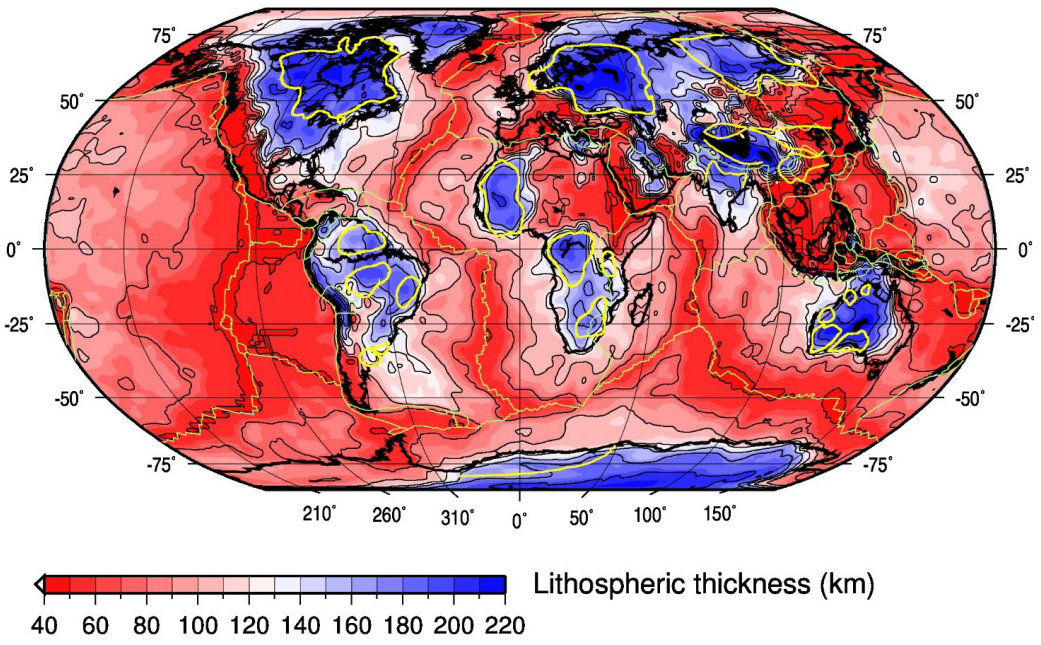

Figure 1. Global lithospheric thickness map based on an update of the surface wave tomography model of Priestley et al. (2013)

* Bullard Laboratories of the Department of Earth Sciences, University of Cambridge, Madingley Rise, Madingley Road, Cambridge UK

Extensive regions of thick lithosphere underlie some, but not all, cratons. With the exception of the Sino-Korean Craton, the regions of Archean crust are underlain by thickened lithosphere. However, the regions of thickened lithosphere in some cases extend for a considerable distance outside the region of the surface-mapped Archean rocks. For example, the thickened lithosphere that underlies the Canadian Shield extends beneath a considerable area of North America. Some tectonically-active regions are underlain by thick lithosphere. Partly because of the limited correspondence between the surface manifestation of the cratons and the regions of thick lithosphere, and partly because seismology provides no age control, we prefer to refer to continuous regions of thick lithosphere as 'cores' rather than as cratons. The strength of the cores resides in the dry crust, which is insulated from the hot convecting mantle by the thick buoyant lithosphere. The structure of the lithospheric cores exercises a strong control on tectonics. The most surprising feature of our lithospheric model is the presence of thick lithosphere beneath Tibet and Iran.

Evolution of the continental lithosphere

Surface wave tomography can also map seismic anisotropy (Ho et al, 2018). Shearing beneath oceanic plates causes horizontally-polarized shear waves to travel faster than those that are vertically polarized; however, the opposite is true beneath cratons (Fig. 2).

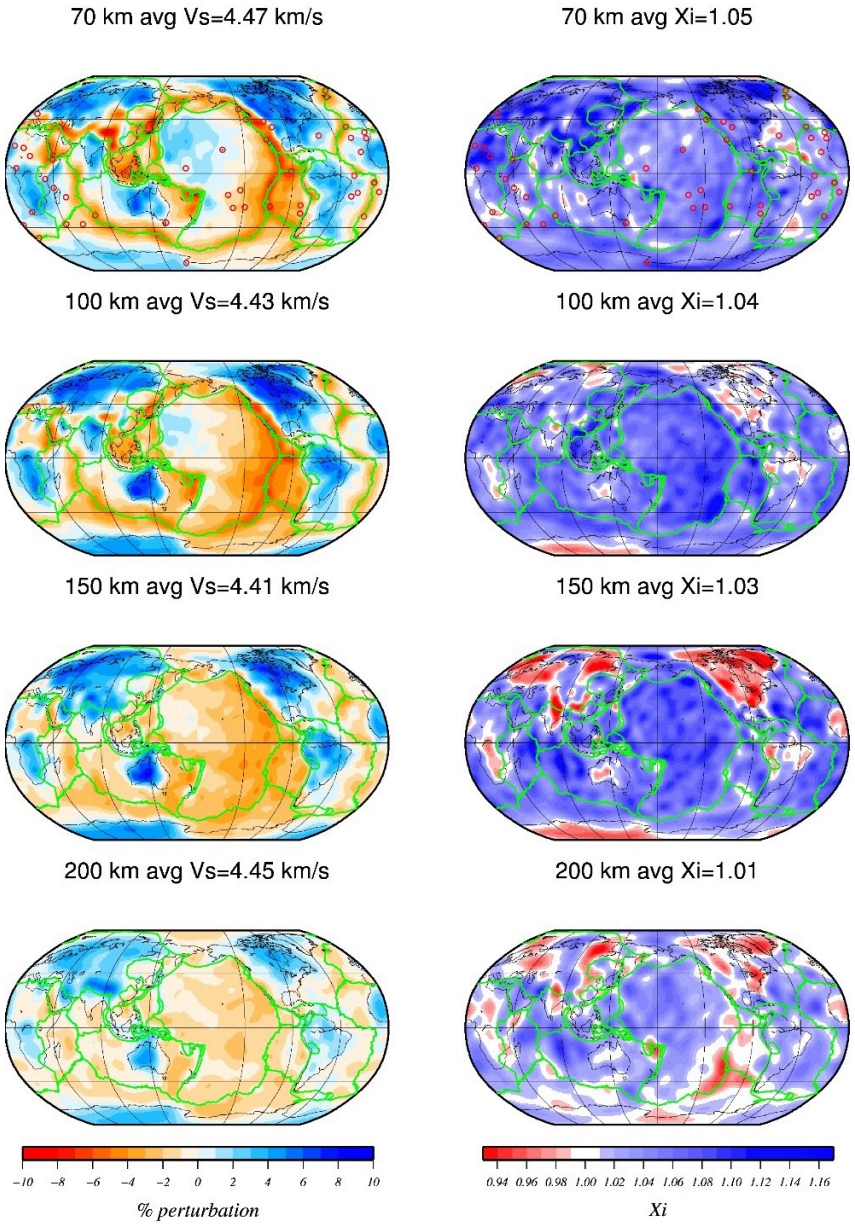

Figure 2. Horizontal depth slices through the radial anisotropy model of Ho et al. (2018). The left column displays the Voigt average isotropic structure and the right column displays the radially anisotropic parameter X. The depth and average value of Vs or X is given above each map. The same color scale is used for all X maps but note the change in color scale with depth for the \vs\ maps. Open red circles on the 70-km depth map denote hot spot locations. White regions are at or below the 1+/–0.01 and therefore below the resolution level

This anisotropic structure beneath the cratons is consistent with craton formation by shortening, and is therefore in agreement with geochemical arguments (Priestley et al, 2018). Surface wave tomography is also relevant to the question of whether cratons are deformed by continental tectonics and whether cratonic roots always move with the overlying crust. Reconstruction of Pangea (Fig. 3) shows that thick lithosphere formed a contiguous arc before Pangea broke up, which thus requires cratonic deformation to have occurred during the assembly of Pangea (McKenzie et al, 2015).

The present lithospheric thickness beneath northeast China and Peninsular India is now less than it was in the early Phanerozoic. Northeast China has since undergone extensive stretching but India has not. Surface wave tomography shows that Tibetan and Iranian Plateaus which are now being shortened, are presently underlain by lithosphere of similar thickness to that existing beneath cratons (Fig.1). Both the elevation and lithospheric thickness of these plateaus can result from pure shear shortening of normal thickness continental lithosphere by about a factor of two. The resulting thermal evolution of the crust and lithosphere is dominated by radioactive decay in the crust which raises the temperature of the lower part of the crust and of the upper part of the lithosphere to above their solidus temperatures, generating granites and small volumes of mafic alkaline rocks from beneath the Moho, as well as generating high temperature metamorphic assemblages in the crust. Thermal models of this process show that they can match the P and T estimates determined from metamorphic xenoliths and can also match the compositions of the alkaline rocks from the region. The Tibetan Core now has a thickness of 250–300 km, and has not been thinned by delamination. If the upper half of the Tibetan crust is removed by erosion (Fig. 4), the resulting velocity structure will be similar to that of cores whose surface is now at sea level, many of which were formed in the Archean (McKenzie and Priestley, 2008, 2016).

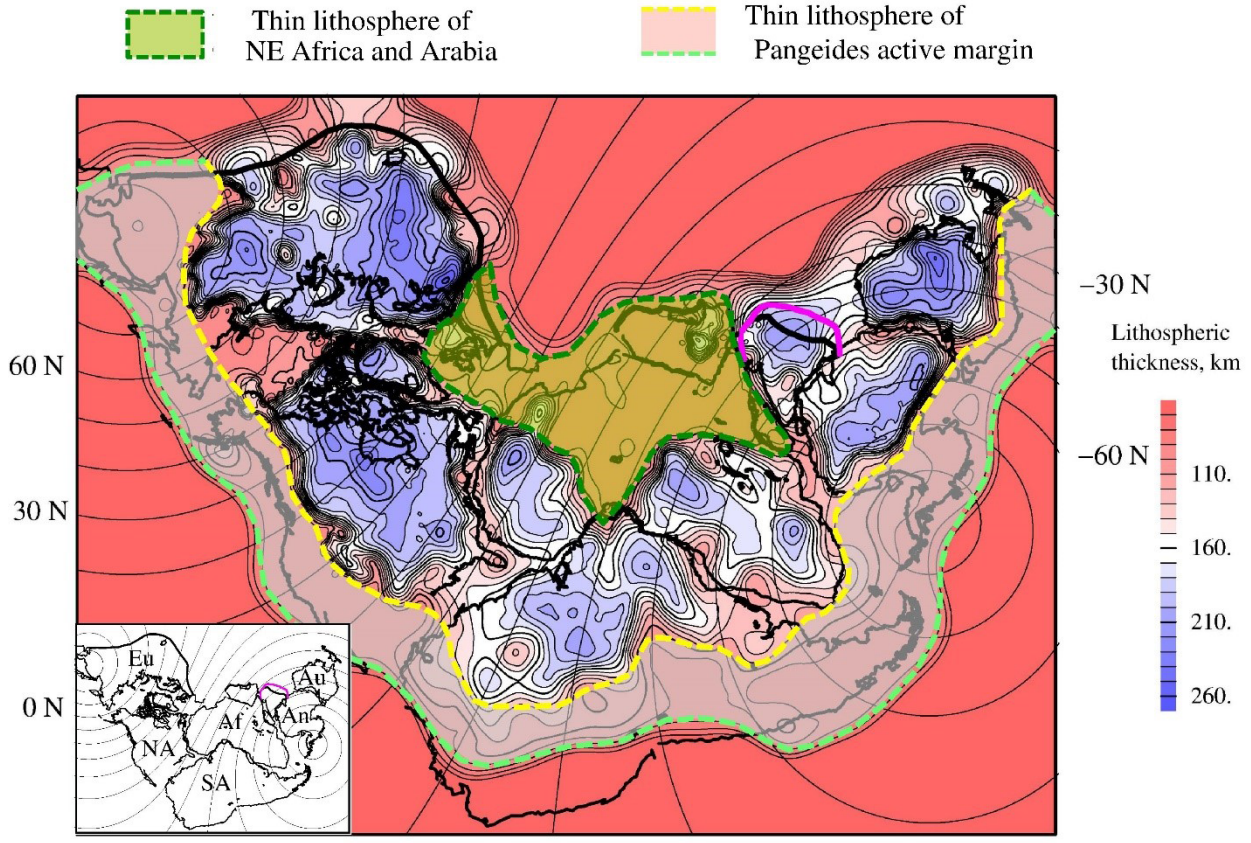

Figure 3. **Pangea reconstruction. Thick black and magenta lines show northern boundaries of India and Arabia and southern boundary of Eurasian craton. Dashed light green line marks outer margin of Pangeides active margin. Dashed yellow line shows approximate boundary between active margin and arc of thick lithosphere. Dashed dark green line outlines area underlain by thinner lithosphere that now underlies North Africa, Arabia, and western Europe. Inset shows same reconstruction without any lithospheric thickness contours. Abbreviations: NA, North America; Eu, Eurasia; SA, South America; Af, Africa; An, Antarctica; Au, Australia. Oblique Mercator projection with axis 30°N, 80°E**

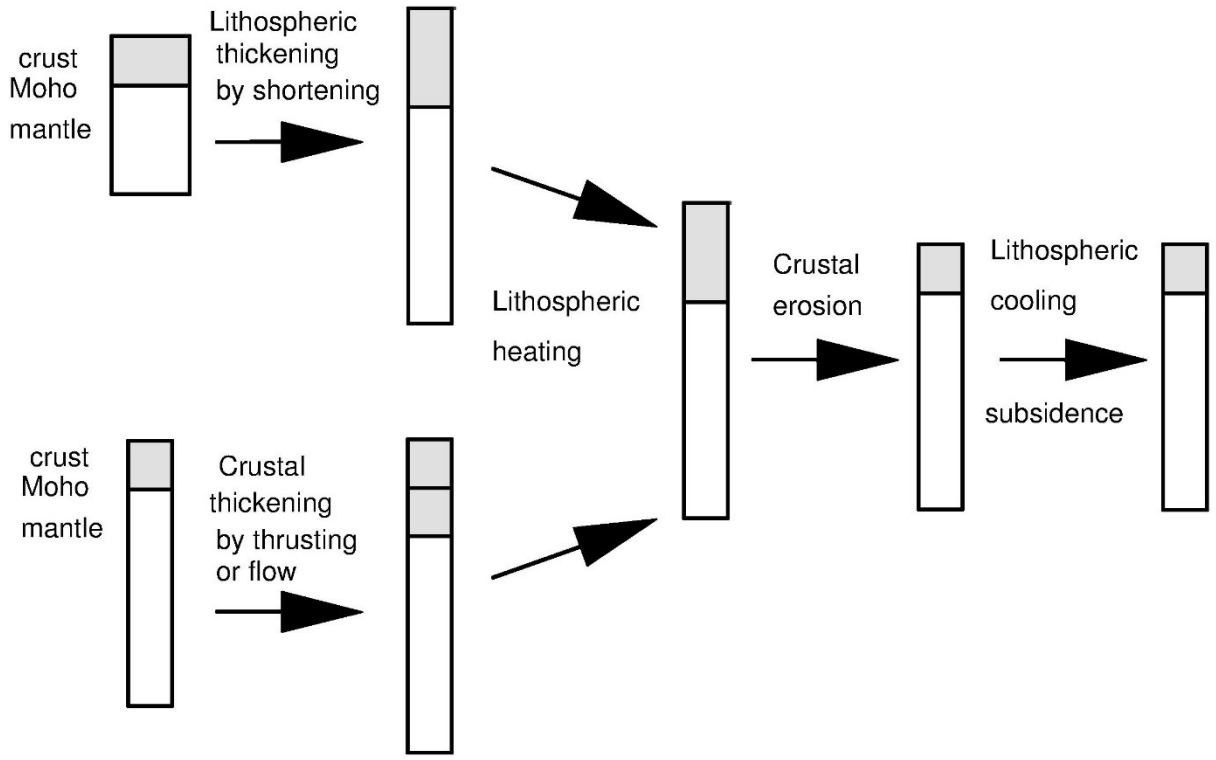

Figure 4. Sketch of two models used to produce thick crust and lithosphere, either by pure shear or by superimposition of a thick crustal layer on an existing craton. Both are followed by erosion which can produce a cratonic basin

References

Ho, T, Priestley, K and Debayle, E 2018, A Global Radial Anisotropy model of the upper mantle from surface wave observations, Geophys. J. Int, submitted.

McKenzie, D and Priestley, K 2008, The influence of lithospheric thickness variations on continental evolution, Lithos, 102, p. 1–11, doi: 10.1016/j.lithos.2007.05.005.

McKenzie, D, Daly, MC and Priestley, K 2015, The lithospheric structure of Pangea, Geol., 43, p. 783–786, doi:10.1130/G36819.1.

McKenzie, D and Priestley, K 2016, Speculations on the formation of cratons and cratonic basins, Earth. Planet. Sci. Lett., 435, p. 94–104.

Priestley, K and McKenzie, D 2006, The thermal structure of the lithosphere from shear wave velocities, Earth. Planet. Sci. Lett., 244, p. 285–310.

Priestley, K and McKenzie, D 2013, The relationship between shear wave velocity, temperature, attenuation and viscosity in the shallow part of the mantle, Earth. Planet. Sci. Lett., 381, p. 78–91, doi.org/10.1016/j.epsl.2013.08.022.

Priestley, K, McKenzie, D and Ho, T 2018, Upper mantle radial anisotropy — a clue to craton formation, Geol., submitted.

Fluid- and melt-rock interaction enable intraplate orogeny

by

T Raimondo[1], M Hand[2], N Daczko[3], S Piazolo[3,4], and C Clark[5]

Very low stresses are typical of plate interiors, meaning that lithospheric-scale extreme rheological weakening is required to facilitate intraplate orogenesis. Yet the processes required for such weakening remain enigmatic. The intraplate Alice Springs Orogen, central Australia, is characterized by fluid- and melt-rock systems that systematically vary in their depth, structural style, sources and magnitude of rehydration and reworking. This offers a remarkable natural laboratory to investigate the contribution of metasomatic processes to intraplate orogenesis through space and time.

Three characteristic styles of fluid- or melt-rock interaction are identified across the eastern Alice Springs Orogen. Discrete metre-scale cataclastic faults in the northwestern Reynolds–Anmatjira Ranges progress into ten- to hundred metre-scale metasomatized shear zones at the southeastern margin of this terrane, associated with low $\delta^{18}O$ and δD values indicative of a meteoric fluid source. Continuing along strike to the southeast, these structures are succeeded by kilometre-scale schist belts transecting Paleoproterozoic granulites in the Strangways Metamorphic Complex, followed by a ~7500 km^2 zone of pervasive Paleozoic amphibolite facies retrogression and voluminous partial melting in the Harts Range and Entia Gneiss Complex further east. Strongly deformed outcrops of the basal sedimentary unit of the Amadeus Basin (Heavitree Quartzite) are preserved in these areas, and discrete shifts to elevated δ18O values suggest that shear zones of the Strangways Metamorphic Complex contain fluids sourced from its prograde dewatering. Similarly, ubiquitous pegmatites of the Harts Range may be derived from burial metamorphism of fertile supracrustal sediments of the Harts Range Group.

Intriguingly, despite being part of a laterally-continuous, anastomosing shear belt that forms the dominant structural network of the Alice Springs Orogen, the fluid- and melt-rock systems described above appear to be diachronous. Ages of deformation, metamorphism and igneous activity hit episodic peaks at c. 450, c. 420, c. 380, c. 360 and c. 330 Ma, spanning approximately 120 Myr of fluid-rock interaction and partial melting. P–T evolutions constrained by petrography, EPMA X-ray maps and calculated pseudosections also demonstrate multiple prograde thermal cycles across this interval, while field relationships indicate the reactivation of contractional structures by overprinting extensional ultramylonites, attesting to a prolonged and episodic history of metasomatism and deformation.

We explore the possibility that the fluid- and melt-rock interaction history of this intraplate orogenic event had a profound impact on its structural and metamorphic expression, and by inference the rheological response of the lithosphere. In particular, we suggest that the spatial and temporal evolution of Alice Springs shear zones may be linked to the availability of fluids and melt in the deep crust and their effects on lithospheric strength through processes such as hydration and reaction softening. Such processes facilitate extreme rheological weakening and explain the deep-seated mechanics of intraplate orogenesis. This interpretation is supported by the episodic temporal link between ages of deformation, metasomatism, igneous activity and sediment shed from the developing orogen. Far from being a purely local phenomenon, therefore, deep crustal fluid- and melt-rock interaction had a profound impact on the dynamics of basement reactivation, acting in concert with other factors such as regionally elevated heat production to critically reduce the long-term strength of intraplate lithosphere and provide impetus for large-scale reworking.

1 School of Natural and Built Environments, University of South Australia, GPO Box 2471, Adelaide SA 5001, Australia (tom.raimondo@unisa.edu.au)
2 School of Physical Sciences, University of Adelaide, Adelaide SA 5005, Australian
3 ARC Centre of Excellence for Core to Crust Fluid Systems and GEMOC, Department of Earth and Planetary Sciences, Macquarie University, Sydney NSW 2109, Australia
4 School of Earth and Environment, University of Leeds, Leeds LS2 9JT, UK
5 Department of Applied Geology, Curtin University, GPO Box U1987, Bentley, WA 6845, Australia

Migrating uplift subsidence in continental interiors due to convective delamination of mantle lithosphere

by

T Stern*

Coupled uplift and subsidence linked to a mantle instability has been identified in a number of continental settings. Examples include the uplift of the Sierra Nevada, USA (Jones et al., 2014) and subsidence of the adjacent Great Valley of California (Saleeby and Foster, 2004), the uplift of the Transantarctic Mountains and geographically linked Wilkes subglacial basin (ten Brink et al., 1997; Brenn et al., 2017), the Pannonian Basin and the Carpathian mountains (Fillerup et al., 2010; Houseman and Gemmer, 2007), and in western North Island (New Zealand) the north to south uplift and subsidence either side of the Taranaki-Ruapehu line (Dimech et al., 2017; Stern et al., 2013). A generalized summary of observations (Fig. 1) shows a mix of phenomena that are observed at some, but not necessarily all, of these regions. Our focus is on those regions where a migration of the uplift and subsidence can be identified in the geological record and a process of 'delamination' of mantle lithosphere can be inferred. The proposition is that delamination couples vertical stresses to the earth's surface creating a moving wave of subsidence and uplift in its wake (Fig. 1). While mantle instability due to uniform convergence and thickening is easily understood and discussed (Molnar and Houseman, 2004), work on instabilities created in an extensional or transtensional setting is not as well documented.

A key difference between instabilities created by uniform convergence and transtensional delamination is that the former removes no more than 50% of the mantle lid, and little if any lower crust (Molnar and Houseman, 2004); delamination, in contrast, can convectively remove both mantle lid and parts of the lower crust (Stern et al., 2013). Mantle instability processes that have the ability to remove lower crust are important as they provide a mechanism where the mafic lower continental crust can be recycled to the mantle so that the continental crust as whole can maintain an andesitic bulk composition through time (Rudnick, 1995). In some cases the removal of crust with a mantle instability have needed to propose eclogisation of the lower crust as a means of enhancing negative buoyancy (Jones et al., 2014). Although eclogite in the lower crust will aid delamination, by dint of its high density, our results show it is not necessary (Fig. 2).

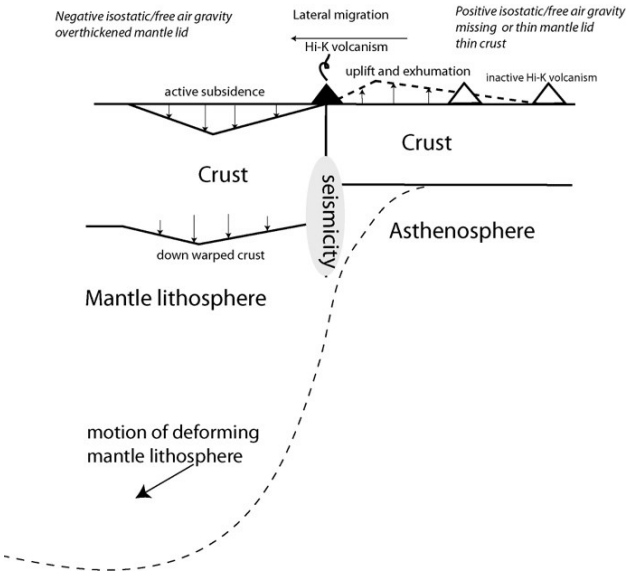

Figure 1. Cartoon for generalized manifestations for migration of an edge instability. Based on examples in Jones et al. (2014); Saleeby and Foster (2004); Houseman and Gemmer (2007); Dimech et al. (2017); Stern et al. (2013)

Our so-called edge-, or step-instability (Fig. 2A) is created by the differential buoyancy from the juxtaposition of lithospheric blocks of contrasting thicknesses (Fig. 2B). A sharp edge is created in the mantle lid that has the dimensionless height of d'= D/L (Fig. 2; Stern et al.,2013). In this model parameterisation is via ~5 dimensionless ratios that include η' and η", which are the ratios of crustal to mantle viscosity, and upper crustal to lower crustal viscosity, respectively. Dimensionless time (t') is defined to be = $t\ \Delta\rho g L/(2\eta_m)$, where t is time in seconds, $\Delta\rho$ is density contrast between the mantle lithosphere and the asthenosphere, L = lithosphere thickness and η_m is viscosity for the top of the mantle lid (Stern et al., 2013).

In the dimensionless variable approach a normalized set of curves describe the surface stress, and hence topography (Fig. 2C), that is created by a migrating instability. In continental regions such as western North Island and the Sierra Nevada, the time scale for instability development

* Victoria University of Wellington, Wellington, New Zealand

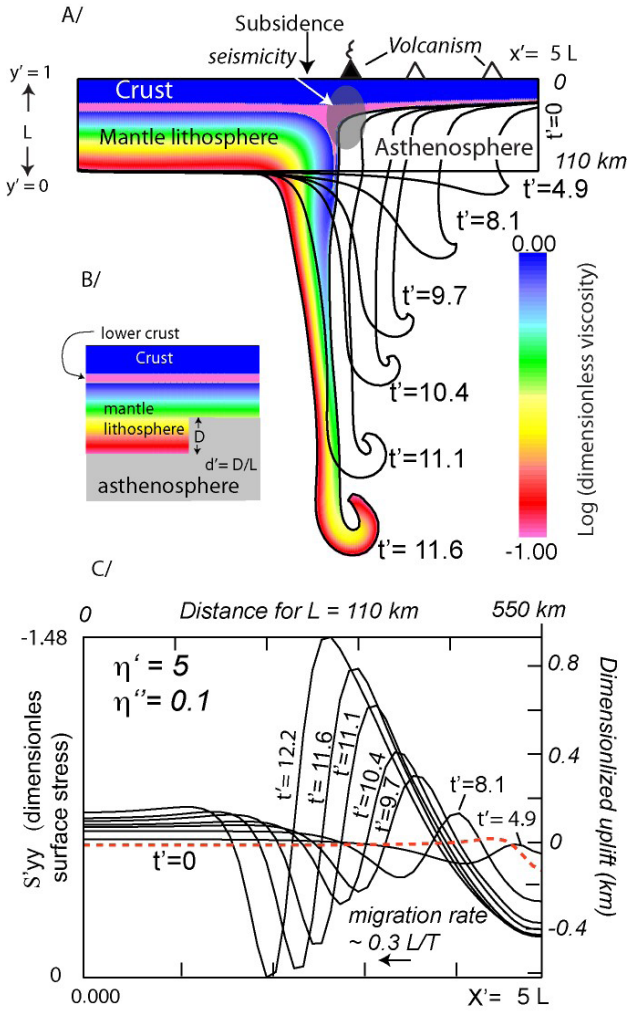

Figure 2. Edge-instability model developed from an initial edge (reference 8). Here we assume a layered, Newtonian, viscosity model (B). Plot 2C shows surface stress as a proxy for topography. The tight hand axis shows dimensionlized topography for the situation: L =110 km, t'= millions of years, ηm = 5 x10^{20} Pa s and Δρ = 30 kg/m^3

is of the order of 10^{-15} my and the lithospheric thickness(L) is ~100 km. The predicted topography curves of Figure 2C can then be dimensionlized such that t' values roughly represent time in millions of years and η_m is ~5 x10^{20} Pa s. Lateral migrations of ~300 km, and surface uplifts and subsidence of ~ 1 km are predicted (Fig. 2C). In the case of long-lived uplifts at stronger and older margins, like the Transantarctic Mountains, η_m ~10^{22} Pa s, L= 250 km and a time scale of ~60 my is implied. Another factor that can create the appearance of a sluggish instability is if d' <0.5 (Fig. 3). In this case there is a long gestation before the exponential phase of the instability growth. This may be useful to explain instability growth millions, to tens of millions, of years after a major transtensional episode.

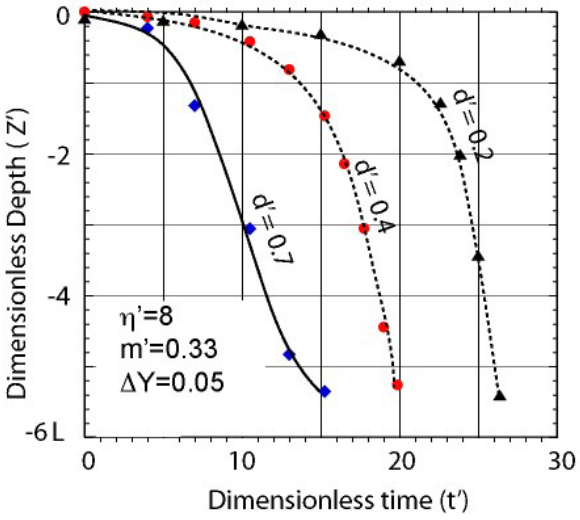

Figure 3. Vertical growth curves for an instability with η' = 8 and no lower crustal layer.The three curves show how varying d' can delay the onset of the instability for significant period of time. A initial condition is that the mantle lithosphere started with a 5% thickening of its bottom surface

References

Brenn, GR, Hansen, SE and Park, Y 2017, Variable thermal loading and flexural uplift along the Transantarctic Mountains, Antarctica: Geology v. 45, p. 463–466, doi:10.1130/g38784.1.

Dimech, JL, Stern, T and Lamb, S 2017, Mantle earthquakes, crustal structure, and gravitational instability beneath western North Island, New Zealand: Geology v. 45, p. 155–158, doi:10.1130/G38476.1.

Fillerup, MA, Knapp, JH, Knapp, CC and Raileanu, V 2010, Mantle earthquakes in the absence of subduction? Continental delamination in the Romanian Carpathians: Lithosphere 2, p. 333–340, doi:10.1130/l102.1.

Houseman, GA and Gemmer, L 2007, Intra-orogenic extension driven by gravitational instability: Carpathian-Pannonian orogeny: Geology 35, p. 1135–1138, doi:10.1130/G23993A.1.

Jones, CH et al. 2014, P-wave tomography of potential convective downwellings and their source regions, Sierra Nevada, California: Geosphere 10, p. 1–29, doi:10.1130/GES00961.1.

Molnar, P and Houseman, G 2004, The effects of buoyant crust on the gravitational instability of thickened mantle lithosphere at zones of intracontinental convergence: Geophys. J. Int. 158, p. 1134–1150.

Rudnick, R 1995, Making continental crust: Nature 378, p. 571–578.

Saleeby, J and Foster, Z 2004, Topographic response to mantle lithosphere removal in the southern Sierra Nevada region, California: Geology 32, p. 245–248.

Stern, T, Houseman, G, Salmon, M and Evans, L 2013, Instability of a lithospheric step beneath western North Island, New Zealand: Geology 41, p. 423–426, doi:10.1130/G34028.1.

ten Brink, US, Hackney, R, Bannister, S, Stern, TA and Makovsky, Y 1997, Uplift of the Transantarctic Mountains and the bedrock beneath the East Antarctic icecap: J. Geophys. Res. 102, p. 27603–27621.

From the crust to the core using recent advances in global seismology, global interferometry and mathematical geophysics

by

H Tkalčić*

Will the Earth's deep interior remain the final frontier of modern observational seismology? The answer to that question depends on several factors: 1) how efficient we will be in expanding spatial coverage of ray-paths through the deep Earth and making new observations; 2) how industrious we will be in developing ground-breaking methods and techniques applied to the existing waveform data; 3) how quickly we will achieve computational capacity to synthetize the seismic wavefield containing frequencies of up to several Hz; and 4) how successful we will be in integrating seismological observations with advances in geodynamics, mineral physics and mathematical geophysics.

I will present several recent developments pioneered by the ANU/RSES Seismology and Mathematical Geophysics group, and subsequent applications and discoveries from the crust to the core. Moving toward the Earth's centre, I will demonstrate the feasibility and advantage of utilizing reflection signals through an improved method of teleseismic *P* wave coda autocorrelation to unveil *P* and *S* wave reflection signals from the ice-rock interface and the Moho. I will then show how we utilized global interferometry to observe a number of reverberations from Earth's internal boundaries in the period range 15–50 seconds, which have never been seen before in traditional seismology. These newly observed seismic phases complement the existing empirical travel time curves, provide new constraints on Earth's internal structure and have significant potential to advance global seismology. Finally, I will demonstrate the use of Bayesian inversion methods in imaging of the lowermost mantle and the inner core. Recent studies have revealed increasingly complex structure of the top of the Earth's inner core and a possible link to heterogeneities in the lowermost mantle. The inner core boundary has proven to be more complex than just a dividing boundary between the liquid outer core and the solid inner core.

On one hand, the above advancements have been achieved due to the availability of new data. On the other hand, most of them are due to better computational facilities, the accessibility and introduction of new mathematical techniques, and a multidisciplinary approach. The Earth Sciences community has to take a unified front in aspiring to install new seismic stations and arrays in the most remote locations of the planet, from landmasses to the ocean bottom borehole seismometers at extreme geographic latitudes. While seismological probes corresponding to large earthquakes recorded on individual stations focus on the established ray-path corridors through the deep Earth, seismic arrays of different apertures provide invaluable new information. The RSES Seismology and Mathematical Geophysics group continues to be at the forefront of these efforts, with recent installations of spiral arrays in Queensland and Western Australia, and a proposed onshore–offshore array at the Macquarie Ridge Complex near the Macquarie island.

References

Pham T-S and Tkalčić, H 2017, On the feasibility and use of teleseismic P-wave coda autocorrelation for mapping shallow seismic discontinuities: J. Geophys. Res., p. 122, doi:10.1002/2017JB013975.

Sambridge, M, Bodin, T, Gallagher, K and Tkalčić, H 2013, Transdimensional inference in the geosciences, Phyl. Trans. R. Soc. A, p. 1–17, doi:10.1098/rsta.2011.0547.

Stipčević, J, Kennett, BLN and Tkalčić, H 2017, Simultaneous use of multiple seismic arrays: Geophys. J. Int., 209, p. 770–783, doi:10.1093/gji/ggx027.

Tkalčić, H, Young, MK, Muir, JB, Davies, R and Mattesini, M 2015, Strong, multi-scale heterogeneity in Earth's lowermost mantle: Scientific Reports, 5, doi:10.1038/srep18416.

Tkalčić, H, 2015, Complex inner core of the Earth: The last frontier of global seismology: Reviews of Geophysics, 53/1, p. 59–94, doi:10.1002/2014RG000469.

Tkalčić, H 2017, The Earth's inner Core Revealed by Observational Seismology: Cambridge University Press, Cambridge, UK, doi:10.1017/9781139583954.

* Research School of Earth Sciences, The Australian National University, ACT 2600

Poster abstracts

Deciphering the fluid evolution of the Nimbus Ag–Zn–(Au) VHMS deposit, Yilgarn Craton, Western Australia

by

S Caruso[1], RJ Baumgartner[1], ML Fiorentini[1] , SP Hollis[2], C LaFlamme[1], and L Martin[3]

In the Yilgarn Craton, volcanic-hosted massive sulfide (VMS) mineralization is mainly restricted to zones of thin juvenile crust as recently identified by regional (Nd, Pb and Hf) isotope studies (Huston et al., 2014; Mole et al. 2014). Interpreted as Archean paleo-rift zones, one such zone trends north–south through the Eastern Goldfields Superterrane and is associated with the high grade c. 2690 Ma Teutonic Bore, Jaguar and Bentley VMS deposits (Hollis et al., 2015). Until recently, the plume-related lower portions of the stratigraphy were considered non-prospective since only minor barren pyritic lenses were recognized.

The Nimbus Ag–Zn–(Au) VMS deposit represents the first notable exception to this paradigm. It is located 250 km south of Teutonic Bore, near the margin of the paleo-rift zone but in comparison with the aforementioned occurrences, it preserves strikingly different features. In particular, is the tectono-stratigraphic position and its age, defined by two new U–Pb zircon SHRIMP ages of 2703 ± 5 Ma and 2702 ± 4 Ma, that associate Nimbus with the 2.7 Ga plume magmatism responsible for world-class Ni-komatiite mineralization. The ore mineralogy is characterized by an abundance of Ag–Sb–Pb–As bearing sulfosalts, high Hg and low Cu contents, and is hosted in a sericite-dominated alteration assemblage. Nimbus may be interpreted as a shallow water and low temperature VMS deposit with epithermal characteristics.

In this study we take advantage of state-of-the-art in situ techniques to investigate the fluid evolution of this peculiar VMS system. From the trace element compositions and S-isotope signatures we suggest that Nimbus experienced a bimodal fluid evolution consisting of: i) an initial intense interaction between deep-magmatic fluids and seawater that developed barren pyritic lenses; and ii) a subsequent closure of the hydrothermal system during which the Ag-rich ore formed sourcing sulfur almost entirely from a deep magmatic source. We also provide evidence supporting a widespread presence of bacterial colonies that promoted the formation of the barren pyrite lenses.

References

Hollis, S, Yeats, C, Wyche, S, Barnes, S, Ivanic, T, Belford, S, Davidson, G, Roache, A and Wingate, MTD 2015, A review of volcanic-hosted massive sulfide (VHMS) mineralization in the Archaean Yilgarn Craton, Western Australia: Tectonic, stratigraphic and geochemical associations: Precambrian Research Elsevier 260, p. 113–135.

Huston, DL, Champion, DC and Cassidy, KF 2014, Tectonic controls on the endowment of Neoarchean cratons in volcanic-hosted massive sulfide deposits: evidence from lead and neodymium isotopes: Economic Geology, 109, p. 11–26.

Mole, DR, Fiorentini, ML, Thebaud, N, Cassify, KF, McCuaig, TC, Kirkland, CL, Romano, SS, Doublier, MP, Belousova, EA, Barnes, SJ and Miller, J 2014, Archean komatiite volcanism controlled by the evolution of early continents: PNAS, 111, p. 10083–10088.

1 CET/CCFS, The University of Western Australia, Crawely 6009 WA, Australia

2 iCRAG (Irish Centre for Research in Applied Geosciences), University College Dublin, Dublin, Ireland

3 CMCA/CCFS, The University of Western Australia, Crawley 6009 WA, Australia

The crustal boundary of a Proterozoic Ocean: the generation, evolution and accretion of Point Malcolm, southeastern Western Australia

by

J Chard*, C Clark*, C Kirkland*, and M Adams*

A combination of U–Pb, Hf and O-isotope and trace elements in zircon and U–Pb and O-isotope in monazite were used to investigate the geodynamic setting and metamorphic evolution of a sequence of metasedimentary rocks at Point Malcolm. This area provides an ideal natural case study to explore the nature of the boundary between Proterozoic ocean (Madura) and continental (Albany–Fraser Orogen; AFO) crust. Point Malcolm is the southeasternmost coastal exposure of Proterozoic rocks before they are overlain by the Eucla Basin to the east. Identifying exposure of the Madura Province is significant because it is currently known through drillcore and geophysical surveys. Spaggiari et al. (2015) regards the Madura Province as an oceanic-arc accretionary terrane. By contrast, the AFO is a Proterozoic deformation belt related to the Yilgarn Craton margin (Smithies et al., 2015). The spatial and isotopic variation between the three samples investigated in this study yielded the following results: 1) the western most sample contains a multimodal age distribution of detrital zircon U–Pb ages between 2622 and 1293 Ma, whereas the two eastern samples yield an age distribution between 1544 and 1330 Ma detrital zircon grains; 2) the maximum age of deposition of the western metasediment was at 1293 ± 23 Ma, compared to 1330 ± 8 Ma of the eastern most sample; 3) the western sample has zircon εHf values ranging from –8.33 to 8.93 and $\delta^{18}O$ values between 5.05 and 8.34 ‰ indicative of sedimentary succession of reworked Yilgarn and AFO; 4) the eastern samples yield zircon εHf values from 0.11 to 6.12 and low $\delta^{18}O$ values between 3.43 and 4.77 ‰. The low $\delta^{18}O$ values are consistent with high-temperature water rock interaction, which is observed in altered oceanic crust; 5) metamorphism was recorded by zircon and monazite U–Pb ages of 1182–1152 Ma. This metamorphic monazite has elevated $\delta^{18}O$ values > 4.1 ‰ across all three samples, consistent with interaction of a continental metamorphic fluid. These observations lead us to the conclusion that accretion between the AFO and Madura Province occurred after 1330 Ma and before 1182 Ma.

References

Smithies, RH, Spaggiari, CV and Kirkland, CL 2015, Building the crust of the Albany–Fraser Orogen; constraints from granite geochemistry: Geological Survey of Western Australia, Report 150, 49p.

Spaggiari, CV, Kirkland, CL, Smithies, RH, Wingate, MTD and Belousova, E 2015, Transformation of an Archean craton margin during Proterozoic basin formation and magmatism: the Albany–Fraser Orogen, Western Australia: Precambrian Research, v. 266, p. 440–466.

* Department of Applied Geology, Curtin University, Bentley WA 6845

Major lithospheric elements of the Gawler Craton and controls on deformation and magmatism

by

S Curtis* and T Wise*

The Gawler Craton has previously been divided into subdomains or provinces, based on the litho-stratigraphic and tectonic history of the rocks exposed at the surface and traced beneath areas of cover using total magnetic intensity (TMI) imagery. However, these data sets do not necessarily reflect differences in the composition of the underlying lower crust and lithospheric mantle. Nd and Hf isotopes and inherited zircon data of peraluminous and metaluminous felsic to intermediate rocks can be used to provide information about the approximate age of the mid to lower crust, given that such rocks are derived from melting of the mid to lower crust, or the mixing of mantle melts with crustal material. Based on the integration of isotope and inherited zircon data with geophysical datasets the Gawler Craton can be divided into four major lithospheric elements. Inherited zircon and Nd and Hf isotopes suggest that the majority of the Gawler Craton is underlain by Archean crust, which in the central and northern Gawler Craton is Meso–Neoarchean in age, and in the eastern Gawler Craton is Neoarchean. In comparison, the southwestern Gawler Craton is typified by Paleoproterozoic depleted mantle model ages. Heat flow data indicates that the eastern Gawler Craton is underlain by a higher heat-producing crust, compared to the rest of the Gawler Craton.

A greater proportion of Paleo–Mesoproterozoic mafic igneous rocks are observed along lithospheric domain boundaries, compared to more felsic igneous rocks in the intra-domain regions. This suggests that mantle-derived magmas have ascended more readily through the mechanically weak trans-lithospheric structures with little crustal contamination, but in the intra-domain regions have ponded to produce felsic lower crustal melts. There are distinct differences in the expression of some episodes of Proterozoic deformation between the domains, which reflect either: i) timing of amalgamation of the domains; ii) that compositional and rheological differences in the lithosphere have affected the capacity of different domains to undergo crustal deformation during these events; or iii) that the trans-lithospheric structures separating domains have formed the boundary to deformational events by accommodating regional stresses.

* Geological Survey of South Australia, Adelaide SA 5000

Sedimentary limestone subduction and its mobilization in the mantle wedge

by

C Chen[1,2], Y Liu[1], SF Foley[2], and MW Förster[2]

Sedimentary carbonate rocks, which exist extensively in the oceanic realm, are subducted to differing degrees during the closure of oceanic basins. However, very few observational data exist to provide details on the mechanisms of transport of carbonate materials from the surface to mantle depths and back to the Earth's surface. Recently, we reported on a carbonatite intruding Neogene alkali basalts in the Hannuoba region, close to the northern margin of the North China Craton (NCC; Chen et al., 2016). This carbonatite intrusion shows geochemical features of recycled limestone, indicating that this carbonatite had a sedimentary limestone precursor. The presence of coarse-grained mantle-derived clinopyroxene, orthopyroxene and olivine, and chemical features of the carbonates (high Ni content and $^{143}Nd/^{144}Nd$ ratio) indicate that the carbonate melts were derived from the mantle. These observations suggest that the carbonatite probably formed by melting of subducted sedimentary carbonate rocks in the mantle. In addition, U–Pb geochronology and Hf isotopic ratios in detrital zircons from the carbonatite intrusion, which show a wide range of ages ranging from Precambrian to Phanerozoic, are used to trace the origin of the subducted limestone precursor (Chen et al., 2017). The age spectrum of the Precambrian zircons in the carbonatites exhibits similar age peaks to those of the southern Central Asian Orogenic belt (CAOB), but is not compatible with a northern NCC lithosphere source. The 300–400 Ma Phanerozoic zircons show positive Hf isotopic compositions similar to those of the southern CAOB, but contrast strongly with those from the northern NCC. These features suggest that the limestone precursor was derived from the Paleo-Asian Ocean and show that this carbonatite intrusion marks the subduction of a carbonate platform of the Paleo-Asian Oceanic slab to mantle depths beneath the NCC.

Melting of limestone is commonly regarded to be restricted to unusually hot regimes (>1520°C at 2–3 GPa; Irving and Wyllie, 1975), which could not occur in subduction-zone forearcs. Subducted limestone may penetrate the mantle wedge in the form of solid buoyant diapirs due to lower density and viscosity (Behn et al., 2011; Fig. 1). However, the behaviour of the limestone in the mantle is unclear. Here, we use laboratory experiments to show that carbonatite melt can form at temperatures as low as 950–1050°C and 2–3 GPa during interaction between limestone and olivine. We find that reaction with olivine strongly depresses the solidus for subducted limestone (Calcite + Olivine => Clinopyroxene + Carbonate melt), creating calcium-rich carbonatite melt in the shallow mantle (60–90 km). Our results suggest that carbonatite melt could originate from the mantle depths as shallow as 60 km. These carbonatite melts react with the mantle during ascent and transform the dunite or lherzolite to clinopyroxenite or wehrlite. Hence, reaction melting of limestone diapirs may dominate the recycling of limestone in the mantle and contribute to lithospheric refertilization.

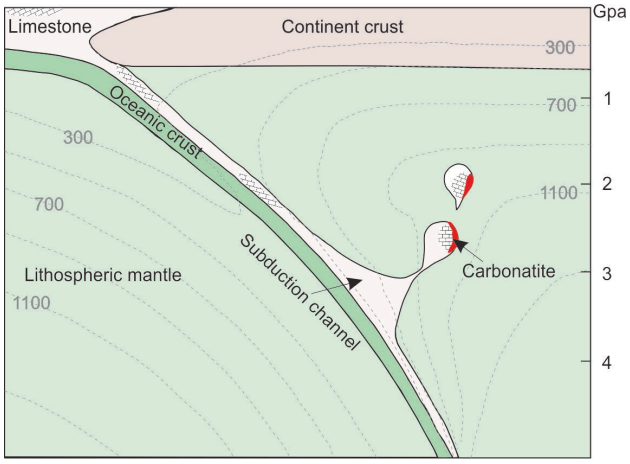

Figure 1. Schematic illustration of recycling of sedimentary limestone. Limestones may detach from the subducted slab to form solid buoyant diapirs. Reaction with peridotite could trigger melting of limestone diapirs, resulting in carbonatite

References

Chen, CF, Liu, YS, Foley, SF, Ducea, MN, He, DT, Hu, ZC, Chen, W and Zong, KQ 2016, Paleo-Asian oceanic slab under the North China craton revealed by carbonatites derived from subducted limestones: Geology, v. 44(12), p. 1039–1042.

Chen, CF, Liu, YS, Foley, SF, Ducea, MN, Han, PY, Hu, ZC 2017, Zircons in carbonatites establish recycling of a carbonate rock from the Paleo-Asian ocean under the North China Craton, submitted to Earth and Planetary Science Letters.

Irving, AJ and Wyllie, PJ 1975, Subsolidus and melting relationships for calcite, magnesite and the join $CaCO_3$-$MgCO_3$ 36 kb: Geochimica et Cosmochimica Acta, v. 39, p. 35–53

Behn, MD, Kelemen, PB, Hirth, G, Hacker, BR and Massonne, H-J 2011, Diapirs as the source of the sediment signature in arc lavas: Nature Geoscience, v. 4, p. 641–646

1 State Key Laboratory of Geological Processes and Mineral Resources, School of Earth Sciences, China University of Geosciences, Wuhan 430074, China

2 ARC Centre of Excellence for Core to Crust Fluid Systems, Dept. of Earth and Planetary Sciences, Macquarie University, North Ryde, New South Wales 2109, Australia

Numerical geodynamic modelling of slab derived carbonate melting at upper-mantle conditions

by

CM Gonzalez*, W Gorczyk*, and ML Fiorentini*

The mantle carbon cycle is an important, yet largely unconstrained and debated problem in the deep Earth volatile cycle. The uncertainty derives from two main causes: 1) the location of the carbonate melting P–T solidus (i.e. f_{O2} and synthetic starting compositions) for subducting altered basalts and sediments; and 2) the physical mechanisms by which carbon removal from the slab into the overlying mantle wedge occur. However, recent high P–T experiments, thermodynamic modelling, and geochemical observations over the last decade have reconciled these processes. Here, we couple, for the first time, experimentally produced solidii for carbonated basalts (MORB + CO_2) and sediments at pressures and temperatures relevant to upper-mantle conditions with the geodynamic modelling code I2VIS to elucidate subduction conditions at which carbonate melting commences beneath a subduction zone. This is accomplished through a robust thermomechanical and petrological modelling framework previous applied to decarbonation of subducting slabs and decarbonation within intracratonic settings. We find that the carbonated basaltic sections do indeed cross the carbonated basalt solidi during subduction and slab breakoff of moderately aged oceanic lithosphere (60 Ma). What remains uncertain is the fate of the carbonated sediments, where when stagnated, have yet to sufficiently attain high enough temperatures to melt. Three implications arise from this work: 1) these models confirm the hypothesis that carbon is likely filtered out at upper-mantle conditions suggesting a carbon increase in the upper mantle over time; 2) carbonate melting in the mantle transition zone may be an important source component for organic carbon signatures of eclogitic diamonds; 3) the base of the subcontinental lithospheric mantle may be enriched by percolation of carbonatitic melts acting as a nucleation point for continental breakup.

* University of Western Australia, School of Earth Sciences, Centre for Exploration Targeting and ARC Centre for Core to Crust Fluids Systems, Crawley WA 6009

New petrogenetic model for the adakitic magmatism of Patagonia and the Austral Volcanic Zone

by

GJ Henriquez[1,2], RR Loucks[1,2], and ML Fiorentini[1,2]

Motivation of research

The 'adakites' from the Patagonian Cordillera and the Austral Volcanic Zone (AVZ) in the southwest margin of South America, have been believed among the few true slab melts on Earth. Their steep REE patterns have been interpreted as implying a substantial role of restite garnet and petrogenesis by partial melting of eclogite in the subducting plate (e.g. Stern and Kilian, 1996; Ramos et al., 2004), by analogy with the alleged slab-melting origin of compositionally similar 'adakites' on Adak Island in the central Aleutian arc (Kay, 1978). These are distinguished from ordinary calc-alkalic arc andesites and dacites by steeper REE patterns with low concentrations of HREE and Y, and high values of Mg#, Cr, Ni, and Sr for their SiO_2 contents mainly in the range 56–63 wt%. However, an alternative interpretation of 'adakite' petrogenesis in Adak due to hydrous magmatic differentiation at high-pressure and temperature can be proposed based on: 1) subsequent descriptions of xenolith suites; 2) finding of a seismically active slab-mantle interface to depths of at least 270 km under the central Aleutians, which means that slab temperature is less than 650°C under the volcanic front (Gorbatov and Kostoglodov, 1997), too cool to be melted; and 3) along-arc variations of tectonic stress. This project aims to explore this alternative non-eclogitic petrogenetic interpretation without slab melting in the the Plio-Holocene volcanic centres from the AVZ, as well as to the mid-Miocene Patagonian 'adakites'.

Why Patagonia?

The western margin of Patagonia has experienced the subduction of the Chile Rise since ~22 Ma. As a result, a series of adakitic igneous complexes are related with the northward-propagating compressive deformation wave, which seems to be associated with the young, warm and buoyant southern part of the Nazca Plate subducted. On the other hand, all six Holocene volcanic centres of the Andean AVZ (49–54°S), associated with subduction of the Antarctic Plate under the South American and Scotia Plates, have erupted exclusively adakitic andesites and dacites (Stern and Kilian, 1996). These two scenarios integrated in one particular tectonic setting, makes Patagonia a perfect location to understand the processes involved in the genesis of the adakitic magmas.

Sampling scope and analytical techniques

This research project aims to integrate both whole-rock geochemistry and U–Pb dating and trace elements (including REE) from zircons by LA-ICP-MS analyses (in situ and detrital) from Patagonian igneous centres. Zircon Cathodoluminescence images will be used to search unzoned cores textures, which could imply deep and slow crystallization of the plutonic rocks. Additionally, we will perform Al-in-hornblende (EPMA) barometry on hornblende phenocrysts in host rock and plutonic enclaves.

To date, rocks and stream sediments were taken from five mid-Miocene igneous centres, during March 2017 at Patagonia (Chile and Argentina). Zircon mineral separation and geochemical sample preparation have already been undertaken at UWA.The next field work to sample two adakitic volcanoes from the AVZ is planned for February – March 2018. Preliminary results of ~2000 Zircon LA-ICP-MS analyses (in situ and stream sediments materials), in addition to 15 whole-rock geochemistry analyses, are expected for December 2017.

References

Gorbatov, A and Kostoglodov, V 1997, Maximum depth of seismicity and thermal parameter of the subducting slab: general empirical relation and its application: Tectonophysics, v. 277, 165–187

Kay, RW 1978, Aleutian magnesian andesites: melts from subducted Pacific Ocean crust: Journal of volcanology and geothermal research, v. 4, p. 117–132.

Ramos, V, Kay, SM and Singer, BS 2004, Las adakitas de la cordillera Patagónica: Nuevas evidencias geoquímicas y geocronológicas: Revista de la Asociación Geológica Argentina, v. 59 (4), p. 693–706.

Stern, CR and Kilian, R 1996, Role of the subducted slab, mantle wedge and continental crust in the generation of adakites from the Andean Austral Volcanic Zone: Contributions to Mineralogy and Petrology, v. 123, p. 263–281.

1 Centre for Exploration Targeting, School of Earth Sciences, The University of Western Australia, Crawley WA 6009

2 Australian Research Council Centre of Excellence for Core to Crust Fluid Systems, The University of Western Australia, Crawley WA 6009

Gold pathways in El Indio Belt: preliminary zircon U–Pb and O-isotopes analyses

by

C Jara[1,2], J Miller[3], M Fiorentini[1,2], H Jeon[1], M Fanning[4], and D Winocur[5]

Project Scope

This study is testing the Mineral System concept hypothesis in one of the most highly Au-endowed provinces of the Andes Cordillera: the El Indio Belt (EIB; Chile and Argentina, 29°20' to 30°30' S), which holds >45 Moz Au mainly hosted in Miocene world-class epithermal systems (Pascua-Lama, El Indio, Veladero, and Alturas). By means of integration of currently available data with new structural and zircon analyses, it intends to define: 1) the trans-lithospheric architecture that acted as the magma/fluids pathway, linking the fertile metal source with the deposits location; 2) the architecture's geodynamic evolution related to metallogenic events.

El Indio Belt Geology

The EIB is associated to a long-lived subduction zone. It is comprised by Permian–Triassic pyroclasts and granites intruding Carboniferous–Devonian metasediments, segmented by Triassic–Jurassic sedimentary basins. During the Cenozoic, a volcanic arc developed over this basement, evolving among different compression and extensional regimes according to variations in the subduction vector and subducting oceanic slab features (Winocur, 2010). Mineralization is linked to the final, localized stages of volcanic arc magmatism, associated with strong compression due to the subduction of an inactive ridge. Location of the deposits is hypothetised to be linked to trans-lithospherical structures that cut accross the volcanic arc. Currently, the EIB is located in an inactive volcanic segment of the Andes over a flat slab.

U–Pb and O-isotope zircon analyses

O-isotope and Lu–Hf analysis are expected to yield clues on first-order variations in the basement and Cenozoic magmas along EIB, highlighting the location of big, deep-seated structures. Both the Permian–Triassic granitic basement and Cenozoic intrusives or in situ domes were sampled for zircon analyses in Chile and Argentina. Zircon grains were obtained following the conventional methods of density, magnetic and heavy liquids separation, mounted in epoxy resin mounts and imaged, including CL. U–Pb SHRIMP-II geochronology in zircon was performed at Curtin University and at Austalian National University. Subsequent O-isotope analyses using CAMECA IMS-1280 at CMCA, UWA.

Preliminary results are compared with the mantle reservoir values of Valley et al. (2005) of 5.3 ± 0.6‰ $\delta^{18}O$ (2σ). There is a marked difference between Permian–Triassic basement and Cenozoic $\delta^{18}O$ values. Basement samples have higher $\delta^{18}O$, between mantle and evolved-crust values, and the oldest inherited cores of all samples show a much higher supracrustal component. The Cenozoic magmatic events show a variation from the Eocene, with $\delta^{18}O$ close to 6.0‰, indicating both a mantle and evolved-crust component in the magmas in a probably compressive regime, towards mantle-like $\delta^{18}O$ during the Oligocene–Miocene, preliminarily indicating almost no evolved crustal component in these later magmas. Only in Argentina they show a higher $\delta^{18}O$ value of 6–7‰, probably indicating a higher crustal involvement in the eastern area of the EIB, where the crust may be thicker and with older Carboniferous–Devonian basement influence. Slightly higher $\delta^{18}O$ values are locally seen in late Miocene dome and dyke samples, possibly pointing towards a longer residence time inside the crust or further interaction with meteoric waters. These samples also show the biggest data spread, with one $\delta^{18}O$ value below the mantle reservoir values.

Metallogenic implications of these preliminary observations are not yet clear, and they need to be thoroughly assessed in light of petrography and geological context, complemented with Lu–Hf isotopic analyses and whole-rock geochemistry. First-order variations are preliminary observed between the east and west domains of EIB, although further analyses are needed to assess the existance of a north–south variation along the belt.

1 Australian Research Council Centre of Excellence for Core to Crust Fluid Systems, The University of Western Australia, 35 Stirling Highway, Crawley WA 6009, Australia

2 Centre for Exploration Targeting. The University of Western Australia, 35 Stirling Highway, Crawley WA 6009, Australia

3 CSIRO, Australian Resources Research Centre (ARRC), 26 Dick Perry Ave, Kensington WA 6152, Australia

4 Australian National University, Research School of Earth Sciences, 142 Mills Rd, Acton ACT 0200, Australia

5 Universidad de Buenos Aires, Buenos Aires, Argentina

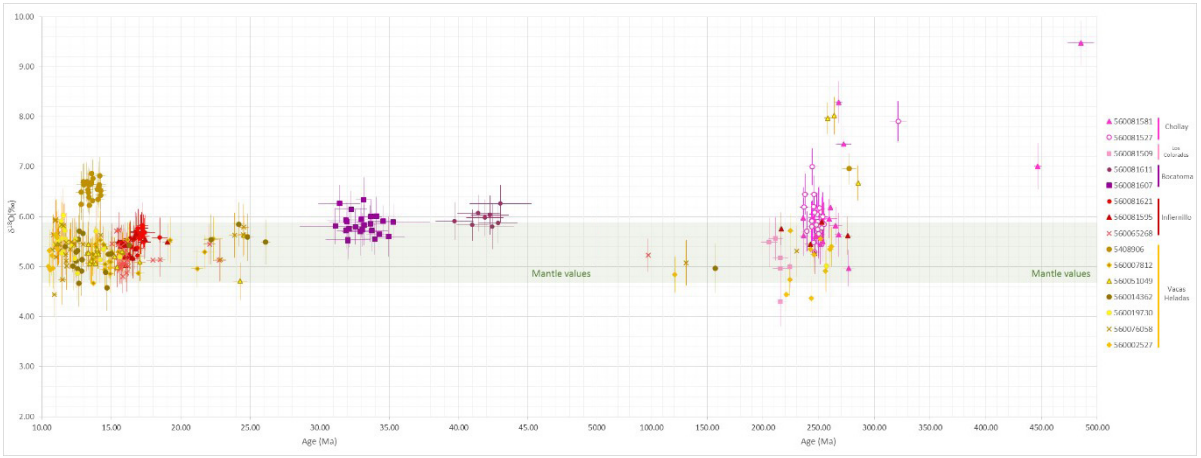

Figure 1. **δ^{18}O vs U-Pb zircon age plot for each sample analysed spots. 10–500 Ma timespan, note change of timescale at 50 Ma. Error bar in 2σ.**

References

Valley, J, Lackey, J, Cavosie, A, Clechenko, C, Spicuzza, M, Basei, M, Bindeman, I, Ferreira, V, Sial, A, King, E, Peck, W, Sinha, A and Wei, C 2005, 4.4 billion years of crustal maturation: oxygen isotope ratios of magmatic zircon: Contributions to Mineralogy and Petrology, v. 150, p. 561–580.

Winocur, D 2010, Geología y estructura del Valle del Cura y el sector central del Norte Chico, Provincia de San Juan y Cuarta región de Coquimbo, Argentina y Chile (Tomos I y II), PhD Thesis, Universidad de Buenos Aires.

Metamorphism and U–Pb monazite dating of the SASCA domain (southwest Ivory Coast)

by

AY Koffi[1], SC Djro[1], L Baratoux[2, 3], AN Kouamelan[1], P Pitra[4], O Vanderhaeghe[2], S Block[2], and FJ-LH Kouadio[1]

The Sassandra-Cavally (SASCA) domain (southwest Ivory Coast), is located in the transition zone between the Paleoproterozoic and Archean domains (Fig. 1). It is characterized by the coexistence of high-grade and low-grade metamorphic units and the existence of Archean relics in the Birimian formations. Heterogeneous gneiss formations comprising migmatites, orthogneisses, garnet-cordierite-sillimanite-garnet metasediment and staurolite-bearing micaschists are affected by three main deformation phases (D1–D3). Therobarometric calculations using Theriak-Domino (De Capitani, 1994) suggest a retrograde evolution from the granulite facies to the amphibolite facies, from Grand Bereby to Sassandra. The metamorphism in the paragneisses of Grand Bereby and in the orthogneisses of San-pedro with quartz–plagioclase–biotite–garnet–sillimanite–ilmenite and quartz–garnet–biotite–ilmenite partial fusion, respectively, evolves at the transition of granulite and amphibolite facies with a maximum pressure of 10 kbar and a temperature of 820 °C. It seems to characterize a decompression period in the granulite facies followed by cooling to the amphibolite facies with an apparent geothermal gradient of 40 °C/km. However, the evolution of staurolite-bearing micaschistes occurred mainly in amphibolite facies with PT conditions corresponding to 3.5 – 6.6 kbar and 550–620 °C. During this evolution, two metamorphic stages are distinguished: a prograde stage and a retrograde stage. The prograde path evolves according to a gradient of 30 °C/km up to a peak of metamorphism estimated at 6.6 kbar – 620 °C in the amphibolite facies for the sample of Kounoukou. This path would correspond to a burial comparable to a thickening of the crust up to about 14 km in depth under an apparent geothermal gradient of 39 °C/km. At this P–T path, the rock passes through a cooling phase with low decompression evolving according to a geothermal gradient of 40 °C/km. This decompression would be associated with a cooling phase recorded in staurolite-bearing micaschiste. U–Pb in situ dating of monazites gives ages of 2044 ± 11 Ma, 2003 ± 11 Ma, 1973 ± 11 Ma in the orthogneiss to quartz-garnet-biotite-ilmenite and 2000 ± 10 Ma for staurolite-bearing micaschistes. These ages correspond to metamorphic ages in the SASCA domain and their meaning will be further investigated.

References

Papon, A 1973, Geology and mineralization of the Southwest of Côte d'Ivoire (Synthesis of the work of the SASCA operation 1962–1968): Same, BRGM, Orleans, France, no. 80, 286p.

De Capitani, C 1994, Gleichgewichts-Phasendiagramme: Theorie und Software: Berichte der Deutschen Mineralogischen Gesellschaft, 6, 48p.

1 University Félix Houphouët Boigny Abidjan-Cocody, UFR STRM, Côte d'Ivoire

2 Geosciences Environment Toulouse, Midi Pyrénées Observatory, IRD,Toulouse, France

3 IFAN, Cheikh Anta Diop, Dakar, Senegal

4 Geosciences Rennes, UMR CNRS 6118, University of Rennes I, France

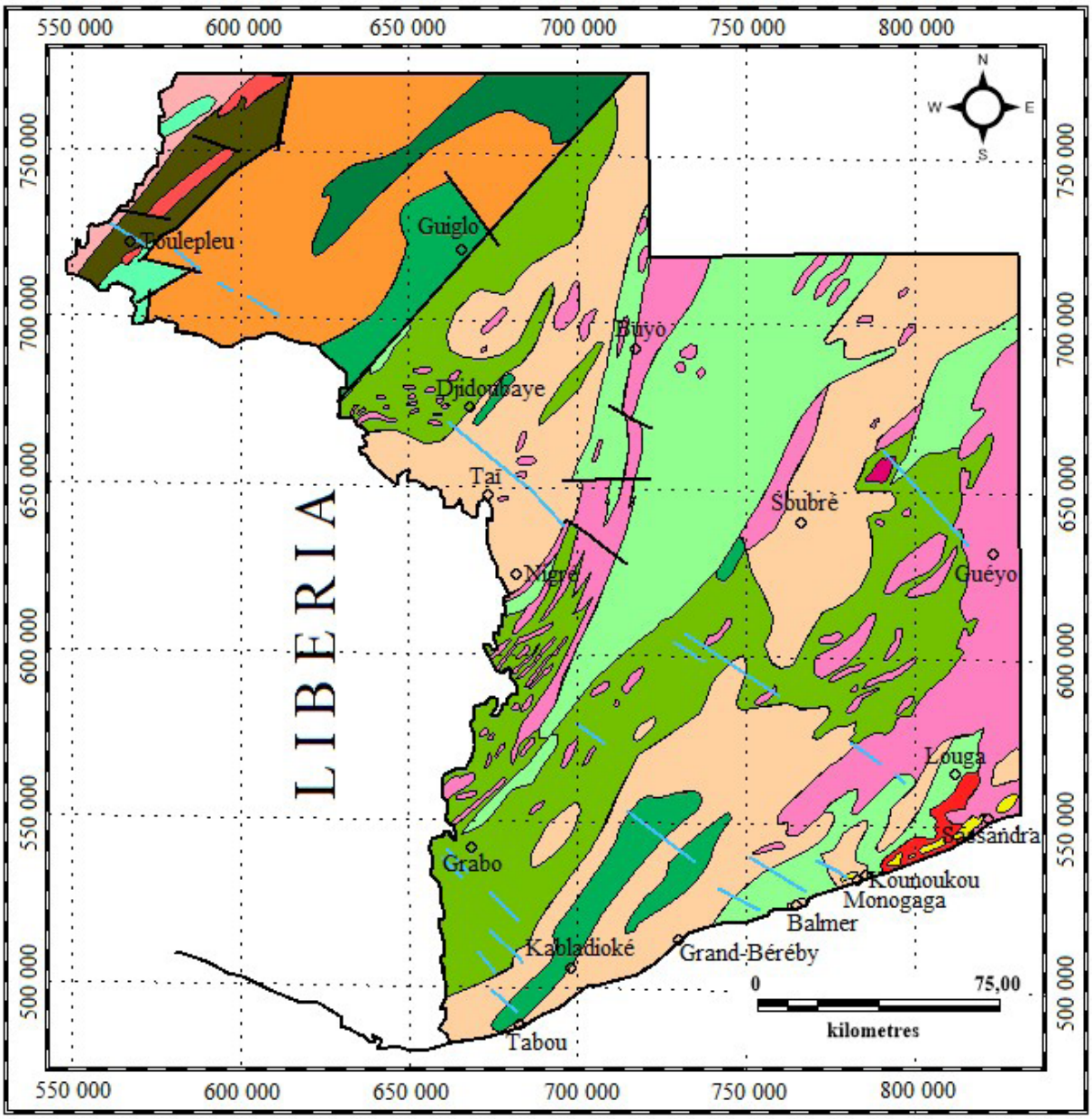

LEGENDE

Tertiaire

Dolérites

DOMAINE DE MAN

- Granodiorites (type Nuon)
- Unité volcano-sédimentaire de Toulepleu-Ity
- Unité d'âge douteux
- Granite et granodiorite gneissifiés
- Formations du mont Douan
- Migmatites, granites liés et formation du mont Gao

DOMAINE DE SASCA

- Syénites du mont Troquoi
- Granodiorites de Sassandra et granties à deux micas
- Unités volcano-sédimentaires des monts Trou, de la Hana-Lobo, de la Davo, de Louga-Kounoukou
- Granite subpegmatitique gneissifié (type Niéga-Pauli-plage)
- Formations de Tabou-Djidoubaye
- Formations de Grabo
- Migmatites, granites liés et formations de Kabiadioké-Balmer

Failles

Figure 1. Geological map of southwest Ivory Coast (modified after Papon, 1973)

Structural controls on Proterozoic gold and nickel mineral systems — insights from East Kimberley, Western Australia

by

F Kohanpour*, MD Lindsay*, S Occhipinti*, and W Gorczyk*

Introduction

It is widely accepted that structure is one of the dominant controls on the localization of mineralization. Deep crustal or lithospheric-scale structures are understood to influence the development of a wide range of mineral deposits, thus identification of controlling structures is critical for mineral systems prospectivity analysis. In addition, damage zones and geological complexities that act as physical throttles for fluid movement are important for prospectivity analysis at camp and deposit scales. In this study, an integration of geophysical, geological data and geodynamic numerical modelling applied to identify major geological features or structures that may be important for controlling the localization of gold and nickel mineralization in the Halls Creek Orogen, east Kimberley (Fig. 1). The Halls Creek Orogen includes the 1910–1805 Ma Lamboo Province that developed between the Kimberley and North Australian Cratons. In the east, the Lamboo Province comprises three parallel, north-northeast trending zones (the Western, Central, and Eastern zones) that have been interpreted as distinct tectonostratigraphic terranes. These zones contain geological units formed during the early Paleoproterozoic that may have originated in different settings and times and then juxtaposed during the 1870–1850 Ma Hooper and 1835–1805 Ma Halls Creek orogenies. The metasedimentary rocks of the Halls Creek Group in the Eastern Zone are known to contain Au that probably formed during the later stage of deformation events in the Halls Creek Orogen. Significant Ni–Cu–PGE mineralization is mainly restricted from c. 1856 to 1830 Ma layered mafic-ultramafic intrusions in the Central Zone of the Lamboo Province.

Geodynamic numerical modelling

The geodynamic evolution of the Halls Creek Orogen has been examined by 2D thermo-mechanical-petrological model based on I2VIS code. The results indicate that the most plausible process that replicates the inferred Paleoproterozoic tectonic evolution of the Halls Creek Orogen can be induced by west-dipping subduction at the margin of Kimberley Craton (Fig. 1). The geodynamic numerical models also reveal the underlying lithospheric settings which lead to voluminous magmatism and heat/fluid flux during the evolution of the Halls Creek Orogen. These processes are not observable without the aid of geodynamic simulation. The second invariant of strain rate (ε_{II}) was used to visualise major fault systems and shear zones during the evolution of numerical models (Fig. 1a). The numerical models illustrate how major fault systems observed in the Halls Creek Orogen developed as a result of both extensional and collisional processes. The geodynamic models also show lithospheric-scale structures can be conduits and pathways for the movement of magmatic and hydrothermal fluids into the upper crust.

Structural interpretation

Regional aeromagnetic, gravity, and Landsat data integrated with mapped geology have been used as a basis for understanding the geological structures associated with gold and nickel mineralization in the Halls Creek Orogen (Fig. 1b). The primary goal was to determine links between the geological structures and mineralization. Critical to the success of this analysis is the identification of deep crustal-scale structures in the region that may have supplied mineralising fluids, and near surface features that acted as physical traps for mineralization.

There is a corridor of gold occurrences in the Eastern Zone associated with a high gravity gradient (Fig. 1c). In the intersection of cross-orogen and orogen-parallel structures, there are some low gravity anomalies proximal to the gold mineralization, which create low first vertical derivative values. These ellipsoid low first vertical derivative figures, showing a similar value to granitic intrusions in the Eastern and Central zones (Fig. 1c). The figures of low first vertical derivative of gravity data below the sites of gold camps could represent unexposed granitoid bodies which may release the gold-bearing fluid or energy. A localized zone of dilation resulting from the intersection of orogen orthogonal features with the extensional faults, may have facilitated igneous intrusion and fluid ascension. In the next step, we identify the structural traps where there is a group of gold deposits. They are sited on second- or third-order faults or shear zones which are in northeast trending, located proximal to first-order major structures. Anticlinal hinges and orogen-normal structures are important features

* Centre for Exploration Targeting, School of Earth and Environment, The University of Western Australia, 35 Stirling Hwy, Crawley WA 6009

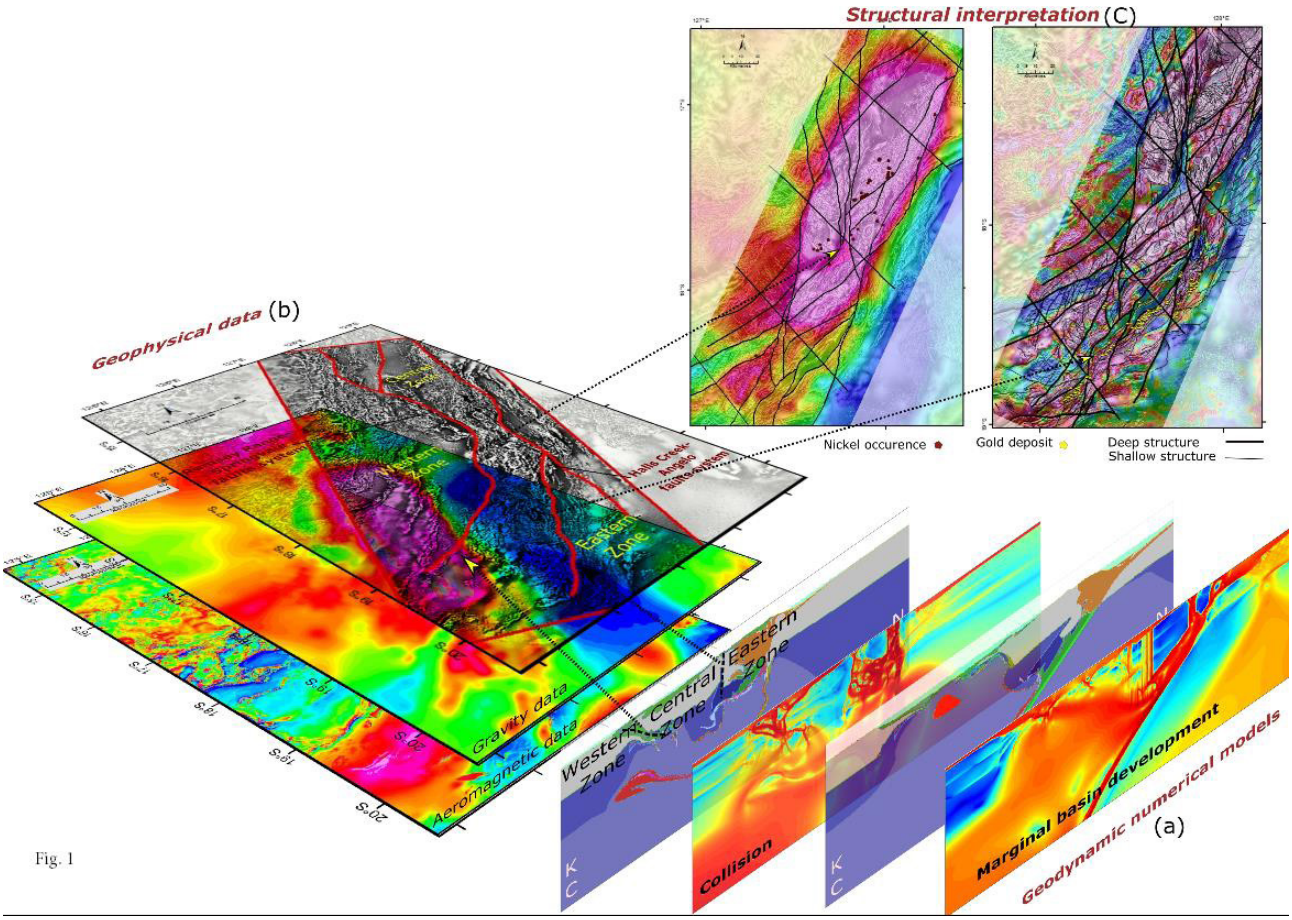

Fig. 1

Figure 1. **Structural control on gold and nickel mineral systems in the Halls Creek Orogen: (a) geodynamic numerical model represents development of the marginal basin and collision in the tectonic evolution of the Halls Creek Orogen; second invariant of strain rate shows how the major shear zones can act as fluid conduits; (b) geophysical data sets include aeromagnetic and gravity data used for structural interpretation; (c) structural controls on gold and nickel presents: the regional distribution of gold mineralization is controlled by shallow second- and third-order structures that splay from the larger and deeper first-order structures; The localization of nickel mineralization at the regional scale are controlled by proximity to ancient cratonic boundaries, and long-lived, lithospheric-scale faults**

of most gold deposits. This is particularly important for trapping fluid to produce deposits. The gold deposits in the HCO are mostly located in fold hinges that are oriented at a high angle to the direction of terrane convergence. It is apparent that gold mineralization is confined to a series of the northeasterly trending folds and shear zones which are mainly related to the D4 and D5 deformation events that occurred during the accretion of the Eastern Zone to the Central Zone and subsequent strike-slip movement.

Nickel occurrences are mainly present in the Central Zone of the Halls Creek Orogen, which is surrounded by two trans-crustal structures developed during the 1835–1805 Ma Halls Creek Orogen (Fig. 1c). Geodynamic models suggest that the Central Zone at the margin of Kimberley Craton rifted during the evolution of the Halls Creek Orogen. At the regional scale, nickel occurrences occur adjacent to major deep structures. These deep lineaments are interpreted to represent deep faults or shear zones through which large amounts of mantle-derived magma can ascend. The geodynamic numerical models suggest asthenosphere upwelling, marginal basin development, and syn- to post-collisional mantle plume activity resulting in crustal extension, and trans-crustal faulting facilitated magma generation and ascent. In the Halls Creek Orogen, mineralized mafic-ultramafic intrusions are associated with a regional positive gravity anomaly (Fig. 1c), likely resulting from the large flux of decompression mantle melt into deep crust during marginal basin development. Deformation of two groups of mineralized mafic-ultramafic intrusions during D3 and D4 suggests that intrusion of ultramafic rocks and nickel mineralization took place prior to the 1835–1805 Ma Halls Creek Orogeny, likely during the extensional tectonic regime related to marginal basin development over the Central Zone.

Zircon composition as a fertility indicator of Archean granites

by

Y-J Lu[1,2] and RH Smithies[1]

Porphyry Cu deposits are major sources of Cu and Mo. They range in age from Archean to modern, but most are Jurassic and younger. Porphyry deposits in Precambrian terranes are rare, and the reasons for this remain unclear. Nevertheless, several porphyry-type deposits occur in the Abitibi and Opatica greenstone belts in the Superior Craton, suggesting that the potential for porphyry deposits in Archean cratons has not been fully recognized.

Lu et al. (2016) proposed that zircon compositions can be an excellent pathfinder for porphyry Cu deposits. The best fertility indicators are zircon Eu/Eu* (>0.3) and 10 000*(Eu/Eu*)/Y (>1) ratios, whereas (Ce/Nd)/Y (>0.01) and Dy/Yb (<0.3) ratios are moderately useful. These distinct zircon trace element ratios are interpreted to reflect a specific differentiation trend, e.g. suppression of plagioclase fractionation and enhanced early amphibole fractionation as a result of high magmatic water content, which is a prerequisite for magmatic–hydrothermal (porphyry) ore formation.

We test the above zircon fertility indicators in Archean granites across the Yilgarn Craton in Western Australia. The studied granites range in age from c. 2930 to 2640 Ma, and from high-Al TTG to potassic granite. These Archean granites lie transitionally between Phanerozoic infertile and fertile granite suites, as defined in Lu et al. (2016), on Eu/Eu* vs (Ce/Nd)/Y and (Eu/Eu*)/Y vs (Ce/Nd)/Y plots. On a Eu/Eu* vs Dy/Yb plot, Yilgarn Archean granites have distinctly higher Dy/Yb ratios (>0.3), and define a positive trend, which contrast with the negative trend for Phanerozoic fertile suites (Fig. 1). This indicates that Archean granites compositional evolution was strongly influenced by garnet (source retention) whereas Phanerozoic fertile suites are strongly influenced by amphibole fractionation. This in turn suggests that Archean granite magmas are typically relatively dry compared to Phanerozoic fertile suites, and is consistent with the absence of amphibole phenocrysts in most granites in the Yilgarn Craton.

The systematic difference in zircon chemistry between Archean granites and Phanerozoic fertile and infertile suites suggests that different processes were involved in forming Archean granites. We argue that Archean granites were mainly formed through lower- or infracrustal partial melting of mafic crust in the garnet stability field, whereas Phanerozoic fertile suites were formed by intracrustal amphibole-dominated fractionation of mafic magmas. Granites formed by the former process have lower potential for porphyry Cu mineralization due to insufficient water and the lack of build-up of copper and sulfur in the melt. Further data is needed from mineralized Archean granites to determine whether they have different genesis from those unmineralized Archean granites.

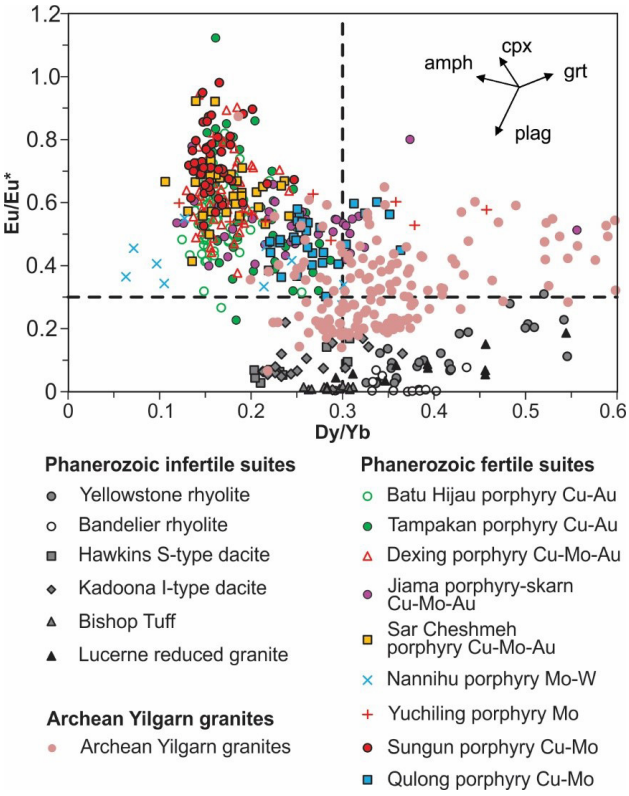

Figure 1. Eu/Eu* vs Dy/Yb plot for zircons from Archean Yilgarn granites and Phanerozoic infertile and fertile suites

References

Lu, YJ, Loucks, RR, Fiorentini, ML, McCuaig, TC, Evans, NJ, Yang, ZM, Hou, ZQ, Kirkland, CL, Parra-Avila, LA and Kobussen, A 2016, Zircon compositions as a pathfinder for porphyry Cu ± Mo ± Au deposits, Society of Economic Geologists Special Publication No. 19, p. 329–347.

1 Geological Survey of Western Australia, 100 Plain Street, East Perth, WA 6004, Australia

2 Centre for Exploration Targeting and Australian Research Council Centre of Excellence for Core to Crust Fluid Systems (CCFS), School of Earth Sciences, The University of Western Australia, Crawley, WA 6009, Australia

Porphyry Cu fertility in the Tibetan Plateau

by

Y-J Lu[1,2], Z-Q Hou[3], Z-M Yang[3], LA Parra-Avila[2], M Fiorentini[2], TC McCuaig[2,4], and RR Loucks[2]

Introduction

Cenozoic porphyry Cu deposits in the Tibetan Plateau, such as in the Gangdese belt of the Lhasa Terrane, southern Tibet, are the archetypal porphyry systems developed in continental collision zones. Understanding the temporal and spatial distribution of these deposits will help unravel the genesis of porphyry deposits in collision zones and exploration targeting of porphyry deposits in similar orogenic belts. Here we present terrane-scale zircon Lu–Hf isotopic mapping and whole-rock geochemical mapping results as well as zircon trace element compositions in the Tibetan Plateau, mainly in the Lhasa Terrane, to unravel the temporal and spatial control on porphyry mineralization.

Zircon Lu–Hf isotopic mapping

Zircon Lu–Hf isotopic mapping results using 652 zircon samples in the Tibetan Plateau are presented in Figure 1. They demonstrate that the majority of porphyry Cu deposits are associated with isotopically juvenile domains along two major suture zones of the Indus-Yarlung and Jinsha suture zones (Fig. 1). Such isotopic mapping can thus help narrow down search space from over 2500 km scale to about 500 km scale.

Whole-rock (Eu/Eu*)/Y ratios

Whole-rock geochemical mapping using c. 1200 Ma samples across the Lhasa Terrane is shown in Figure 2. All porphyry Cu deposits are located within high 10 000*(Eu/Eu*)/Y (>800) domains. Other whole-rock fertility indicators such as V/Sc, Eu/Eu*, Sr/Y ratios (Loucks, 2014) are less effective in discriminating Cu-porphyries from barren ultrapotassic rocks on contour maps. Thus, the (Eu/Eu*)/Y ratio, similar to the (Eu/Eu*)/Yb_N ratio of Loucks (2013), is the best whole-rock fertility indicator, and is interpreted to indicate extremely high magmatic water content which induces early and prolific hornblende fractionation and suppresses early plagioclase crystallization.

Zircon trace element fertility indicator

Zircon U–Pb and trace element data were obtained from 66 igneous samples of Jurassic–Miocene (181–11 Ma) age in the eastern Gangdese belt (Fig. 3). Both xenocrystic and magmatic zircons show systematic temporal compositional evolution from Jurassic to Miocene. From c. 200 to 55 Ma, zircon Eu/Eu* (0.1 – 0.4), 10 000*(Eu/Eu*)/Y (0.1 – 10), and (Ce/Nd)/Y (0.001 – 0.05) ratios remain broadly similar (Lu et al., 2016). However, these zircon trace element ratios increase rapidly after c. 55 Ma and culminate at c. 13 Ma with Eu/Eu*, 10 000*(Eu/Eu*)/Y, and (Ce/Nd)/Y ratios up to 1, 70, and 2, respectively. Similar temporal trends are also observed for whole-rock Sr/Y, La/Yb, and (Eu/Eu*)/Y ratios, although whole-rock Eu/Eu* ratios appear to be similar throughout the Jurassic-Miocene period. In addition, Cretaceous samples show juvenile Hf-O isotopic signatures, whereas Eocene–Miocene intrusions show increasing zircon $\delta^{18}O$ values and decreasing epsilon Hf values, suggesting increasing amounts of supracrustal materials were incorporated in magma genesis after c. 55 Ma.

These whole-rock geochemical, zircon trace element, and Hf-O isotopic trends are interpreted to indicate increasing maturation of the collision-related magmas, which interacted with an increasing length of the crustal column. This was probably the result of steadily increasing compression that has progressively impeded magma ascent, forcing magmas to evolve at a series of deep-intermediate level chambers between the lower and upper crust. Increased compression may have been related to subduction of buoyant Indian continental lithosphere.

1 Geological Survey of Western Australia, 100 Plain Street, East Perth, WA 6004, Australia

2 Centre for Exploration Targeting and Australian Research Council Centre of Excellence for Core to Crust Fluid Systems (CCFS), School of Earth Sciences, The University of Western Australia, Crawley, WA 6009, Australia

3 Institute of Geology, Chinese Academy of Geological Sciences, Beijing 100037, PR China

4 BHP, 125 St Georges Terrace, Perth WA 6000 Australia

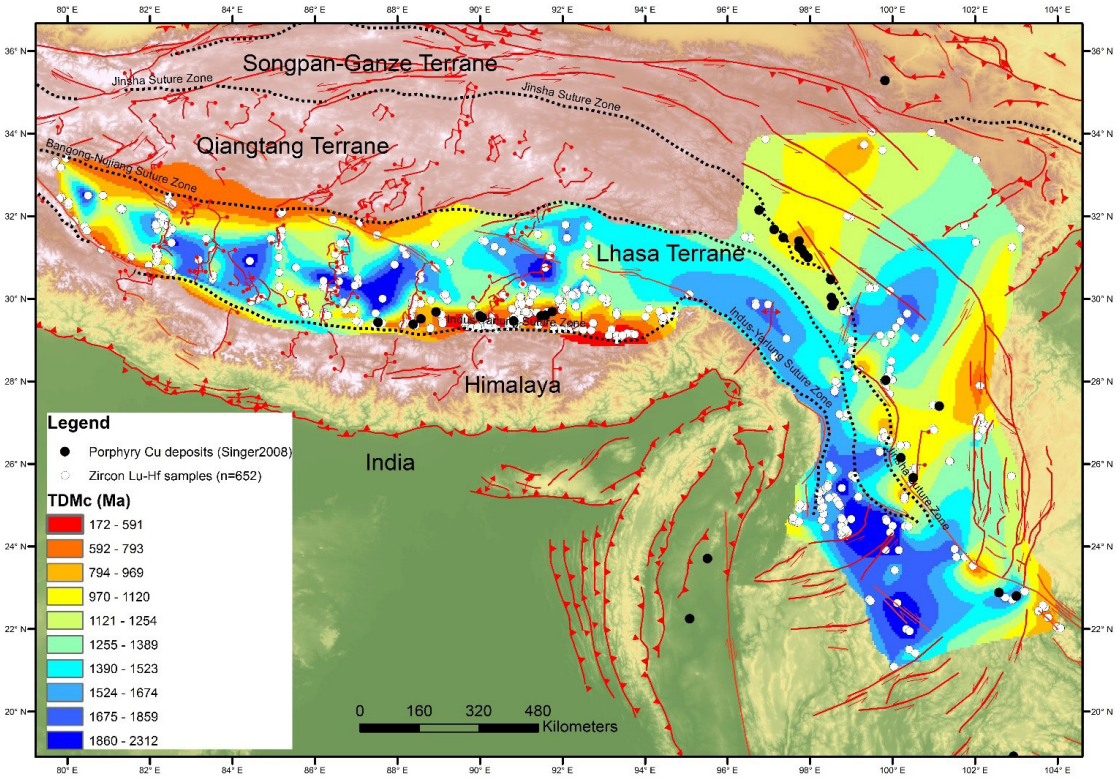

Figure 1. **Contour map of zircon two-stage depleted mantle model ages (TDMc) for granitoid and felsic volcanic rocks in the Tibetan Plateau. Zircon data sources: Hou et al. (2015); Wang et al. (2016); and Hou et al. (submitted to Nature Communications). Suture zones and faults of the Tibetan Plateau are from the HimaTibet Map (Styron et al., 2010). Locations of porphyry copper deposits are from Singer et al. (2008)**

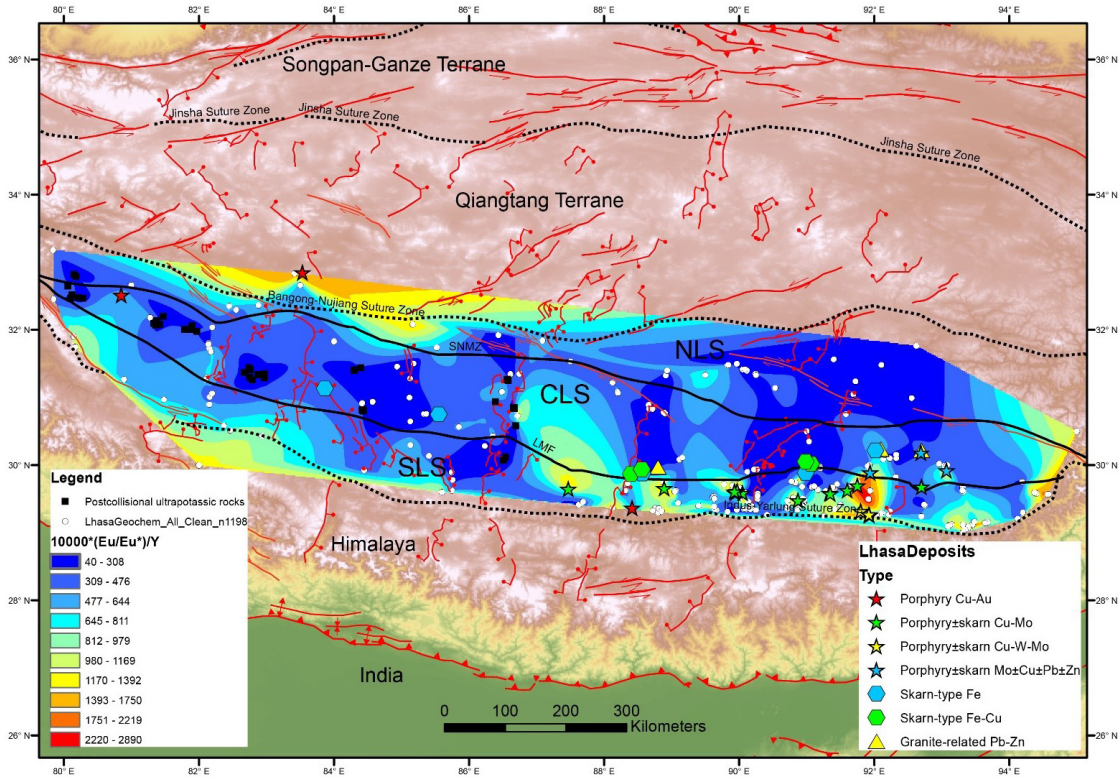

Figure 2. **Contour map of whole-rock geochemical ratio of 10 000*(Eu/Eu*)/Y for mafic to felsic intrusive and volcanic rocks in the Lhasa Terrane, southern Tibet. Also shown are major mineral deposits in the Lhasa Terrane (Hou et al., 2015; Yang et al., 2016). Whole-rock geochemistry of igneous rocks in the Lhasa Terrane were compiled from Hou et al. (2015), Yang et al. (2016) and Lu et al. (unpublished). Abbreviations: NLS, Northern Lhasa Subterrane; CLS, Central Lhasa Subterrane; SLS, Southern Lhasa Subterrane**

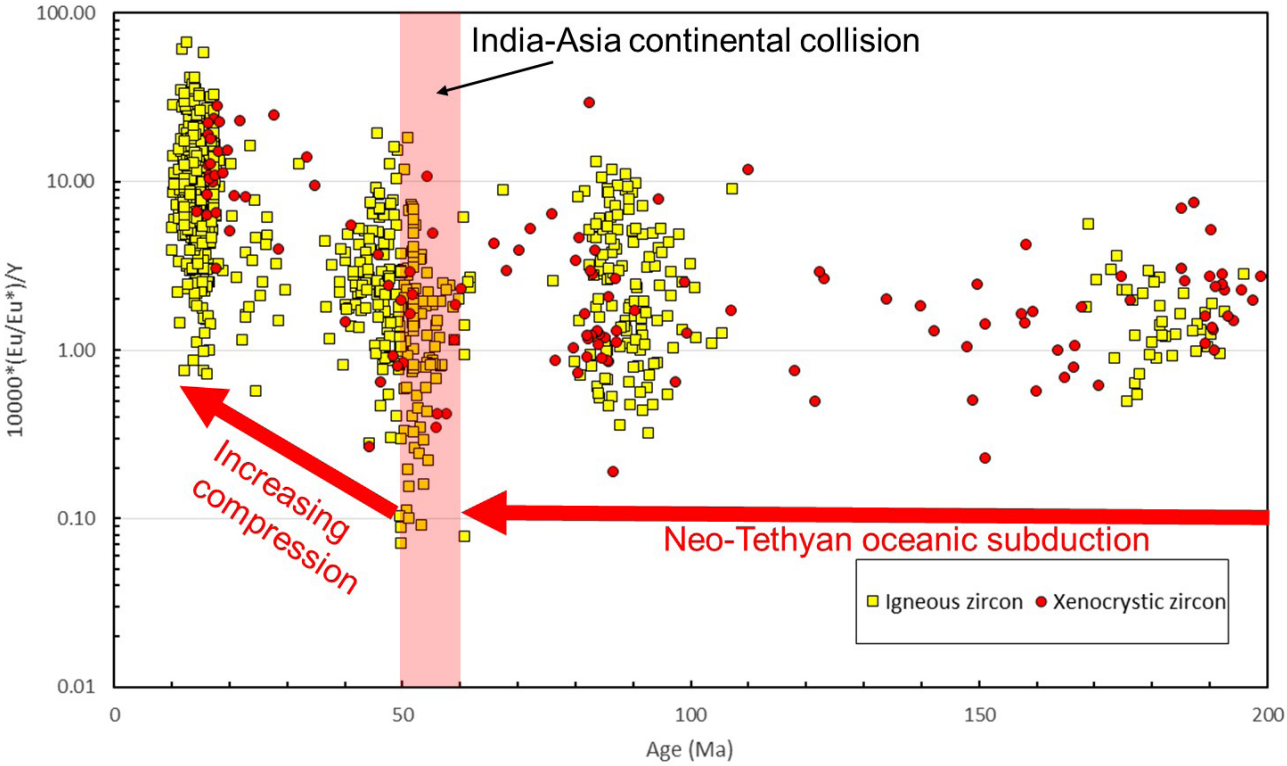

Figure 3. Zircon 10 000* (Eu/Eu*)/Yratio vs Age (Ma) for 66 magmatic rocks in the eastern Gangdese belt, Lhasa Terrane, southern Tibet. Data Source: Lu et al. (unpublished)

Conclusion

Exploration is a scale reduction process. Zircon Lu–Hf isotopic mapping is powerful in identifying juvenile crust domains which are preferable for porphyry Cu formation. All porphyry Cu deposits in the Lhasa Terrane are characterized by intrusive phases with juvenile compositions compare to surrounding regions and distinctly high whole-rock 10 000*(Eu/Eu*)/Y ratios (>800), which is the best fertility indicator. The combined isotopic mapping and whole-rock 10 000*(Eu/Eu*)/Y ratio mapping has great potential to help focus exploration on prospective areas.

References

Hou, ZQ, Duan, LF, Lu, YJ, Zheng, YC, Zhu, DC, Yang, ZM, Yang, ZS, Wang, BD, Pei, YR, Zhao, ZD and McCuaig, TC 2015, Lithospheric architecture of the Lhasa Terrane and its control on ore deposits in the Himalayan-Tibetan orogeny: Economic Geology, v. 110, p. 1541–1575.

Loucks, RR 2013, Distinctive Composition and Genesis of Copper Ore-forming Arc Magmas: Mineralogial Magazine, v. 77, p. 1642. doi:10.1180/minmag.2013.077.5.12.

Loucks, RR 2014, Distinctive composition of copper-ore-forming arc magmas: Australian Journal of Earth Sciences, v. 61, p. 5–16.

Lu, YJ, Loucks, RR, Fiorentini, ML, McCuaig, TC, Evans, NJ, Yang, ZM, Hou, ZQ, Kirkland, CL, Parra-Avila, LA and Kobussen, A 2016, Zircon compositions as a pathfinder for porphyry Cu ± Mo ± Au deposits: Society of Economic Geologists Special Publication No. 19, p. 329–347.

Styron, R, Taylor, M and Okoronkwo, K 2010, HimaTibetMap-1.0: new 'web-2.0' online database of active structures from the Indo-Asian collision: Eos, v. 91, no. 20.

Wang, CM, Bagas, L, Lu, YJ, Santosh, M, Du, B and McCuaig, TC 2016, Terrane boundary and spatio-temporal distribution of ore deposits in the Sanjiang Tethyan Orogen: Insights from zircon Hf-isotopic mapping. Earth-Science Reviews, v. 156, p. 39–65.

Yang, ZM, Goldfarb, R and Chang, ZS 2016, Generation of Postcollisional Porphyry Copper Deposits in Southern Tibet Triggered by Subduction of the Indian Continental Plate: Society of Economic Geologists Special Publication no. 19, p. 279–300.

Singer, DA, Berger, VI and Moring, BC 2008, Porphyry copper deposits of the world: database and grade and tonnage models: U.S. Geological Survey Open-File Report 2008-1155, 45p., http://pubs.usgs.gov/of/2008/1155/.

The timing of gold mineralization in Yaouré: towards the understanding of the metallogenic evolution of central Côte d'Ivoire, West Africa

by

Nicolas Mériaud[1], Nicolas Thébaud[1], Quentin Masurel[1], Patrick Hayman[2], Mark Jessell[1], and Steffen Hagemann[1]

Abstract

The West African Craton hosts a wide range of gold deposit types including orogenic gold, intrusion-related, skarns, paleoplacer and Cu–Au porphyry systems totalizing 318 Moz throughout 60 deposits (Goldfarb et al., 2017). In comparison to its neighboring countries, the understanding of gold mineralization in Côte d'Ivoire remains poorly constrained. This study focuses on the Yaouré deposit, one of the 7 gold deposits currently mined in the country. It is located 35km northwest of Yamoussoukro, the capital city. The deposit sits on the southeastern edge of a 100km-long northeast-striking Birimian granite-greenstone belt called the Bouaflé greenstone belt. The stratigraphy comprises tholeiitic basalts intruded by a series of dykes ranging in composition from felsic to intermediate. These units are overlain by a narrow fault-bounded basin stratigraphically composed of immature alluvial fans, andesitic mass flow and dacite. The interpretation of geophysical datasets, combined with drill core logging and ore mineralogy investigation allow to recognize a diachronous gold mineralization during a compressive event at Yaouré. Gold endowment is controlled by two distinct types of mineralized shears including: 1) north–south trending thrusts; and 2) northwest–southeast and southwest–northeasterly trending conjugated strike-slip faults. These two sets of fault zones orientations and kinematics are consistent with a protracted east–west shortening event. At a regional scale, the neighboring Oumé-Fétékro greenstone belt display a similar structural evolution to that of the Bouaflé greenstone belt. It is however remarkable that the timing of mineralization in the Yaouré deposit precedes that of the Hire and Bonikro deposits of the Oumé-Fétékro greenstone belt. Our preliminary results further support a polyphase gold mineralization for the West African Craton.

References

Goldfarb, RJ, André-Mayer, A-S, Jowitt, SM and Mudd, GM 2017, West Africa: The world's premier Paleoproterozoic gold province: Economic Geology, v. 112, p.123–143.

1 Centre for Exploration Targeting, The University of Western Australia, Crawley WA 6009

2 Queensland University of Technology, Brisbane QLD 4000

New seismological views of the ancient and modern lithospheric rifts

by

WD Mooney*, F Pollita*, and Z Yao*

North American rifts

Using seismic surface waves recorded with Earthscope's Transportable Array, we apply surface wave imaging to determine 3D seismic velocity in the crust and uppermost mantle. Our images span several North American Proterozoic and early Cambrian rift zones (Mid-Continent Rift, Rough Creek Graben, Rome trough, Birmingham trough, Southern Oklahoma Aulacogen, and Reelfoot Rift). While ancient rifts are generally associated with low crustal velocity because of the presence of thick sedimentary sequences, the Reelfoot Rift (central USA) is unique in its association with a pronounced low mantle S-wave seismic velocity. Its mantle low-velocity zone (LVZ) is exceptionally pronounced and extends down to at least 200 km depth. This LVZ is of variable width, being relatively narrow (~50 km wide) within the northern Reelfoot Rift, which hosts the New Madrid Seismic Zone (NMSZ). We hypothesize that this mantle volume is weaker than its surroundings and that the Reelfoot Rift consequently has relatively low elastic plate thickness, which would tend to concentrate tectonic stress within this zone. No other intraplate ancient rift zone is known to be associated with such a deep mantle low-velocity anomaly, which suggests that the NMSZ is more susceptible to external stress. Our results provide an explanation for the concentration of earthquakes, including the 1811–1812 New Madrid sequence, in the NMSZ.

Red Sea Rift

We measured phase velocities at 13 periods from 20 s to 143 s using Rayleigh-wave data recorded at recently-installed, dense (135) broadband seismic stations in the Arabian shield and determined the shear-wave velocity structure. Our results clearly reveal a 300-km wide upper-mantle seismic low-velocity zone (LVZ) beneath the western Arabian shield at a depth of 60 km and with a thickness of 130 km. The LVZ has a north–south trend and follows the late-Cenozoic volcanic areas. The lithosphere beneath the western Arabian shield is remarkably thin (60–90 km). The 130-km thick mantle LVZ does not appear beneath the western Red Sea and the spreading axis. Thus, the Red Sea at 20–26° north is an asymmetric rift, with thin lithosphere located east of the Red Sea axis, as predicted by the low-angle detachment model for rift development. Passive rifting at the Red Sea and extensional stresses in the shield are probably driven by slab pull from the Zagros subduction zone. The low shear-wave velocity (4.0 – 4.2 km/s) and the geometry of LVZ beneath the western shield indicate northward flow of hot asthenosphere from the Afar hot spot. The upwelling of basaltic melt in fractures or zones of localized lithospheric thinning has produced extensive late Cenozoic volcanism on the western edge of the shield, and the buoyant LVZ has caused pronounced topography uplift there. Thus, the evolution of the Red Sea and the Arabian shield is driven by subduction of the Arabian plate along its northeastern boundary.

References

Pollitz, FF and Mooney, WD 2014, Seismic structure of the Central US crust and shallow upper mantle: Uniqueness of the Reelfoot Rift, Earth and Planetary Science Letters, 402, p. 157–166.

Yao, ZX, Mooney, WD, Zahran, H and Youseff, SE-H, Upper mantle seismic velocity structure beneath the Arabian shield from Rayleigh wave surface wave tomography and its implications, in revision after through USGS internal review.

* Earthquake Science Center, USGS, Menlo Park, California 94025 USA

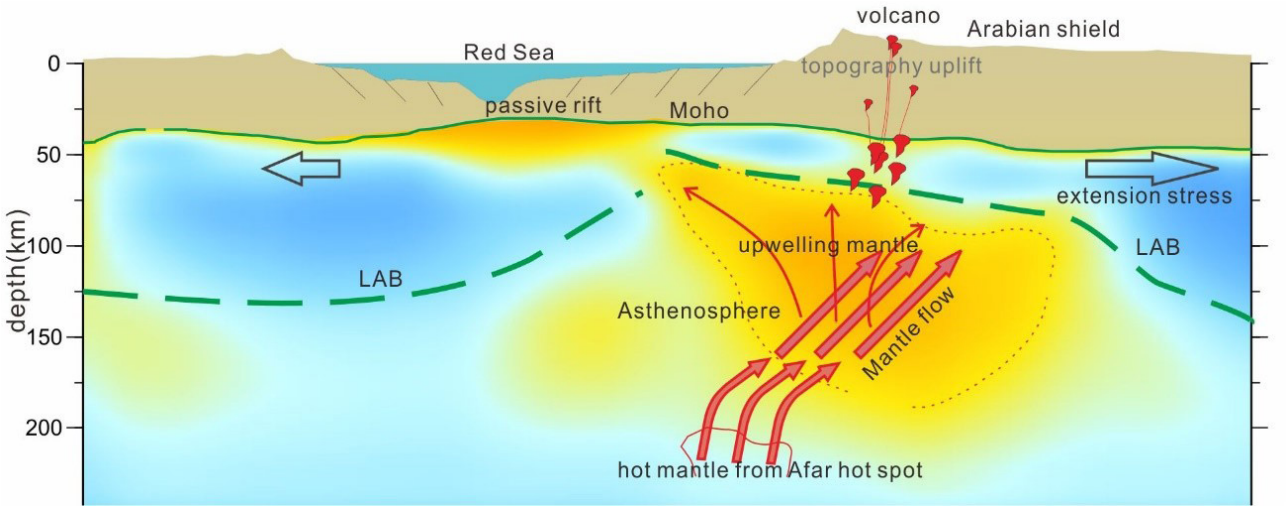

Figure 1. **Red Sea S-wave velocity cross section at 20° north from Sudan to western Saudi Arabia. Blue colors are higher S-wave velocities, yellow are lower. The Red Sea has opened on a low angle detachment fault and hot asthenosphere (yellow) upwells to the east of the Red Sea spreading axis. Thus, the Red Sea is an asymmetrical rift with much thinner (60 km) lithosphere to the east as compared with the west (>100 km). From Yao et al., 2017**

Controls on high-grade ore shoots at Callie world-class gold deposit, Northern Territory, Australia

by

L Petrella[*], N Thébaud[*], C LaFlamme[*], and S Occhipinti[*]

Preliminary observations ranging from geological and structural mapping to smaller scale petrographic study have been used in order to document possible controls on gold mineralization at Callie deposit in Northern Territory, Australia. With an endowment of 14 Moz Au, Callie is a world-class deposit characterized by visible, high-grade, gold mineralization (commonly returns intervals around 100 g/t Au). High-grade ore shoots are primarily controlled by a series of vein corridors (approximately 5m wide) that cut across a plunging folded sequence of medium to fine-grained Paleoproterozoic metaturbidites. The vein corridors are trending 70º and dipping 70º to the southeast. They consists of numerous, highly continuous quartz veins which acted as a conduit for the mineralising fluid. Depending on the nature of the host unit two contrasting styles of Au mineralization are found at Callie. One type of Au mineralization consists of disseminated sulphides occurring in iron-rich, fine-grained siltstones within the vein corridor vicinity. The main sulphides present are pyrrhotite and arsenopyrite which crystallized as a result of sulphidation of the iron-rich minerals present in the iron-rich siltstone. Visible gold is found mainly as filling micro-fractures within the arsenopyrite crystals. The other mineralization style found at Callie consists of higher-grade visible Au constraint within quartz veins intersecting specific stratigraphic horizons characterized by finely laminated siltstones. Highest Au grade occurrences within the quartz veins are located along secondary direction. The secondary direction corresponds to later carbonate-rich vein sets cutting through the earlier quartz veins. Both vein sets are concomitant with a distinct deformation event and each contains a specific alteration footprint indicating contrasting fluid composition. Considering that Au is present in the second carbonate-rich vein type only when it intersects the earlier vein set it is unlikely that the second hydrothermal event brings further mineralization into the deposit but rather locally remobilises it. The presence of both vein sets and alteration types appears to be instrumental in the formation of high-grade oreshoots and therefore can be used as a vector towards high-grade Au mineralization.

* Centre for Exploration Targeting. The University of Western Australia, 35 Stirling Highway, Crawley WA 6009

Death of an orogen, birth of a craton

by

AM Piechocka[1], S Sheppard[1], SP Johnson[2], B Rasmussen[1], and F Jourdan[1]

Orogens represent unstable portions of the Earth's crust that with repeated reworking become progressively strengthened and, ultimately, cratonized. Reactivated intraplate orogens typically display significant crustal thickening and vertical exhumation but this style may not apply to all intraplate orogens. The Proterozoic Capricorn Orogen, Western Australia, records a complex history of intraplate reworking and reactivation over about 1.5 billion years. Initial reworking at 1.8 Ga spanned the entire width of the orogen but subsequent reworking events affected progressively smaller areas with a final event at 1.03 – 0.90 Ga confined to a narrow corridor in the center of the orogen. This history of reworking was followed by a major episode of mainly dextral strike-slip reactivation of discrete faults and shear zones across the orogen. New $^{40}Ar/^{39}Ar$ geochronology of muscovite and biotite combined with in situ SHRIMP U–Pb geochronology of xenotime shows that orogen-wide reactivation of pre-existing crustal scale structures occurred between 0.92 and 0.86 Ga just as reworking came to an end. Reactivation involved lateral extrusion of Archean to Paleoproterozoic crust of the Gascoyne Province toward the west as it was squeezed out from between the Pilbara and Yilgarn cratons, most likely during north–south compression. We find no evidence for substantial crustal thickening during reactivation, and our findings do not support earlier suggestions of tectonic activity caused by collision with an unknown craton to the west. Our new data shows that progressive funneling of reworking and orogenic activity was succeeded by a breakout reactivation event that marked cratonization of the orogen.

1 Department of Applied Geology, Curtin University, Kent Street, Bentley WA 6102

2 Geological Survey of Western Australia, 100 Plain Street, East Perth WA 6004

Hadean continental crust in the southern North China Craton: evidence from the Xinyang felsic granulite xenoliths

by

X Ping[1,2], J Zheng[1], H Tang[1], Q Ma[1,3], WL Griffin[2], Q Xiong[1,2], and Y Su[1]

Most of our understanding of the Hadean aeon on Earth is based on the zircon record from the metasedimentary rocks at Mount Narryer and Jack Hills in the Narryer Terrane of Western Australia (e.g. Kemp et al., 2010). In China, more and more Hadean zircons have also been reported (e.g. Xing et al., 2014) and provide further opportunities to unravel the nature and evolution of the Hadean crust. However, most of these zircons were found as detrital or xenocrystic grains in the Phanerozoic orogenic belts, and the nature of the oldest crustal material in China remains unclear.

Four xenoliths of garnet-free felsic granulites, entrained by the Mesozoic Xinyang volcanic rocks in the southern North China Craton (NCC), were selected for U–Pb dating and Lu–Hf isotopes of zircon, as well as whole-rock major and trace element analysis. Their petrography and geochemical composition reveal that the xenoliths are of igneous origin. The magmatic zircons yield ages including 3.5 – 3.6 Ga and c. 2.1 Ga. The 3.5 – 3.6 Ga zircons have widely variable εHf(t) of –7.8 to +4.0 and model ages (T_{crust}) of 3.51 – 4.12 Ga; the c. 2.1 Ga zircon grains have very negative εHf(t) (–29.0 to –26.2) and Hadean model ages (T_{crust} = 3.96 – 4.10 Ga). The metamorphic zircons from the studied xenoliths record several thermal episodes at c. 2.73 Ga, 2.13 – 2.35 Ga and 1.77 – 1.86 Ga. These results suggest that Hadean crustal components may exist in the deep crust of the southern NCC, and probably suffered complex modification during Paleoarchean-Paleoproterozoic time.

Combined with published data, the Hf crustal model ages of zircons from the NCC (peak at c. 3.94 Ga) are older than those from the South China Craton (peak at c. 3.77 Ga) (Fig. 1). This means that there is much more likelihood of finding more Hadean continental crust in the NCC than in the South China Craton. By comparison with the ancient crustal components in the Anshan and Caozhuang areas of the northern NCC, the Xinyang area in the southern NCC may be more prospective for further occurrences of Hadean zircons and/or rocks.

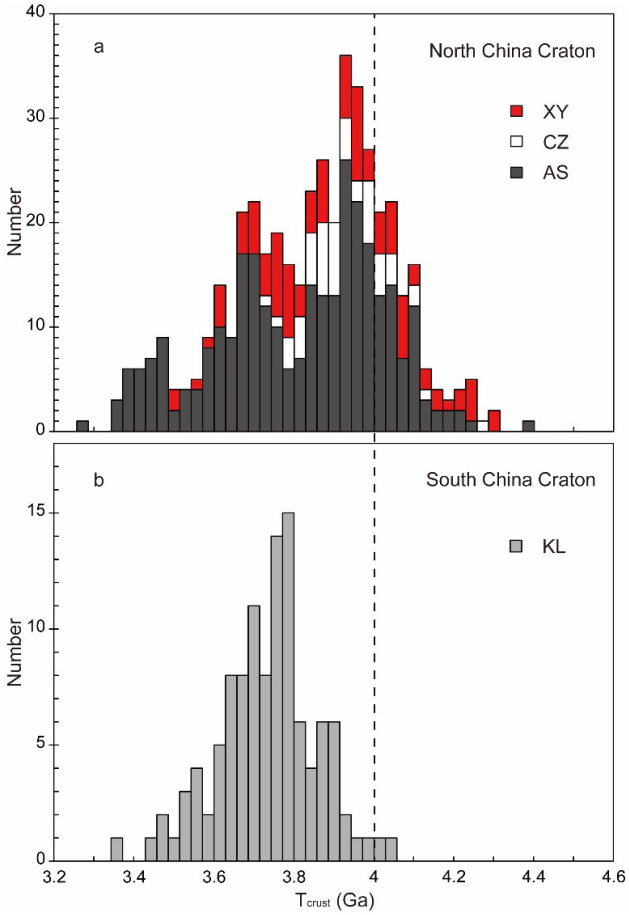

Figure 1. **Distribution of two-stage Hf model ages (Tcrust) of zircons from Eoarchean-Paleoproterozoic rocks from the North China Craton (a) and South China Craton (b). Data sources: a) Zheng et al. (2004), Wu et al. (2005, 2008), Liu et al. (2008), Diwu et al. (2013) and this study; b) Guo et al. (2014). Abbreviations: XY, Xinyang; CZ, Caozhuang; AS, Anshan; KL, Kongling**

1 School of Earth Sciences, State Key Laboratory of Geological Processes and Mineral Resources, China University of Geosciences, Wuhan 430074, China

2 ARC Centre of Excellence for Core to Crust Fluid Systems and GEMOC National Key Centre, Department of Earth and Planetary Sciences, Macquarie University, Sydney NSW 2109, Australia

3 State Key Laboratory of Isotope Geochemistry, Guangzhou Institute of Geochemistry, Chinese Academy of Sciences, Guangzhou 510640, China

References

Kemp, AIS, Wilde, SA, Hawkesworth, CJ, Coath, CD, Nemchin, A, Pidgeon, RT, Vervoort, JD and DuFrane, SA 2010, Hadean crustal evolution revisited: new constraints from Pb-Hf isotope systematics of the Jack Hills zircons: Earth and Planetary Science Letters 296, p. 45–56.

Xing, GF, Wang, XL, Wan, YS, Chen, ZH, Jiang, Y, Kitajima, K, Ushikubo, T and Gopon, P 2014, Diversity in early crustal evolution: 4100 Ma zircons in the Cathaysia Block of southern China; Scientific Reports 4, article number 5143, doi:10.1038/srep05143.

Zheng, JP, Griffin, WL, O'Reilly, SY and Lu, FX 2004, 3.6 Ga lower crust in central China: new evidence on the assembly of the North China Craton: Geology, v. 32, p. 229–232.

Wu, FY, Yang, JH, Liu, XM, Li, TS, Xie, LW and Yang, YH 2005, Hf isotopes of the 3.8 Ga zircons in eastern Hebei Province, China: implications for early crustal evolution of the NCC: Chinese Science Bulletin 50, p. 2473–2480.

Wu, FY, Zhang, YB, Yang, JH, Xie, LW and Yang, YH 2008, Zircon U–Pb and Hf isotopic constraints on the Early Archean crustal evolution in Anshan of the North China Craton: Precambrian Research, v. 167 (no. 3–4), p. 339–362.

Liu, DY, Wilde, SA, Wan, YS, Wu, JS, Zhou, HY, Dong, CY and Yin, XY 2008, New U–Pb and Hf isotopic data confirm Anshan as the oldest preserved segment of the North China Craton: American Journal of Science, v. 308, p. 200–231.

Diwu, CR, Sun, Y, Wilde, SA, Wang, HL, Dong, ZC, Zhang, H and Wang, Q 2013, New evidence for ~4.45 Ga terrestrial crust from zircon xenocrysts in Ordovician ignimbrite in the North Qinling Orogenic Belt, China: Gondwana Research, v. 23, p. 1484–1490.

Guo, JL, Gao, S, Wu, YB, Li, M, Chen, K, Hu, ZC, Liang, ZW, Liu, YS, Zhou, L, Zong, KQ, Zhang, W and Chen, HH 2014, 3.45 Ga granitic gneisses from the Yangtze Craton, South China: Implications for Early Archean crustal growth: Precambrian Research, v. 242, p. 82–95.

Stratigraphy and architecture of the Paleoproterozoic Bryah and Padbury Basins, Capricorn Orogen: towards an understanding of basin evolution

by

L Ramos*, A Aitken*, S Occhipinti*, and M Lindsay*

The Paleoproterozoic Bryah and Padbury Basins are located in the southeastern part of the Capricorn Orogen, which is currently the target of a major multi-institution and multidisciplinary research project — The Capricorn Distal Footprints Project. This project aims to understand the crustal evolution, tectonic processes, and mineralization systems of the Capricorn Orogen. In this context, magnetic and gravity data together with petrophysics, drillcore logging, geological mapping, and 2D geophysical modelling were integrated aiming the characterization of the stratigraphy and architecture of the Bryah and Padbury Basins, and hence to better understand the basin evolution.

The Bryah Basin formed along the northern Yilgarn Craton margin due to extension and tectonic processes prior to the Glenburgh Orogeny. This lithospheric extension resulted in the deposition of sedimentary and magmatic rocks of the Bryah Group (c. 2030 to 2014 Ma), which has its bulk formed by the Narracoota Formation's magmatism. The Padbury Basin overlies the Bryah Group, and is formed by carbonate, siliciclastic and banded iron formation rocks of the Padbury Group (c. 2000 to 1890 Ma) deposited in a pro-foreland basin. Deposition in these basins ceased with the initiation of the Capricorn Orogeny at c. 1820 Ma, which was responsible for the structural reworking of the basins, resulting in the reactivation of pre-existing faults, and the input of hydrothermal fluids that resulted in gold mineralization.

Different geophysical data and methods can be used to characterize volcano-sedimentary basins. The Bryah and Padbury Basins are characterized by long magnetics lineaments which are both easterly and northerly trending. However, only easterly trend features are exhibited in the gravity data, in a convex geometry (northwest–southeast/southwest–northeast trend). These are sub-parallel to structures related to the southern boundary of the basins (e.g. Goodin and Murchison Faults). Based on the magnetic data, fourteen magnetic domains are distinguished in the Bryah and Padbury Basins and surroundings terranes, while four main domains based on the Bouguer Anomaly are recognized. In the southern part of the basins, a regional positive gravity anomaly trending east–west/northeast–southwest is coincident with mafic magmatism in the Narracoota Formation. This anomaly may be due to an approximately 5 km thick package of higher density mafic rocks, and it can help to elucidate processes that occurred during the precursor rift of the early stages of the Bryah Basin. This anomaly is also particularly important to delineate contacts between magmatic rocks and the sedimentary fill, which can assist VMS exploration models. Additionally, observations made in drill holes at several localities in the basins provided a better understanding of the basins infill, subsurface lithologies and structural information, as well as the contact between the Archean basement and the sediments in the underlying Yerrida Group that was formed in a sag basin.

* Centre for Exploration Targeting. The University of Western Australia, 35 Stirling Highway, Crawley WA 6009

Identifying open-system behaviour in Sm–Nd and U–Pb data in titanite

by

E Scibiorski*

Titanite is a valuable chronometer as it occurs in a wide variety of geological settings, and may record multiple stages of high-grade metamorphism and fluid mobility. Although titanite is most commonly used for U–Pb geochronology, Sm–Nd data may be used to obtain the Nd isotope composition at the time of titanite growth. In these cases, the U–Pb isotope system provides valuable context for the interpretation of titanite Sm–Nd data.

Here, we use three titanite-bearing samples from the Mesoproterozoic Albany–Fraser Orogen of Western Australia to investigate the behaviour of the U–Pb and Sm–Nd isotopic systems in titanite. We used LA-SS-ICPMS to analyse the U–Pb, Sm–Nd and trace element composition of titanite in situ in thin section. The samples were selected to encompass a range of processes, from a simple system with a single titanite population, to a more complicated case showing evidence of open-system behaviour.

Chondrite-normalized REE abundance patterns discriminate between multiple populations of titanite in each sample. These populations correlate with distinct BSE microstructures and petrographic context, as well as the behaviour of the U–Pb and Sm–Nd isotope systems.

In one sample, a single compositional population of titanite yields a homogenous cluster of U–Pb data. Similarly, the Sm–Nd data define a single isochron with low dispersion in $^{147}Sm/^{144}Nd$ values. This suggests that titanite in this sample remained a closed system following crystallization.

In a second sample, two compositional populations of titanite were subjected to age resetting during metamorphism, and yield a single U–Pb age. The two titanite populations differ slightly in Sm–Nd characteristics, primarily in $^{147}Sm/^{144}Nd$ and εNd values, but define a single isochron line, suggesting a single Sm–Nd reservoir for titanite in this sample. Therefore, differences in the Sm and Nd content may be a product of titanite recrystallization during metamorphism.

In the third sample, the U–Pb data are distributed along a mixing line between radiogenic and common (non-radiogenic) Pb. Analyses of titanite with a high proportion of radiogenic Pb define an isochron in Sm–Nd space, whereas titanite analyses that contain a high proportion of common Pb are discordant, and plot below the Sm–Nd isochron. This suggests that the incorporation of common Pb into the titanite was accompanied by open system behaviour in Sm–Nd.

* ARC Centre of Excellence in Core to Crust Fluid Systems (CCFS) and Centre for Exploration Targeting, University of Western Australia, 35 Stirling Highway, Crawle WA 6009

Evolving 3D magnetotelluric models across South Australia

by

S Thiel[1,2], K Robertson[1,2], A Reid[1,2], S McAvaney[1], and G Heinson[2]

Introduction

The Australian Lithospheric Architecture Magnetotelluric Project (AusLAMP) is an eventual continent-wide deployment of long-period (10–10 000 s) magnetotelluric (MT) instruments in a half-degree (~55 km) interval grid across Australia to map the electrical resistivity structure of the continental lithosphere. AusLAMP aims to provide constraints on the tectonic evolution of the continent and the mineral exploration potential as part of the UNCOVER initiative (UNCOVER, 2015; Amira International, 2015). The coverage of sites in South Australia is nearing completion with about 370 out of 400 sites acquired to date. Areas of economic potential or interest covered by the survey include the Mesoproterozoic Coompana Province, the Archean–Proterozoic Gawler Craton and its mineral-rich cover of the Neoproterozoic Stuart Shelf, extending across to the east and covering the Neoproterozoic Ikara-Flinders Ranges and Paleo-Mesoproterozoic Curnamona Province. MT images regions of enrichment or depletion, with fluids/melts/sediments released from subducting plates or interactions with mantle plumes changing the conductivity and high temperature events such as high-grade metamorphism and melt events may serve to deplete the lithosphere of hydrogen and carbon thus leaving a resistive lithosphere. Given the retainment of these signatures for billions of years, we have a tool capable of imaging the effects of a rich and complex tectonic history across the cratonic parts of South Australia (Gawler Craton; Thiel and Heinson, 2013), near cratonic (e.g. Musgrave Province, Curnamona Province, Coompana Province) and younger overprinted regions (e.g. Ikara-Flinders Ranges, Stuart Shelf).

Method

MT is a passive electromagnetic technique involving the measurement of naturally occurring magnetic and electric fields generated by a combination of the interaction of solar particles with the magnetosphere, and lightning strikes across the globe traversing within the ionosphere which acts as a waveguide. To date, a total of 370 long period (10–10,000 s) MT sites have been collected across South Australia since November 2013. Standard long-period MT sets from the AuScope instrument pool were used, with two 50 m dipoles using Pb–PbCl non-polarizing electrodes to record the electric field in perpendicular directions (along a north-south axis, Ex and an east–west axis, Ey), and a fluxgate magnetometer to record the magnetic field in three directions (north–south, Bx, east–west, By, and vertical, Bz). Instruments recorded for at least three weeks unless damage was sustained in the field, but generally at least one week of recording would result in usable data. Time series data were processed to the frequency domain using the bounded influence robust remote referencing processing code of Chave and Thompson (2004) with sites that recorded simultaneously used for remote referencing to improve the signal to noise ratio of the response. With MT sounding, a more resistive subsurface and longer period measurements result in a greater penetration depth than a conductive subsurface and shorter period measurements. Generally most sites recorded good data across a period range of about 5–10 000 s, capable of imaging the entire lithosphere across most of South Australia.

Results

Models of subsets of AusLAMP SA have already been presented (Robertson et al 2016, Thiel et al 2016), however final stages of modelling are currently underway to incorporate these smaller subsets into a model space covering almost all of South Australia (Model Area 1, red rectangle, Fig. 1) along with new results from the northeast SA area (Model Area 2, purple rectangle, Fig. 1). Modelling is conducted using the ModEM software package (Egbert and Kelbert, 2013; Kelbert et al., 2014) for the full impedance tensor and the tipper.

The central Gawler Craton is imaged as a resistive zone with conductive margins surrounding the core of the cratonic block at shallow upper-mantle depths. Contrary to seismic tomography models, showing a fairly homogeneous and fast velocity structure, the Curnamona Province shows a highly heterogeneous resistivity distribution with low resistivity zones in the crust beneath the Province. The most recent acquisition covers the NE of the state in the Cooper Basin and the Simpson Desert, an area that has not been covered by any deep-probing geophysical techniques and preliminary results indicate the presence of a north-south trending conductor. The results of the inversion of the AusLAMP data highlight the correlative significance with other geochemical data and points towards MT as a geophysical fertility vector for mineral discovery.

1 Geological Survey of South Australia, Adelaide SA 5000

2 The University of Adelaide, Adelaide SA 5005

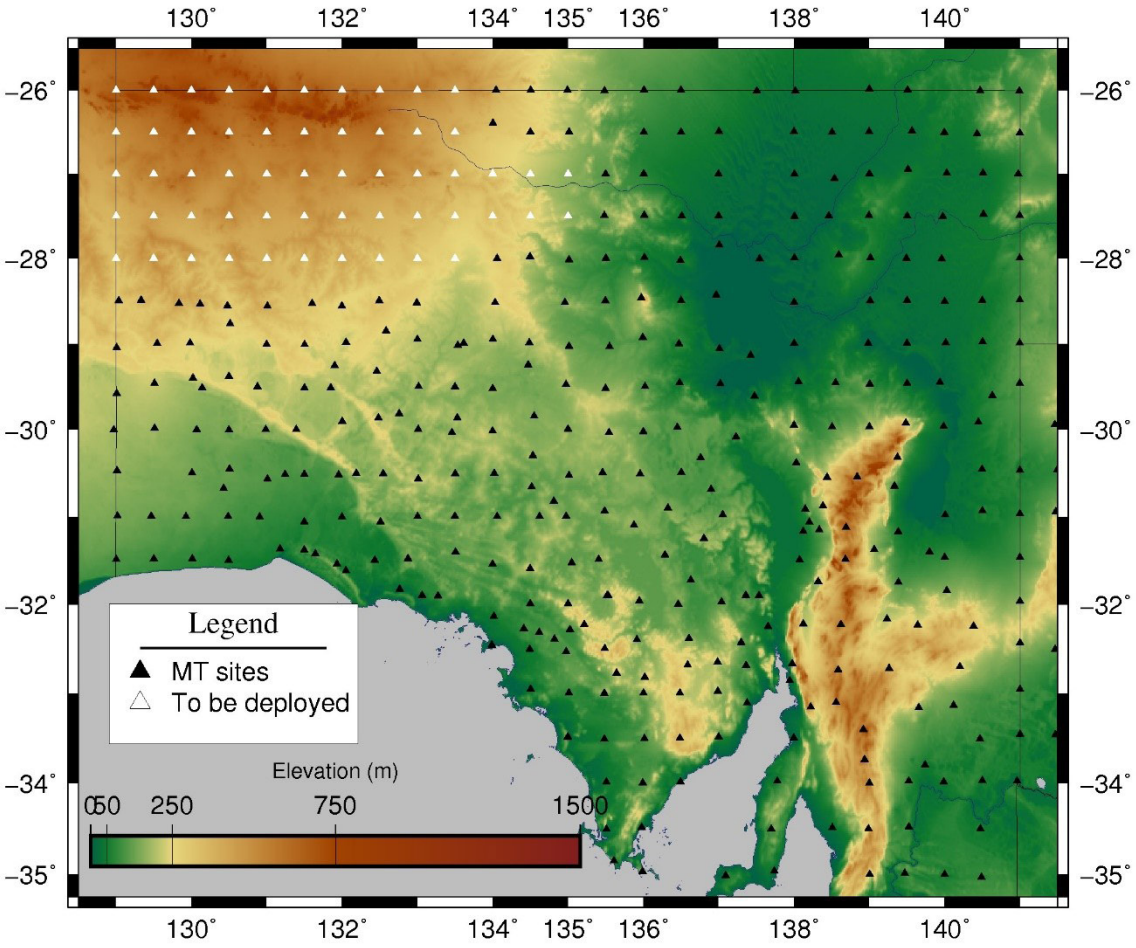

Figure 1. **AusLAMP long-period MT site deployed locations (black) and intended locations (white) over topography. Model Area 1 is shown by the red rectangle and Model Area 2 is shown by the purple rectangle.**

Preliminary work on the near-statewide AusLAMP dataset shows that tectonic provinces with varying tectonothermal histories are imaged as changing electrical resistivity structure with enriched lithosphere in graphite, carbon and sulphides imaging as (such as the margin of the Gawler core and the crust of the Curnamona Province) and depleted regions as resistive such as the interior core of the Gawler Craton. Regions of anomalous conductivity may underlie regions of mineralogical potential such as that which occurs along the IOCG-U belt in the Stuart Shelf (Heinson et al., 2006) and the Beverley Uranium mine (Thiel et al., 2016b).

Conclusions

AusLAMP is nearing completion across South Australia with approximately 5% remaining to be covered in the northwest of the state. A total of 370 long-period MT sites reveal distinct large scale changes in the electrical structure across the state and for the first time we have shown data and described preliminary modelling results of the northeast of South Australia, a region that until now has not been covered by deep-penetrating geophysical techniques and thus has very little known about the lithosphere. Major features observed across the state include a resistive interior core of the Gawler Craton surrounded by a conductive margin, a resistive Ikara-Flinders Ranges with the exception of two conductive anomalies and a conductive crust of the Curnamona Province.

Acknowledgments

AusLAMP in SA is a collaborative project between the GSSA, the University of Adelaide and Geoscience Australia with funding from the GSSA's PACE Copper initiative, Geoscience Australia and NCRIS. The core field team comprises Philippa Mawby, Bruce Goleby and Geoff Axford and other field crew for collecting the data, and to Goran Boren for instrument maintenance. The instruments were provided by the AuScope instrument pool. Thanks to landholders and traditional owners for allowing access to the lands and to Naser Meqbel for providing 3D grid software. Modelling was undertaken on the NCI, and Phoenix. Figures were generated using GMT 5 (Wessel et al., 2013).

References

Australian Academy of Science 2015, UNCOVER, Searching the deep earth: A vision for exploration geoscience in Australia.

Amira International 2015, Final Report- Unlocking Australia's hidden potential: An Industry Roadmap – Stage 1, P1162.

Chave, AD and Thompson, DJ 2004, Bounded influence magnetotelluric response function estimation: Geophysical Journal International, v. 157, p. 988–1006.

Egbert, GD and Kelbert, A 2012, Computational Recipes for Electromagnetic Inverse Problems: Geophysical Journal International, v. 189, p. 251–267.

Kelbert, A, Meqbel, NM, Egbert, GD and Tandon, K 2014, ModEM: A modular system for inversion of electromagnetic geophysical data: Computational Geoscience, v. 66, p. 40–53.

Heinson, G, Direen, N and Gill, R 2006, Magnetotelluric evidence for a deep-crustal mineralizing system beneath the Olympic Dam iron oxide copper-gold deposit, southern Australia: Geology, v. 34(7), p. 573–576.

Robertson, K, Heinson, G and Thiel, S 2016, Lithospheric reworking at the Proterozoic–Phanerozoic transition of Australia imaged using AusLAMP Magnetotelluric data: Earth and Planetary Science Letters, v. 452, p. 27–35.

Thiel, S and Heinson, G 2013, Electrical condcutors in Archean mantle-Result of plume interaction?: Geophysical Research Letters, v. 40, p. 2947–2952.

Thiel, S, Heinson, G, Reid, A and Robertson, K 2016, Insights into lithospheric architecture, fertilisation and fluid pathways from AusLAMP MT: ASEG Extended Abstracts.

Wessel, P, Smith, WHF, Sharroo, R, Luis, J and Wobbe, F 2013, Generic Mapping Tools: Improved Version Released: EOS Transactions. AGU, v. 94(45), p. 409–410.

Finite-frequency P-wave tomography of the upper mantle beneath Capricorn Orogen and adjacent areas

by

X Xu[1], L Zhao[1,2], H Yuan[3,4,5]*, SP Johnson[4], M Dentith[5], R Murdie[4], K Gessner[4], FJ Korhonen[4], and P Piña-Varas[5]

Abstract

The Proterozoic Capricorn Orogen located in central Western Australia, recorded the assembly of the Archean Pilbara and Yilgarn Cratons to form the West Australian Craton during two stages of Paleoproterozoic Orogenies. To better understand the associated early tectonic evolution, we applied a finite-frequency P-wave tomography technique to obtain the 3D body-wave velocity model of the upper mantle of this region. The P-wave relative travel-time residuals were picked by applying a multichannel cross-correlation technique to the waveforms collected at eight permanent and 57 broadband seismic stations of the Capricorn Orogen Passive-source Array. Overall a dataset including 6788 P-wave travel-time data was obtained from 344 teleseismic events (distance range from 20 to 98º, magnitude from from Mw5.0 to Mw8.0). A preliminary results show an excellent spatial correlation with the geologic structure in this region, but also reveal intriguing features in the orogenic lithosphere that my shed light onto the regional tectonics. The Capricorn Orogen is imaged clearly as a significant low-velocity zone extending downward to ~250 km, likely reflecting the effects of punctuated lithospheric reworking and reactivation during the over-a-billion-years of cratonization of the West Australian Craton. The Glenburgh Terrane is underlain by a high-velocity anomaly with ~200 km thickness, consistent with an Archean megablock origin of the Glenburgh Terrane. The Pilbara Craton is characterized by high-velocity anomalies downward to ~300 km, but with alternating low-velocity anomalies inside: The amplitude of the high-velocity is substantially lower compared with the Yilgarn Craton. To the northeast of Pilbara Craton, a slow velocity anoamaly is found beneath the Paterson Orogen. The most intriguing feature of the model is the high-velocity slab-like anomalies that extend northwards to over 200 km depth beneath the Capricorn Orogen, favoring the operation of a 2.0 Ga Paleoproterozoic subduction during the final assembly of the West Australian Craton.

References

Cawood, PA and Korsch, RJ 2008, Assembling Australia: Proterozoic building of a continent: Precambrian Research, v. 166, p. 1–35.

Dahlen, FA, Hung, SH and Nolet, G 2000, Fréchet kernels for finite-frequency traveltimes-I, Theory: Geophys J Int, v. 141, p. 157–174.

Hung, SH, Dahlen, FA and Nolet, G 2000, Fréchet kennels for finite-frequency traveltimes-II, Examples: Geophys J Int, v. 141, p. 175–203.

Sheppard, S, Rasmussen, B, Muhling, JR, Farrell, TR and Fletcher, IR 2007, Grenvillian-aged orogenesis in the Palaeoproterozoic Gascoyne Complex, Western Australia: 1030-950 Ma reworking of the Proterozoic Capricorn Orogen: Journal of Metamorphic Geology, v. 25, p. 477–494.

Reading, AM, Tkalčić, H, Kennett, BL, Johnson, SP and Sheppard, S 2012, Seismic structure of the crust and uppermost mantle of the Capricorn and Paterson Orogens and adjacent cratons, Western Australia, from passive seismic transects, Precambrian Research, v. 196, p. 295–308.

Vandecar, JC and Crosson, RS 1990, Determination of teleseismic relative phase arrival Times using multi-channel cross-correlation and least-squares: Bull Seismol Soc, Am, v. 80, p. 150–169.

1 State key Laboratory of Lithospheric Evolution, Institute of Geology and Geophysics, Chinese Academy of Science, Beijing 100029, China

2 CAS Center for Excellence in Tibetan Plateau Earth Sciences, Beijing, China

3 ARC Centre of Excellence for Core to Crust Fluid Systems, Department of Earth and Planetary Sciences, Macquarie University, Sydney NSW 2109, Australia (huaiyu.yuan@gmail.com)

4 Geological Survey of Western Australia, Mineral House, 100 Plain Street, East Perth WA 6004, Australia

5 Centre for Exploration Targeting, University of Western Australia, 35 Stirling Highway, Crawley WA 6009, Australia

Indication from finite-frequency tomography beneath North China Craton: the heterogeneity of Craton destruction

X Xu[1] , L Zhao[1,2], K Wang[1], J Yang[1]

Abstract

Using a multi-frequency joint inversion tomographic technique, we constructed new 3D P and S velocity models of the North China Craton (NCC) upper mantle with high resolution. Our research was based on previous work in the region but was augmented by a much denser station coverage in the western NCC. The new data set is composed of 65629 P- and 447050 S-wave travel time residuals in multiple frequency bands, measured from 793 teleseismic events recorded by 738 permanent stations of the upgrade China National Seismic Network and 685 broadband stations of 10 temporary arrays in the region. The new P and S models provide several salient features which we draw possible inferences on the regional tectonics. High-velocity anomalies are observed in the mantle transition zone (MTZ), with great morphological heterogeneities suggesting the buckling and/or fragmentation of the subducted Pacific slab. Some of the slab materials may be inferred from the high velocity anomalies visible below 660 km discontinuity, which further sink into the lower mantle. The velocity structure of the eastern NCC is dominated by small-scale lateral heterogeneities. At shallow depth, the high-velocity anomalies beneath the southern part of the eastern NCC and the Yanshan region likely represent the remnant cratonic lithosphere, which may suggest the craton destruction of the NCC is spatially non-uniform. A high-velocity anomaly is also observed in the Sulu Orogen, which is seemingly associated with the Tanlu Fault. The northern boundary of this anomaly spatially coincides with the Yantai–Qingdao–Wulian Fault, and it is likely a remnant of the Yangtze Cratonic lithosphere subducting northwestwards. Significant low-velocity anomalies imaged beneath the central NCC exhibit a spatial discordance between its northern and southern parts, in which the northern low-velocity anomaly extends downwards to the top of MTZ with a lateral northwest–southeast trend, while the southern one extends downwards only to ~200–300 km. Slow-velocity anomalies are present beneath the Phanerozoic orogenic belt surrounding the NCC, the Paleoproterozoic Trans-North China Orogen and the Tanlu Fault. This feature not only shows the excellent spatial correlation with the orogens at surface, but also exhibits a consistent vertical continuity between 60 and 250 km depth. This intriguing feature suggests that the collisional orogenic belts are the inherited weak zones, which may intent to play an important role in the craton destruction. Combining the multidisciplinary results in this area, we suggest that the spatial heterogeneities associated with the NCC craton destruction most likely result from a combined effect of the spatially non-uniform distribution of the wet upwellings triggered by the subducted Pacific slab and the pre-existing weak zones in the cratonic lithosphere.

References

Chen, L 2010, Concordant structural variations from the surface to the base of the upper mantle in the North China Craton and its tectonic implications: Lithos, 120(1), p. 96–115.

Dahlen, FA, Hung, SH and Nolet, G 2000, Fréchet kernels for finite-frequency traveltimes-I. Theory, Geophys J Int, 141, p. 157–174.

Hung, SH, Dahlen, FA and Nolet, G 2000, Fréchet kennels for finite-frequency traveltimes-II, Examples, Geophys J Int, 141, p. 175–203.

Yang, JF, Zhao, L, Kaus, BJP, Lu, G, Wang, K and Zhu, RX 2017, Slab-triggered wet upwellings produce large volumes of melt: Insights into the destruction of the North China Craton, Tectonophysics

Zhao, L, Allen, RM, Zheng, TY and Zhu, RX 2012, High-resolution body wave tomography models of the upper mantle beneath eastern China and the adjacent areas, Geochem Geophys Geosyst, 13: Q06007, doi: 10.1029/2012GC004119

Zhu, RX, Zhang, HF, Zhu, G, Meng, QR, Fan, HR, Yang, JH, Wu, FY, Zhang, ZY and Zheng, TY 2017, Craton destruction and related resources, Int J Earth Sci, p. 1–25.

1 State Key Laboratory of Lithospheric Evolution, Institute of Geology and Geophysics, Chinese Academy of Sciences, Beijing, China

2 CAS Center for Excellence in Tibetan Plateau Earth Sciences, Beijing, China

Bayesian transdimensional inversion for a probabilistic shear-wave velocity model of the crust in the central West Australian Craton

by

H Yuan[1,2,3] and T Bodin[4]

Introduction

The velocity of seismic waves is one of the frequently used parameters to study tectonic processes associated with crustal growth and evolution. By using a modified Bayesian transdimensional tomography technique, we targeted the crustal shear-wave velocity model beneath a high-density temporary deployment that straddles the north boundary of the Glenburgh Terrane, an exotic block in the core of the Paleoproterozoic Capricorn Orogen in central Western Australia. The region played important roles in initializing and finalizing the West Australian Craton, and provides us an ideal laboratory to characterize the seismic signature associated with the associated tectonic processes. We first explored the feasibility and benefits of obtaining a probabilistic crustal shear-wave velocity model by combining the array dispersion measurements with a regional background velocity model that contains a Moho topography. We then compared the inverted shear-wave velocity model with the surface geological futures as well as higher resolution crustal models from the active-source reflection profiling and receiver function studies.

The crustal shear-velocity model

A high resolution crustal shear-wave velocity model was obtained along a ~200km long cross-section, which straddles the suture zone associated with the 2.2 Ga Ophthalmian Orogeny leading the assembly of the West Australian Craton. The crustal velocity model adds great details to the crustal architecture, and provides complementary information to support that the Glenburgh Terrane is a microcontinent originated in the

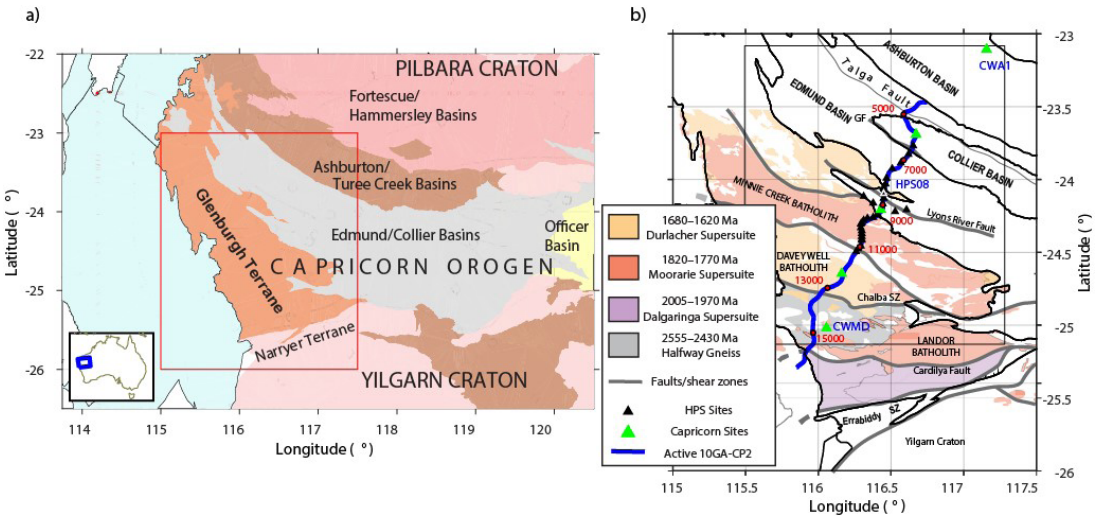

Figure 1. Tectonic setting of the Paleoproterozoic Capricorn Orogen in the West Australian Craton (a), and the close view of the Glenburgh Terrane (b) as indicated by the red rectangle in a). Features in b) include: the passive-source seismic array (black and green triangles for HPS and COPA, respectively), and the active-source transect 10GA-CP2 (blue line). Numbers along the active-source line show the common depth point (CDP) locations discussed in the text. Major faults (gray lines) are marked. Black contours are the terrane structural boundaries. Color coded in b) are the regions affected by the major tectono-thermal events during the cratonization

1 ARC CCFS, Department of Earth and Planetary Sciences, Macquarie University, NSW 2109, Australia
2 Geological Survey of Western Australia, Mineral House, 100 Plain Street, East Perth WA 6004, Australia
3 Centre for Exploration Targeting, University of Western Australia, 35 Stirling Highway, Crawley WA 6009, Australia
4 Univ Lyon, Universite Lyon 1, Ens de Lyon, CNRS, UMR 5276 LGL-TPE, F-69622 Villeurbanne, France

Archean. The average slow velocity favors a felsic or granitic composition of the Glenburgh Terrane, which was perturbed during the intraplate thermal events in the stabilization of the West Australian Craton. The distinct pattern in the velocity domains helps delineate the northern margin of the Glenburgh Terrane. Compared with previous crust models, the terrane extends further north and extrudes into the crust beneath the Proterozoic basins. The fast-velocity lower crust in the terrane margin is spatially coincident with crustal wedges recognized in both the active source reflection and receiver function images, which may be typical in convergent continental regions. Along with the isotope evidence that suggests a magmatic arc origin of the deep crust source, the seismic observations favor the operation of a Paleoproterozoic subduction processes leading the 2.2 Ga Ophthalmian Orogeny.

References

Johnson, SP, Thorne, AM, Tyler, IM, Korsch, RJ, Kennett, BLN, Cutten, HN, Goodwin, J, Blay, O, Blewett, RS, Joly, A, Dentith, MC, Aitken, ARA, Holzschuh, J, Salmon, M, Reading, A, Heinson, G, Boren, G, Ross, J, Costelloe, RD and Fomin, T 2013, Crustal architecture of the Capricorn Orogen, Western Australia and associated metallogeny: Australian Journal of Earth Sciences, v. 60, p. 681–705.

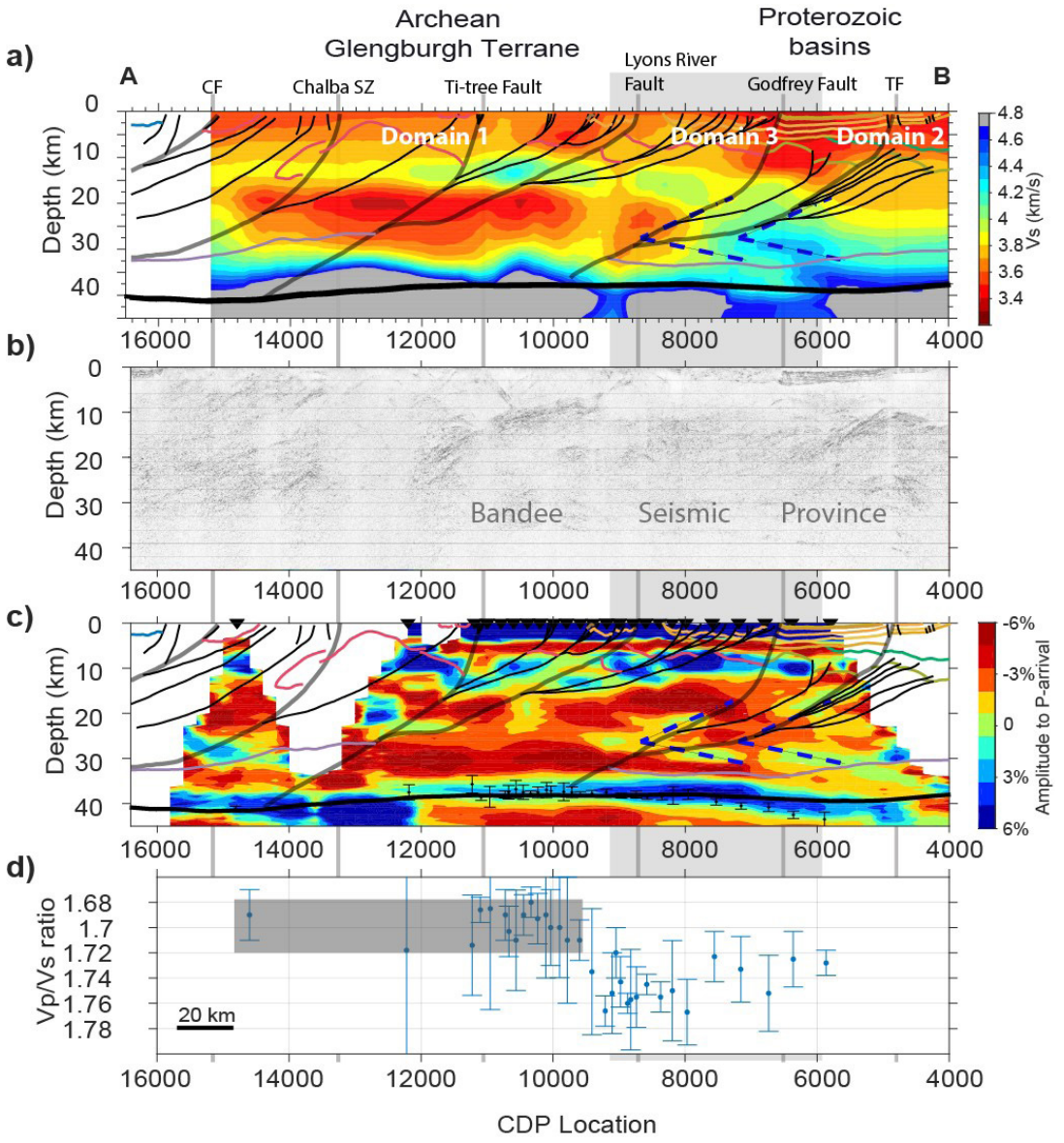

Figure 2. **Comparison between the velocity structure, surface geology and available crustal models: a) the annotated velocity model with the active-source interpretations modified from Johnson et al. (2013). Faults and suture zones at surface are marked and indicated as vertical grey lines. The vertical gray bar shows the approximated boundary for the transition region Domain 3. Blue dashed lines indicate the tectonic wedges inferred from the active source and receiver function results. The thick black line is the Moho interface from the AuSREM model. The active source interpretations include: thin grey and black lines, the fault systems; red lines in the shallow crust, the base of granite batholiths; and green lines, the base of Proterozoic basins; b) the migrated active source image without the interpretations; c) receiver function common conversion point (CCP) results with the active-source interpretations; d) Vp/Vs ratios and errors from receiver function H-k technique. The grey-shaded region indicates the small Vp/Vs ratios (~1.70) in the Glenburgh Terrane.**

Modelling the dominant driving force for supercontinent breakup: plume push or subduction rollback?

by

N Zhang*, C Huang*, Z Dang*, and Z Li*

Understanding the dominant force responsible for supercontinent breakup is crucial for establishing Earth's geodynamic system that drives supercontinent cycles and plate tectonics. Conventionally, two forces have been considered: the push by mantle plumes from the subcontinental mantle that is called an active force for breakup, and the dragging force from oceanic slab rollback which is called a passive force for breakup. However, the relative importance of each of these forces is unclear. Here we model supercontinent breakup coupled with global mantle convection in order to address this question. Our global model features a spherical harmonic degree 2 structure, which includes a major subduction girdle and two large upwelling systems. Based on this global mantle structure, we examine the distribution of stress applied to the supercontinent by both sub-supercontinent mantle upwelling and subduction rollback at the supercontinent peripheral. Our results show that: 1) at the central half of the supercontinent, plume push force is up to three times larger than that induced by subduction rollback; 2) a hot anomaly smaller than 50 K beneath the supercontinent can produce a push force strong enough to cause the initialization of supercontinent breakup; (3) the extensional force induced by subduction rollback concentrates on a ~600 km wide zone on the peripheral of the supercontinent, but has far less impact to the interior of the supercontinent. We therefore conclude that although circum-supercontinent slab rollback assists supercontinent breakup, sub-supercontinent mantle superupwell is an essential force.

* Earth Dynamics Research Group, ARC Centre of Excellence for Core to Crust Fluid Systems (CCFS), Department of Applied Geology, Curtin University, GPO Box U1987, Perth, WA 6845

RECORD 2018/7

3RD LITHOSPHERE WORKSHOP

5–6 NOVEMBER 2017, THE UNIVERSITY OF WESTERN AUSTRALIA

Gorczyk and Gessner

This Record is published in digital format (PDF) and is available as a free download from the DMIRS website at <www.dmp.wa.gov.au/GSWApublications>.

Further details of geological products produced by the Geological Survey of Western Australia can be obtained by contacting:

Information Centre
Department of Mines, Industry Regulation and Safety
100 Plain Street
EAST PERTH WESTERN AUSTRALIA 6004
Phone: +61 8 9222 3459 Fax: +61 8 9222 3444
www.dmp.wa.gov.au/GSWApublications